ABSTRACT

Title: COMPARISON OF ASSISTIVE MOBILITY DEVICES WITH AXILLARY SUPPORTS

James Borrelli, Master of Engineering 2006

Directed By: Professor Henry Haslach, Department of Mechanical Engineering

Assistive ambulatory devices with axillary supports are compared using a multidisciplinary approach. Axillary supports are commonly referred to as "shoulder supports" on standard crutches. A framework is presented that compares axillary supports based on loading characteristics during initial contact and during a stride. The underlying goal of this research is to lay the foundation for an axillary support design that is safe. The force normal to the axillary support of two types of assistive devices, axillary crutches and the Strutter, is found experimentally for 2-point gait and 2-point gait with no hands. A dynamic model is developed to estimate the force tangential to the axillary support required for axillary crutches and the Strutter to have the same stride time. Models for the Strutter are also developed to study the response of the axillary support to impact loads due to initial contact.

Comparison of Assistive Mobility Devices with Axillary Supports

By

James Borrelli

Thesis submitted to the Faculty of the Graduate School of the
University of Maryland, College Park, in partial fulfillment
of the requirements for the degree of
Master of Engineering
2006

Advisory Committee:
Henry Haslach, Chair
Amr Baz, Professor
Adam Hsieh, Assistant Professor

Dedicated to my father, Guy Borrelli Sr.

Acknowledgements

There are many people who helped me throughout the course of my thesis. I would like to thank Al Aaron for teaching me how to use the mill and lathe in the machine shop, Dr. Balakumar Balachandran for allowing me access to the shaker table and advice on dynamic experiments, Xinhua Long and He Li for helping me with operation of the dynamic equipment. I would like to thank Dr. Robert Bonenberger for assistance with the destructive testing of aluminum tubes and Dr. Amr Baz for use of his lab where the experiments with human subjects took place.

I would like to thank my family and I would also like to thank my advisor, Dr. Henry Haslach whose guidance and patience has meant a lot to me.

Table of Contents

List of Tables

List of Figures

1 Introduction

People with low-level spinal cord injury (SCI) may use forearm crutches to aid ambulation. Forearm crutches used by low-level SCI sufferers make up for loss of leg function by supporting the weight through the hands and arms. Supporting the weight of the body through the arms is tiring and contributes to the high-energy cost of ambulating. Alternatively, people with short-term disabilities use axillary crutches to aid ambulation. Axillary crutches are intended to be used by supporting weight through the hands but are typically used incorrectly by users who support weight by resting their underarm on the axillary cushion. Supporting the weight of the body through the underarm or axillary region is not a commonly accepted method of crutch walking because it has been shown to cause nerve damage.

Short-term users tend to use axillary crutches incorrectly as they grow tired from the high cost of ambulating with crutches. This indicates that using an axillary support is easier than supporting weight through the hands. Finding a "safe" axillary support directly benefits people with SCI because despite benefits from standing and walking, many individuals with a low-level SCI choose to cease walking with crutches in favor of using a wheelchair around the time of adolescence. Perceived comfort is used as an indicator of relative safety with the hope that people perceive safe axillary supports as more comfortable relative to ones that are un-safe.

The long-range goal is to develop a means of evaluating the safety, comfort, mechanical integrity and ease of use of such devices. This thesis reports the progress toward this goal with the aim of establishing relationships between user perceived comfort and reactions between the user's underarm and the axillary supports of the

Strutter and axillary crutches so that favorable design features of each axillary support may be established. This evaluation involves comparing the forces felt by the user at the axillary support during a stride and from an impact of the footpad with the ground and trying to relate the forces to the perceived comfort for the Strutter and axillary crutches. Perceived comfort is used to assess the "safety" of a device since the axillary nerve and axillary artery cannot be observed directly.

The fracture morphology of aluminum tubes with holes is found in chapter 3 so that when confronted with a failure, investigators can deduce the cause. Aluminum tubes are a material common in forearm and axillary crutches as well as the Strutter. The tubes typically have evenly spaced radial holes, which are used to adjust the height of the device. The external force in the normal direction during gait is found through human experiments in chapter 4. Following the experiments with human subjects, the subjects were surveyed to find the perceived comfort of the Strutter and axillary crutches. The tangential force on the axillary support is estimated by assuming an angular acceleration that gives the same stride times for axillary crutches and the Strutter in section 5.3, at which time the reason for estimating the force is explained. The dynamic model is used to examine the pins of the Strutter or prototype for yielding (chapter 5). The force transmitted to the axillary support caused by an impact of the footpad with the ground is examined in chapter 6.

2 Background

2.1 Assistive Ambulatory Devices

The three assistive ambulatory devices with axillary support that are studied are the Strutter by Orthotic Mobility Systems, axillary crutches and a prototype design created by Borrelli and Haslach (Figure 2.1).

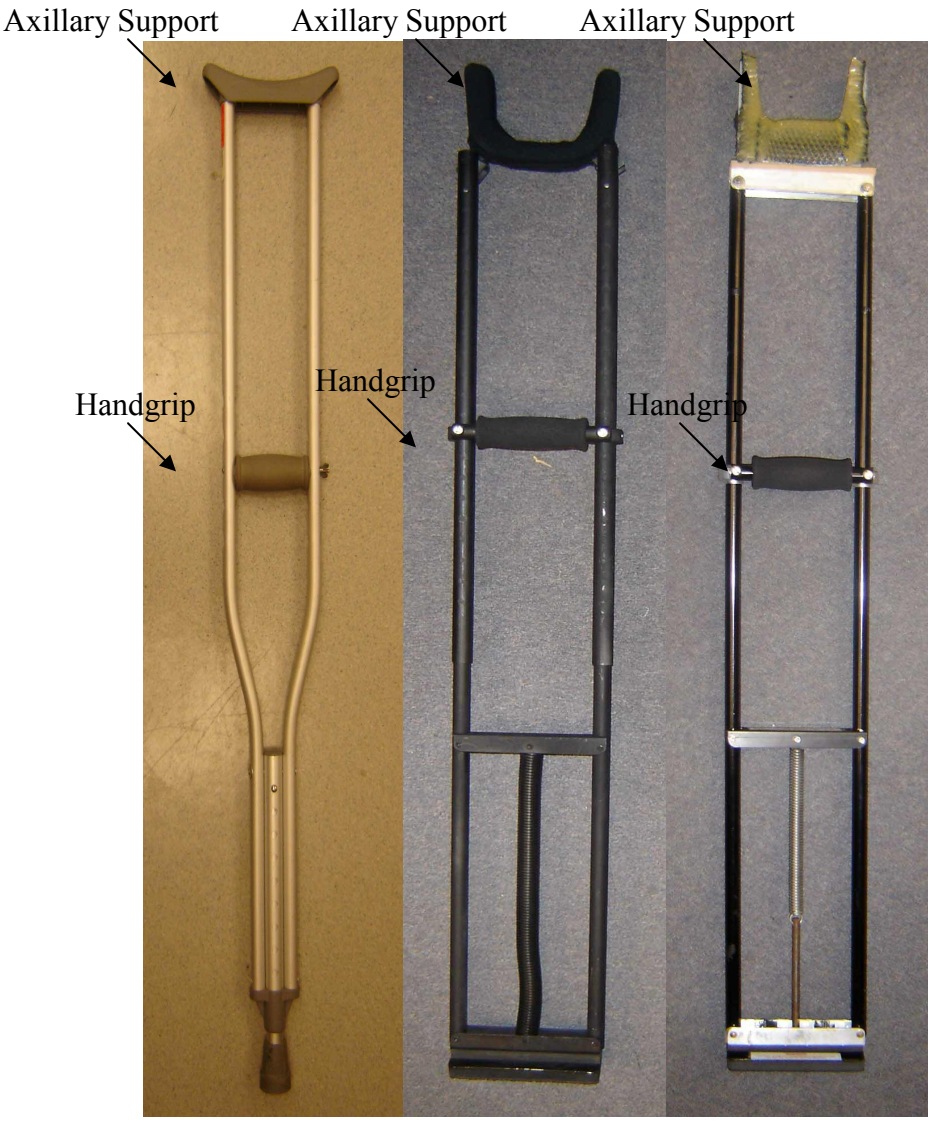

Figure 2.1: Axillary crutch (a), the Strutter (b) and a prototype assistive ambulatory device (c).

The axillary support on the Strutter and the prototype as labeled in Figure 2.1 are intended for weight bearing whereas the axillary support of axillary crutches is not. Axillary crutches are supposed to be used in a similar fashion as forearm crutches. Users support themselves by carrying their weight through the hands and bracing the device against their body. The axillary support of axillary crutches is braced against the ribs and the forearm cuff of forearm crutches is braced against the forearm (Figure 2.2).

Figure 2.2: Forearm crutches (themedicineshop.com, 2006)

The axillary support on axillary crutches may have originally been designed for users to support their weight. However a link was established between axillary nerve damage and supporting the weight of the body on the axillary supports of axillary crutches so that

users are warned against using the axillary pad of a standard axillary crutch for weight bearing (McFall et al. 2004, Rudin and Levine 1996, Perlmutter 1999, Feldman et al. 1995).

The Strutter manufactured by Orthotic Mobility Systems of Kensington, MD makes use of a pinned parallelogram with an internal spring that helps pull the user through a stride. The spring holds the Strutter vertical until the user acts on the Strutter. When the Strutter is placed in front of the body, the spring stretches and stores some energy. From this position, the Strutter spring helps pull the user through their stride,

Figure 2.3.

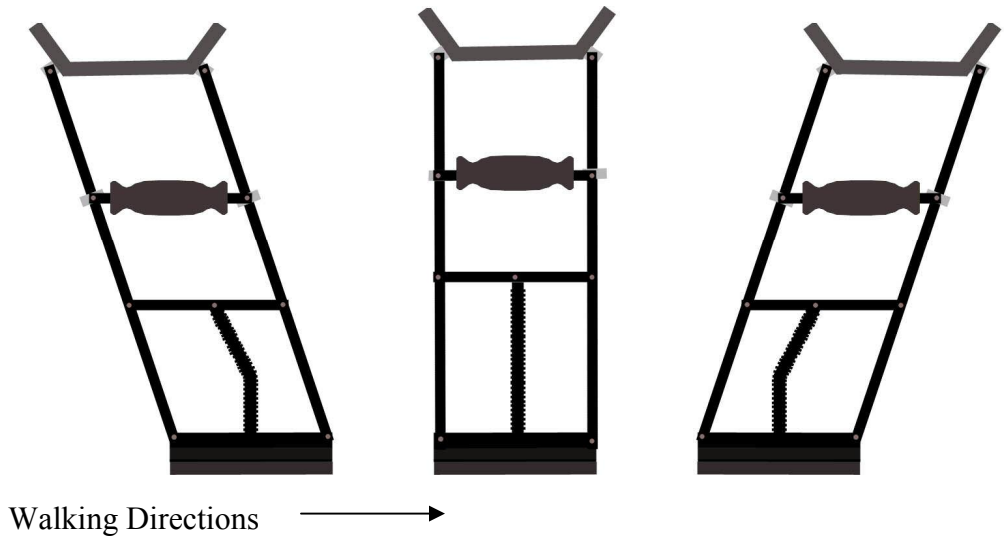

Figure 2.3: The Strutter going through a stride. Notice the shoulder support, handgrip and footpad remain horizontal through the entire stride.

Once the Strutter reaches vertical, if the user progresses further, the Strutter spring resists their motion. If falling is a risk factor, then this is a good thing. However if the user has no risk associated with falling, then this force only impedes the user. Gottschall and Kram (2002) showed that an assistive force created by pulling on subject's torso with an elastic cord decreases energy expenditure for walking. The Strutter pulls on the user's

hand or underarm via the handgrip or axillary support respectively. The handgrip and axillary support of the Strutter and prototype remain horizontal throughout the stride of the user whereas the axillary support and handgrip of an axillary crutch rotate during a stride.

The prototype is a modified Strutter. The shoulder support of the prototype is centered over the vertical support tubes whereas the shoulder support of the Strutter is cantilevered on the vertical support tubes. This change is made to reduce axial and torsion stresses in the vertical support tubes caused by a cantilevered shoulder support. The prototype has a hard saddle shape below the cushion compared to the aluminum bar of the Strutter that serves as a foundation for a cushion (Figure 2.4). The idea behind the saddle shaped hard support is to improve the perceived comfort of the user by implementing an ergonomically shaped support.

(a) (b)

Figure 2.4: Shoulder supports of the Strutter (a) and the prototype (b). The prototype's shoulder support has a honeycomb cushion glued to the hard support.

The prototype was compared to the Strutter with regard to its force transmitted to the underarm however it was not used for experiments with human subjects. The shoulder support is a somewhat complex design that is made of ABS plastic. The shoulder support

constructed to date is only a proof of concept, and the plastic it is made of is not strong enough for use. Although the force transmissibility of the prototype is found in chapter 6, the methodology applied to the Strutter to find the tangential force and stride time also applies directly to the prototype. The axillary crutches tested are standard axillary crutches.

2.2 Users of Assistive Ambulatory Devices

Assistive ambulatory devices serve to reduce weight bearing by the lower extremities and/or increase stability by adding points of contact. People who have difficulty ambulating on their own fall into two categories, short-term and long-term users of assistive ambulatory devices. Short-term users are typically recovering from an injury such as an ankle break or sprain while long-term users are suffering from a permanent spinal injury or disease. Individuals with low-level SCI make up a large portion of long-term assistive ambulatory device users.

A SCI is damage to the spinal cord that results in loss of control of muscle function as well as other ailments. The hip abductors and leg muscles of individuals with low level SCIs have limited abilities. The location of damage to the spinal cord is a good indicator of the degree of disability someone with a SCI experiences. As damage occurs higher up the spine, (moving towards the neck), a person is able to control fewer muscles than a person with lower level damage. Injuries to the spinal cord occur for a variety of reasons ranging from direct trauma, e.g. a fall or violence to disease, e.g. spina bifida, muscle dystrophy or polio.

Spina bifida is a fairly common disability with the more severe forms occurring in approximately 1 in 1000 live births in the US. Spina bifida is a neural tube defect in

which a fetus' spinal cord does not develop properly during the first month of pregnancy. Nerve damage causes varying degrees lower limb impairment. Persons with S1 (sacral level lesion, 1st vertebra), L4 (lesion at 4th lumbar vertebra) and L5 level lesions are generally capable of unassisted gait whereas persons with slightly higher-level lesions generally require ankle foot knee orthoses as well as forearm crutches to ambulate upright (Duffy 1996). Damage to the thoracic levels generally does not permit ambulation with crutch-like assistive devices. Figure 2.5 shows which muscle function is affected by damage to the different regions of the spinal cord. Muscle function below where spinal damage is located is compromised. For example, a person with damage to the L5 region of the spinal cord may lose some bowel, bladder, leg muscle and sexual function.

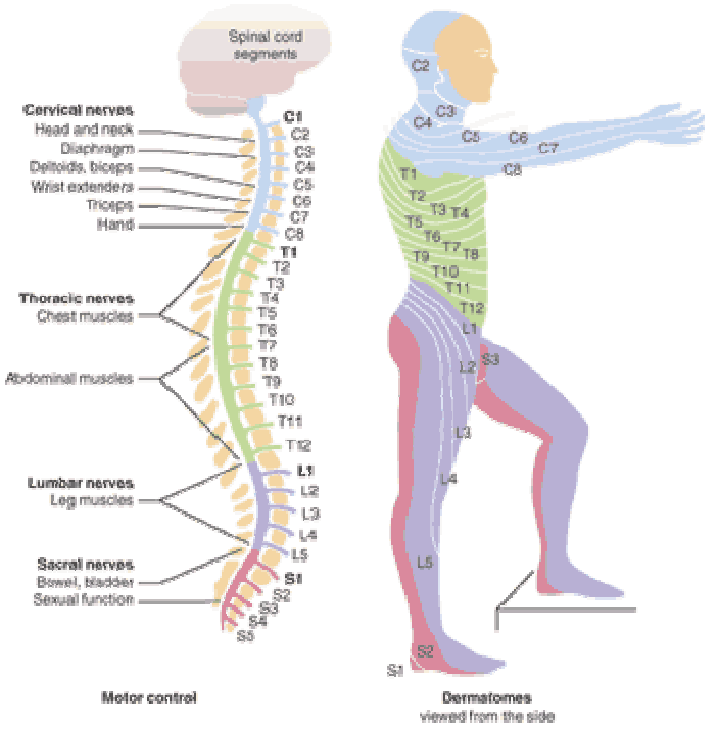

Figure 2.5: Regions of the spinal column (spinal-research.org, 2006).

A person with a low-level SCI typically loses some hip abductor, hip flexor and hip adductor muscle control. The abductors, flexors and adductors are a few of several muscle groups responsible for walking. The purpose of the hip flexors is to advance the leg forward, lifting the leg for toe clearance. Adequate frontal plane torque from the hip adductors is crucial for stability during gait. The hip adductors help to stabilize the hip and assist the hip flexors.

Walking is a very deliberate coordination of the muscles of the hip, the knee, the foot and ankle, and the trunk. The hip has five subcategories of muscles, the hip extensors, the hip flexors, the hip abductors, the hip adductors and rotators. People with damage to the spinal cord at L5 lose some or all muscle function of three of the five subgroups of the muscles of the hip. Duffy et al. (1996) stated that a lack of functioning hip abductors results in significant trunk movement and an energy expensive compensatory gait that is referred to as Trandelenburg.

Different assistive ambulatory devices are risk factors for certain other disorders such as axillary nerve damage, axillary artery damage or carpal tunnel syndrome. The remedy for these disorders is stopping the use of the assistive device or surgery for more advanced cases. When short-term users of assistive ambulatory devices resume normal walking, the symptoms are usually alleviated. For long-term users, the cessation of assistive ambulatory device use can prevent upright ambulation. Ambulating upright as opposed to in a wheelchair has the benefits of improved bone growth, improved blood circulation, reduced bladder infections, reduced pressure sores and prevention of contractures (LeBlanc 2004). A contracture is a shortening of muscle or scar tissue that results in distortion or deformity at a joint of the body, which is often permanent.

Axillary/forearm crutch use increases the load on the hands and wrist and can cause carpal tunnel syndrome (Sala et. al 1998). In addition to carpal tunnel syndrome, axillary crutches can also cause axillary nerve and artery damage when weight is incorrectly supported through the axillary pad (McFall et al. 2004, Rudin and Levine 1996, Perlmutter 1999, Feldman et al. 1995). Despite being risk factors for development of further disorders, forearm and axillary crutches remain the standard of care for individuals with a SCI who are unable to ambulate on their own because no alternatives are widely accepted.

Many studies of alternatives to axillary and forearm crutches have been published (LeBlanc et al. 2004, Hall and Clarke 1991, Deathe 1992, Dalton, et al. 2004, Lee 1987, Stallard, et al. 1978). With few exceptions, most compensate for reduce weight bearing abilities of the lower extremities by supporting some weight with the hands or the arms, with the exception of the Strutter. The Strutter is designed to support the weight of the user through the handgrip and axillary support. Nyland et al. (2004) showed that use of the Strutter required 25% less energy expenditure than axillary crutches for post unilateral knee/hip replacement patients. This suggests that using the underarm and hands for weight bearing may reduce energy expenditure compared to a conventional crutch gait where only the hands are used for weight bearing.

Two studies have considered different handgrip designs in an effort to improve the comfort of axillary and forearm crutches. Sala et al. (1998) used the Fscan pressure sensor system, which is explained later in chapter 4, to map the pressure on the palm of users of forearm crutches. Sala et al. (1998) evaluated two handgrips based on the average and maximum load for different parts of the palm and for the entire palm. The

study also considers the palm's total weight bearing area. Sala et al. (1998) found that cylindrical and wide handles have similar loading patterns but wide handles distribute force over a greater area. Comin et al. (1999) compared four different handgrips used on forearm crutches. A pressure sensitive film and a survey of subjects was used to compare the various designs. The pressure sensitive film was used to measure the percent of palmar contact area where the pressure is greater than 4 kg/cm^2 (392 kPa). A relationship between perceived comfort and the size of areas of high pressure was found with handgrips having smaller areas of high pressure being more comfortable. Fransson-Hall and Kilborn (1993) report the maximum pressure threshold that a woman believed she could bear without experiencing discomfort is approximately 37 kPa (the maximum for men is 104 kPa). The study also reports that higher pressures reduced the amount of time before the pressure became uncomfortable.

These studies show that the force distribution and handgrip geometry are related to perceived comfort. This thesis attempts to extend these ideas to axillary supports since damage to the axillary nerve or axillary artery cannot be directly observed.

3 Fracture Morphology of Aluminum Tubes Similar to the Adjustable Vertical Supports of the Commercial Strutter

The safety of users of a mobility assistive device must be ensured since a catastrophic failure induced fall would be devastating for a user. A catastrophic failure is a failure that occurs without warning. The vertical support tubes are one potential site of failure. Those conducting design testing must be able to identify the type of loading causing an observed fracture of the vertical support tubes in order to design against such a failure. The load required to fracture a vertical support tube is greater than what a person is likely to be able to apply with their weight. However, the growth of fatigue cracks resulting in complete fracture may occur under much lower loads.

When loaded by the user's weight, the shoulder support and handgrip of an assistive device like the Strutter can permit axial, bending and torsion loads in situations where an axillary crutch permits only axial loads. The shoulder support and handgrip of the Strutter are cantilevered on the vertical support tubes (Figure 3.1). This configuration differs from a conventional axillary crutch, which has a handgrip and shoulder support that lie in the plane of the vertical support tubes. As a consequence, axial tests of the adjustable vertical tubes of axillary crutches do not apply directly to the commercial mini and adult-Strutters. The shoulder support of the Strutter is offset from the center of the vertical support tubes by 1 and 15/16 inches in the front and 15/16 inches in the back. Offsetting the shoulder support relative to the vertical support tubes aims to avoid chaffing from the support tubes brushing against the body and allow the axillary support to be angled so it fits in the armpit.

Figure 3.1: The shoulder support of the mini-Strutter is cantilevered on the red vertical support tube.

The height adjustment tube of the mini-Strutter has 12 adjustment holes (the adult Strutter has 24 adjustment holes) through it. The holes allow the overall height of the axillary support to be increased or decreased. The outer vertical support tubes slide up and down on the inner support tubes. A pushpin at the top of the inner support tubes locks the outer support tube in place by filling in one of the adjustment holes in the vertical support tube (Figure 3.2). This form of height adjustment mechanism is also often used in standard axillary crutches (Figure 3.3).

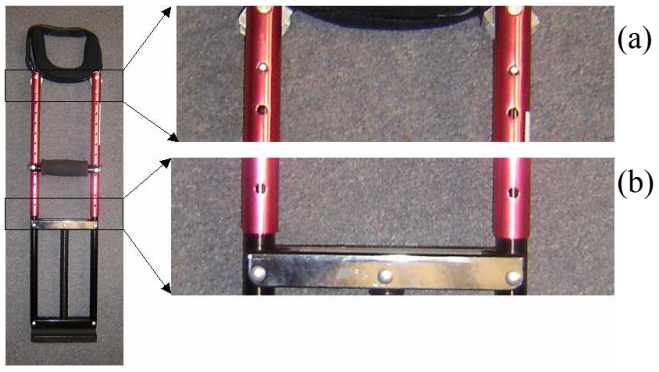

Figure 3.2: Close up of the height adjustment mechanism of the mini-Strutter. A pushpin supports the height adjustment tube (a). The height adjustment tube with the long lower tube inside (b).

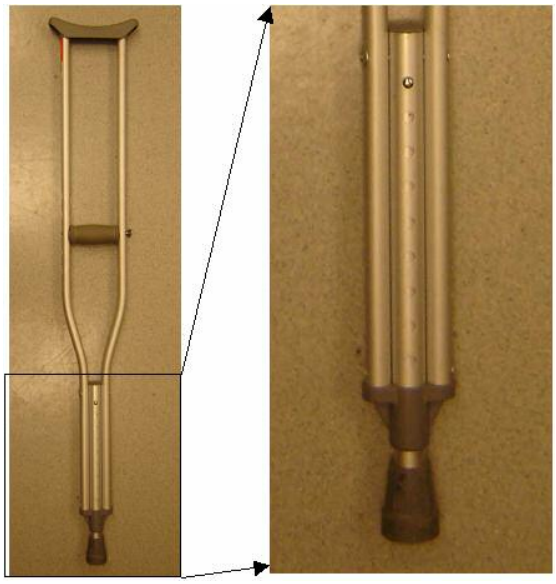

Figure 3.3: Close-up of the height adjustment mechanism of an axillary crutch.

It is likely that the Strutter or mini-Strutter will experience axial, bending, torsion loads or any combination of the three during normal use. The types of fracture morphology caused by these loads are examined, as well as the direction of the crack. The crack direction distinguishes bending from torsion-induced fracture. Buckling and torsion experiments characterize the fracture morphology under these types of loadings. Then when confronted with a tube fractured in use, the type of load that caused a crack can be deduced by comparing the tube fractured in use with the morphology obtained in the experiment. These experiments lay the foundation for forensic investigations into the type of loading that caused an observed fracture crack.

3.1 Combined Loading Procedure

A fixture is used with an Instron compression tester to apply a combined axial and bending load on a vertical support tube of the mini-Strutter comparable to that induced in the support tubes by a vertical load on the axillary support as shown in Figure 3.4.

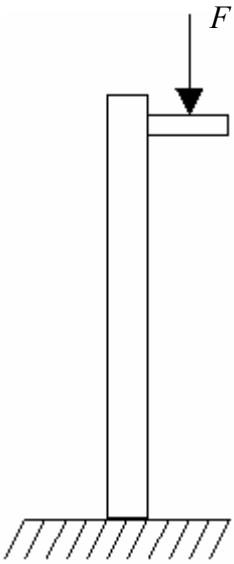

Figure 3.4: Diagram of the mini-Strutter vertical support tube during testing. The load, *F* is the load due to the weight of the user.

The outer support tube is 15.5 inches long and has 12 holes that are used for height adjustment and one hole for a pin that the shoulder support is cantilevered on. The tubes have an outer diameter of 0.875 inches and an inner diameter of 0.765 inches.

The fixture is made of 6061-aluminum. The fixture consists of two portions, the top and bottom as labeled in Figure 3.5 and the top is shown individually in Figure 3.6 and the bottom in Figure 3.7. The force transducer is connected to a computer via a serial cable.

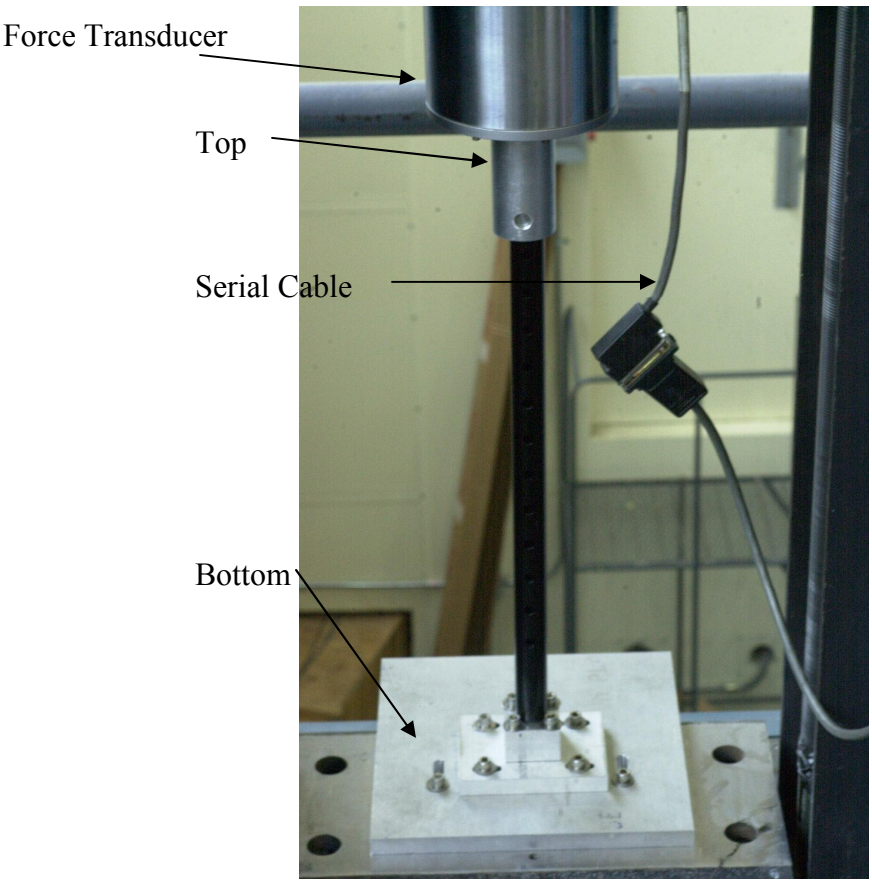

Figure 3.5: Instron compression tester with aluminum fixture for bending the vertical support tube of the mini-Strutter.

The top portion of the testing fixture is a 1.5 inch diameter aluminum rod that is 3 inches long that is threaded onto the force transducer. There is a 3/8 inch diameter hole through the diameter of the rod to accept a horizontal pin (Figure 3.6). The horizontal pin represents the pin that the axillary support of the Strutter is cantilevered on.

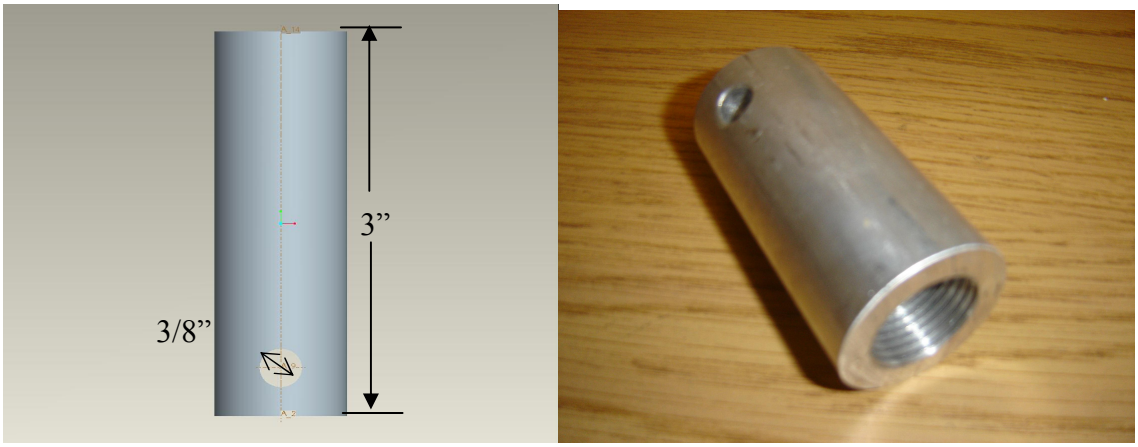

(a) (b)

Figure 3.6: Cad drawing (a) and photo (b) of the top portion of the testing fixture.

The bottom portion of the fixture consists of 4 pieces of aluminum, which are held in place using ¼”-20 screws (Figure 3.7). The three vertical slots in the fixture (Figure 3.7) allow the specimen to move 1.25 inches forward from center. The four horizontal slots allow for minor variations in dimensions of the vertical support tubes.

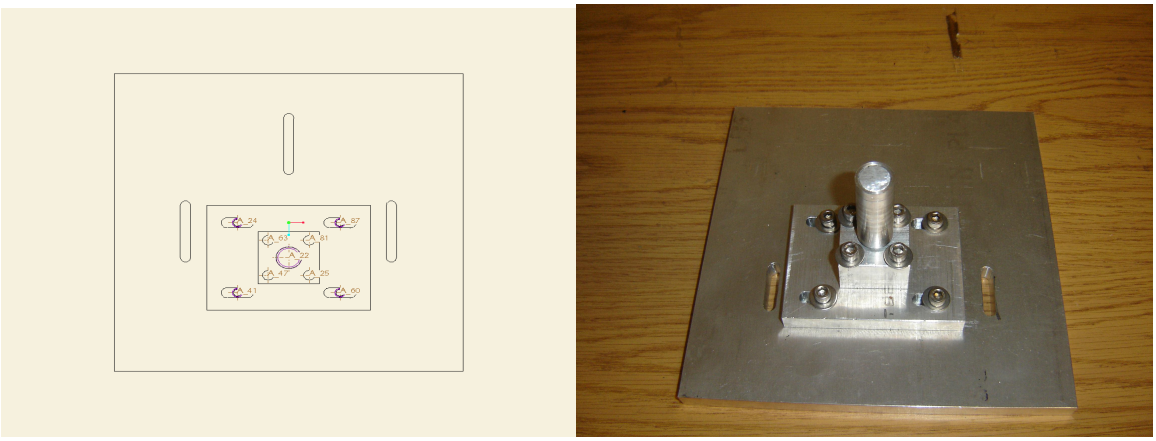

(a) (b)

Figure 3.7: Cad drawing (a) and photo (b) of the bottom portion of the testing fixture.

A 3/8 inch diameter aluminum rod is inserted into the specimen (Figure 3.8) that connects the tube to the top portion of the fixture (Figure 3.6).

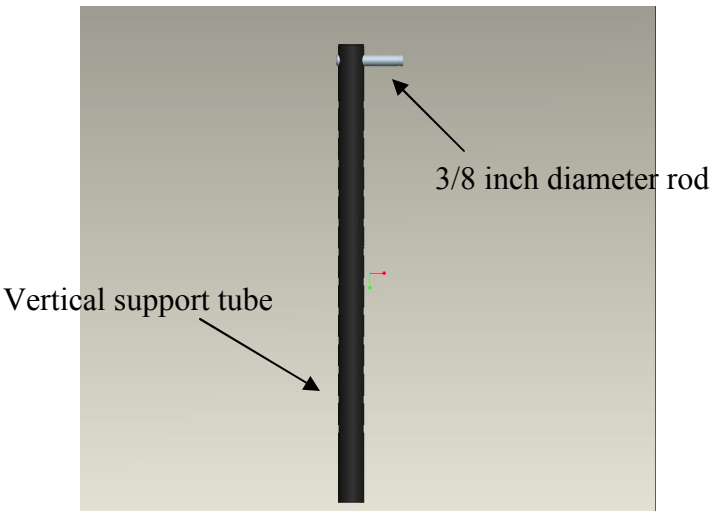

Figure 3.8: Side view of the vertical support tube with the 3/8 inch rod in the top.

The Instron is a deformation-controlled tester. The test specimen is compressed until it fractures or until a maximum compressive force of 5,000 lbs is reached. The force applied to the 3/8 inch rod was recorded at a rate of 1 sample per second.

3.2 Results

Three tests were performed on 6063-T832 aluminum tubes with holes similar to the vertical support tubes of the mini-Strutter. Two tests were at a rate of 0.1 cm/min (Figure 3.9 and Figure 3.10) and one at a rate of 0.5 cm/min (Figure 3.11). The maximum force reached in the tests before the specimens buckled was 2,215.7lbs, 2,664.2 lbs, and 2,143.3 lbs respectively.

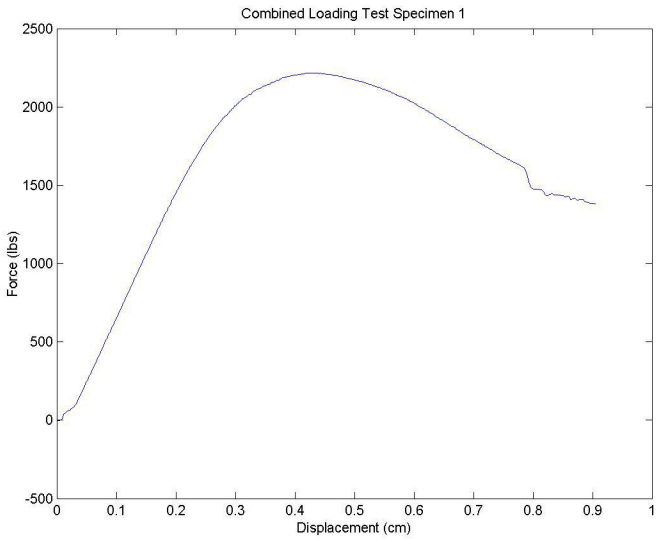

Figure 3.9: Force vs. displacement curve for a specimen with a deformation rate of 0.1 cm/min.

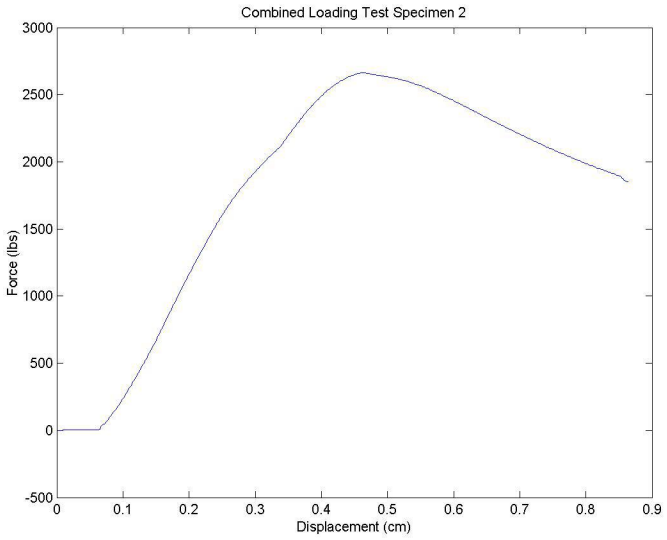

Figure 3.10: Force vs. displacement curve for test specimen 1 with a deformation rate of 0.1 cm/min.

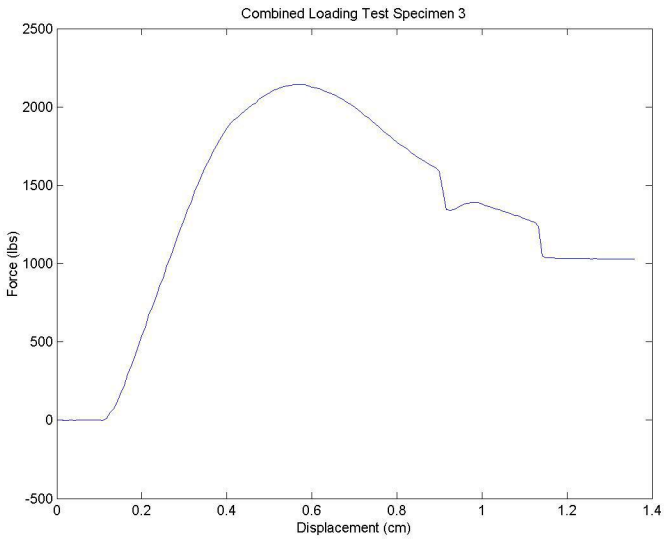

Figure 3.11: Force vs. displacement curve for a specimen with a deformation rate of 0.5 cm/min.

Test speimen 1 (Figure 3.9) and test specimen 2 (Figure 3.10) were stopped before the fracture occurred but the front side of the hole in the buckled region is deformed. A photograph of each specimen after testing is shown in Figure 3.12, Figure 3.13 and Figure 3.14. Test specimen 3 fractured on the side of the tube that was in tension, shown in Figure 3.15. The tube fractured around the third hole from the top 90 degrees from the vertical in the buckled region.

A significant amount of the powder coating chipped off around the third hole from the top of the vertical support tube in Figure 3.12 and Figure 3.14 forming a similar pattern on both vertical support tubes. On the side of the tube that was compressed, the tube buckled around a height adjustment hole and the powder coating chipped off forming lines radiating away from the hole above and below the buckled region. The vertical support tube in Figure 3.12 is not powder coated but painted, and none of the paint chipped off. The line pattern indicates the stress field as in classical brittle coating tests. A brittle coating cracks in response to the surface strain beneath it. Brittle coatings

crack at a predetermined value in a direction perpendicular to the principal tensile strain. Since the cracks in the powder coating occur only around the height adjustment holes, it is safe to say that the stress in that region is highest.

A possible source of error during testing comes from the 3/8 inch diameter aluminum rod (Figure 3.8) that is used to connect the vertical support tube to the top portion of the fixture (Figure 3.6). The rod is held in place in test specimen 3 because it is interference fit (Figure 3.14). The rod is not interference fit in the specimens 1 and 2, Figure 3.12 and Figure 3.13 respectively. Note that the test specimen 3 had observable cracks and buckling occurred at the lowest of the three loads at buckling. So an interference fit may slightly increase the risk of failure.

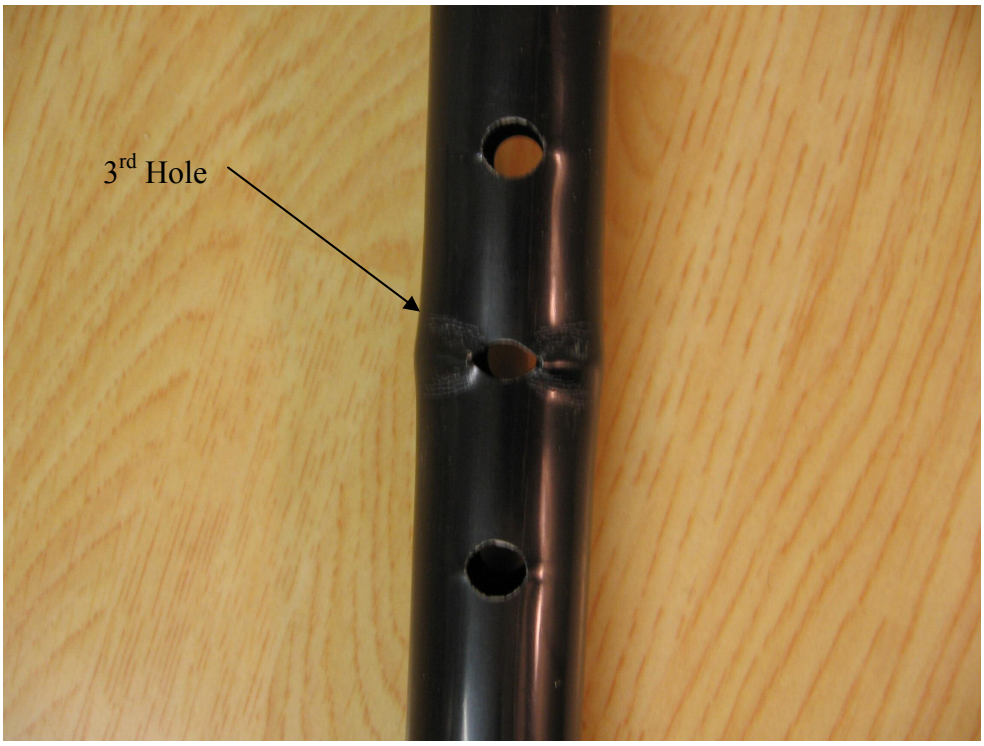

Figure 3.12: Backside of test specimen 1 (Figure 3.9) after testing, deformation is concentrated around the third hole from the top.

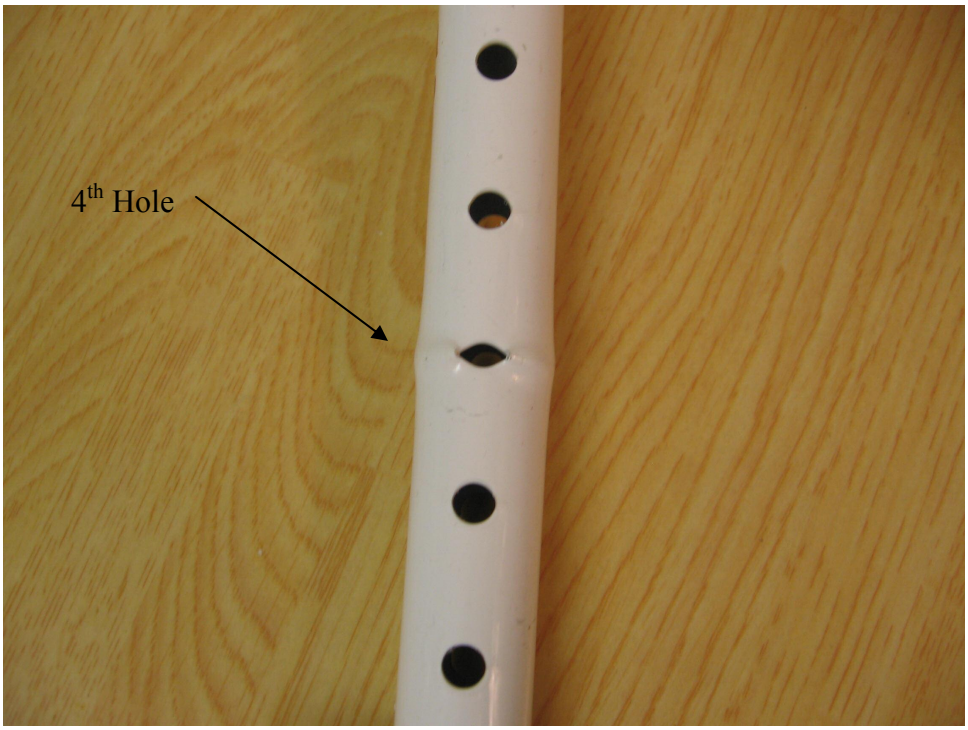

Figure 3.13: Backside of the test specimen 2 (Figure 3.10) after testing, plastic deformation is concentrated around the fourth hole from the top.

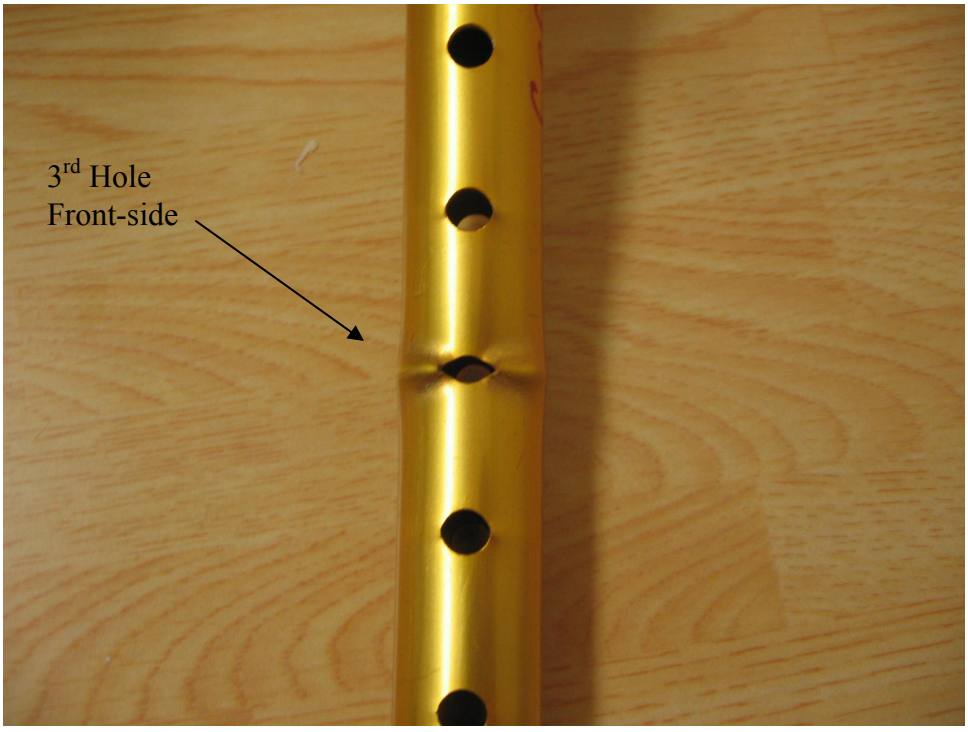

Figure 3.14: Backside of test specimen 3 (Figure 3.11) after testing, plastic deformation is concentrated around the third hole from the top.

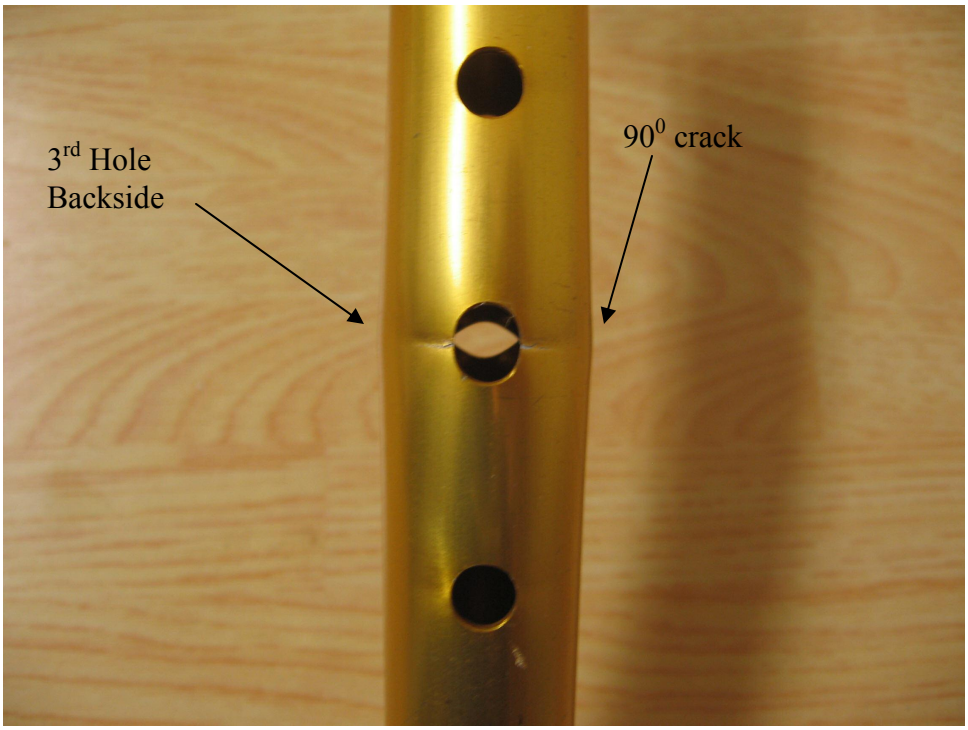

Figure 3.15: Close up of the fracture around the third hole from the top of the front side of test specimen 3 (Figure 3.11).

3.3 Torsion Test Procedure

The cantilever that the axillary support of the Strutter rests on may apply a torque to the vertical support tubes when acted on by the user. Torsion tests were performed on a Tinius Olsen torsion tester. The Tinius Olsen machine has two chucks that face one another (Figure 3.16). One of the chucks is static (does not rotate) and the other turns at a user prescribed rate.

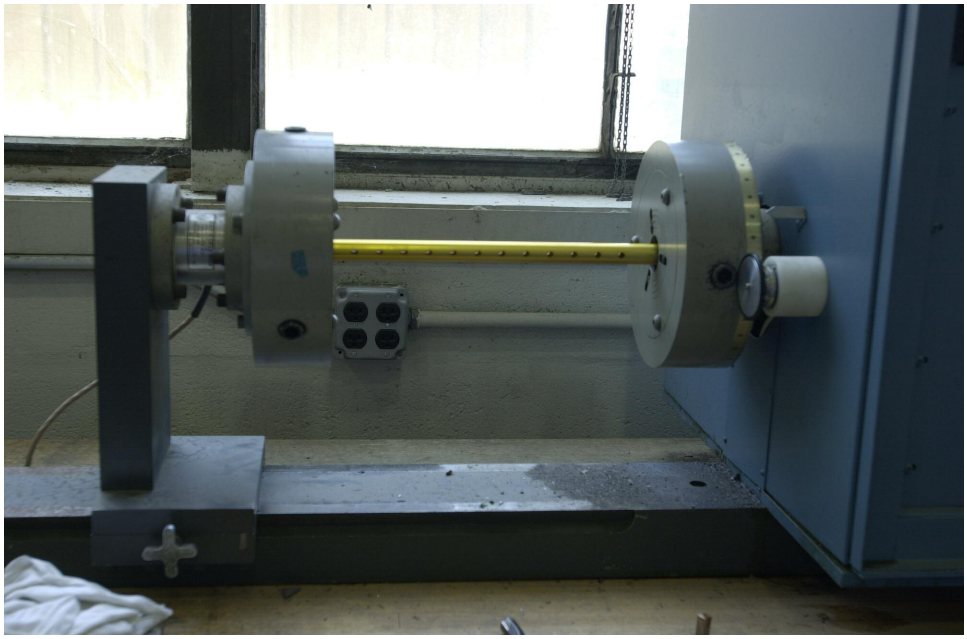

Figure 3.16: Photo of the chucks of the Tinius Olsen machine. The static chuck is on the left.

A solid aluminum plug is placed in the side of the vertical support tube that does not have a hole for the rod that the shoulder support is cantilevered on. The plug extends one inch into the tube to prevent the chuck of the torsion tester from crushing it. The side of the vertical support tube with the hole for the rod that the shoulder support is cantilevered on has a plug in it from the factory. The plug reinforces that side of the tube and does not require further reinforcement.

The side of the vertical support tube with the hole for the rod that the shoulder support is cantilevered on is clamped in the chuck that rotates (the chuck on the right in Figure 3.16). The other side of the vertical support tube is clamped in the static chuck. The maximum torque is set to 1,000 in-lbs, the torque readout is zeroed and a rate between 5-360 degrees/min is selected. The computer records the torque and angle of the tube until fracture when the test stops. The layout of the Tinius Olsen is shown in Figure 3.17.

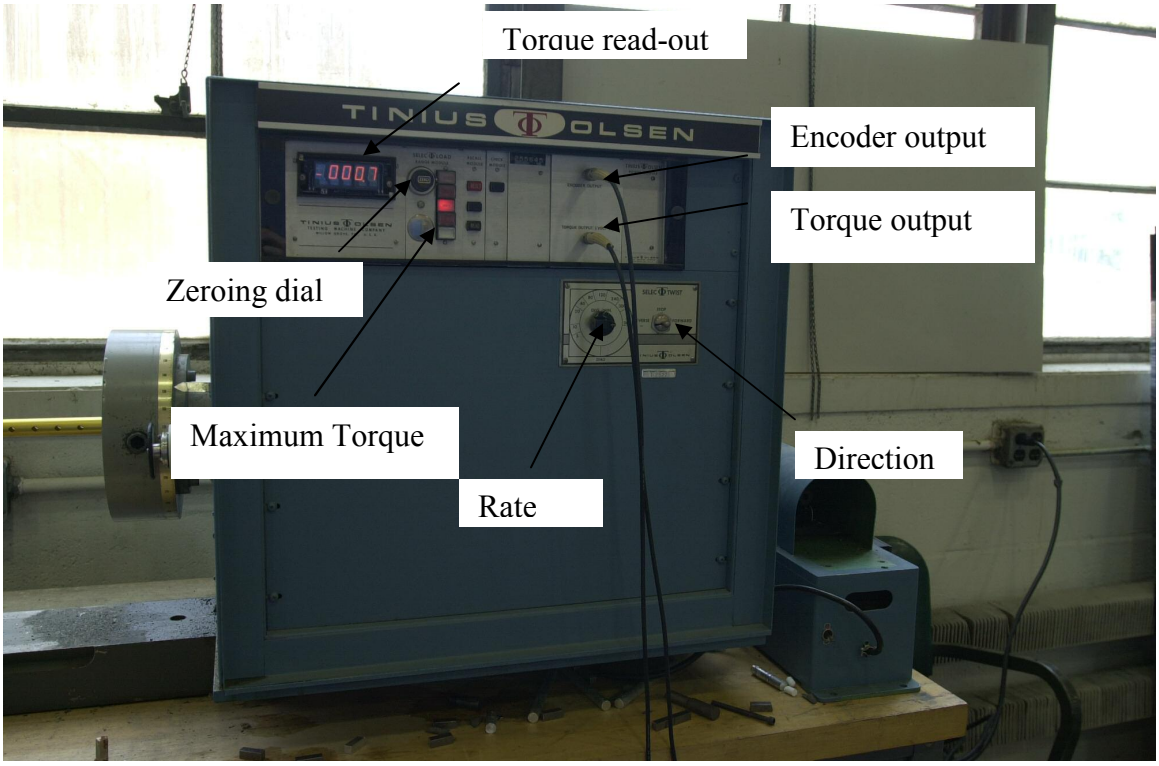

Figure 3.17: The front of the Tinius Olsen machine.

3.4 Results

The test is performed in deformation control. Torque vs. angle graphs for three tests with twist rates of 360 degrees/min, 200 degrees/min, 80 degrees/min are shown in Figure 3.18, Figure 3.19 and Figure 3.20 respectively. The test specimens are vertical 6063-T832 aluminum tubes with holes similar to those of the mini-Strutter. The distance between the chucks during testing is 13.25 inches, 13.25 inches and 13 inches, respectively. The torque at fracture is 645.3 in-lbs, 598.3 in-lbs, and 602.2 in-lbs and the angle at fracture is 1.155 radians, 1.022, and 1.240 radians respectively.

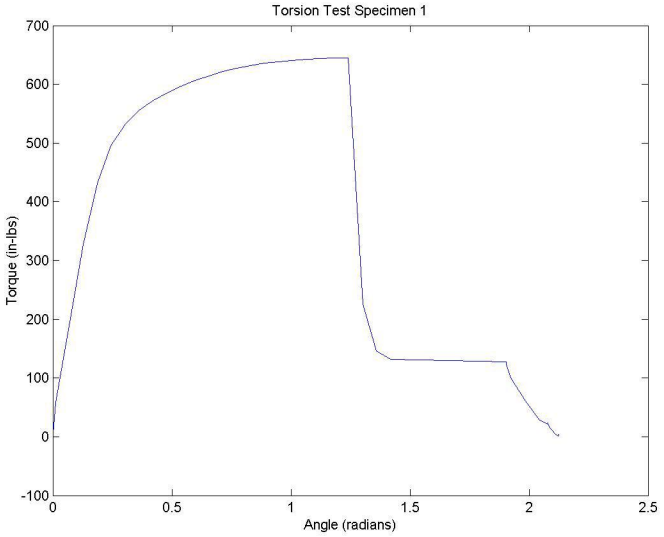

Figure 3.18: Torque vs. angle graph for test specimen 1 with a rate of 360 degrees/min. The tube fractured at 645.3in-lbs. Yielding begins at approximately 400 in-lbs.

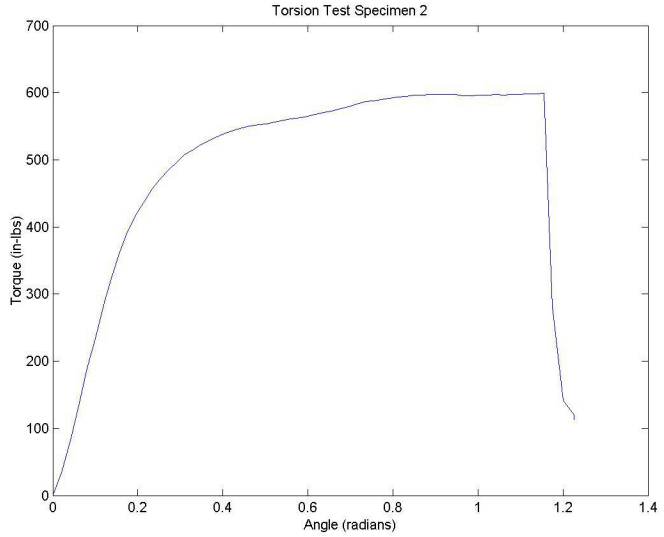

Figure 3.19: Torque vs. angle graph for test specimen 2 with a rate of 200 degrees/min. The tube fractured at 598.9 in-lbs. Yielding begins at approximately 400 in-lbs.

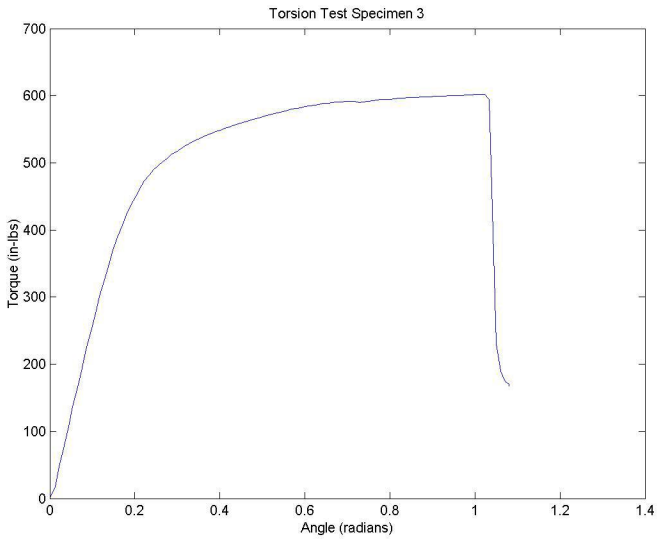

Figure 3.20: Torque vs. angle graph for test specimen 3 with a rate of 80 degrees/min. The tube fractured at 602.2 in-lbs. Yielding begins at approximately 400 in-lbs.

The three vertical support tubes fractured on the inner surface, at the 6th adjustment hole from the top in Figure 3.21, the 5th adjustment hole from the top in Figure 3.22, and the top adjustment hole in Figure 3.23. The fractures occur around height adjustment holes at angle 45 degrees relative to the vertical axis of the tubes. The fracture surface is at an angle 45 degrees from the plane perpendicular to the surface of the tube.

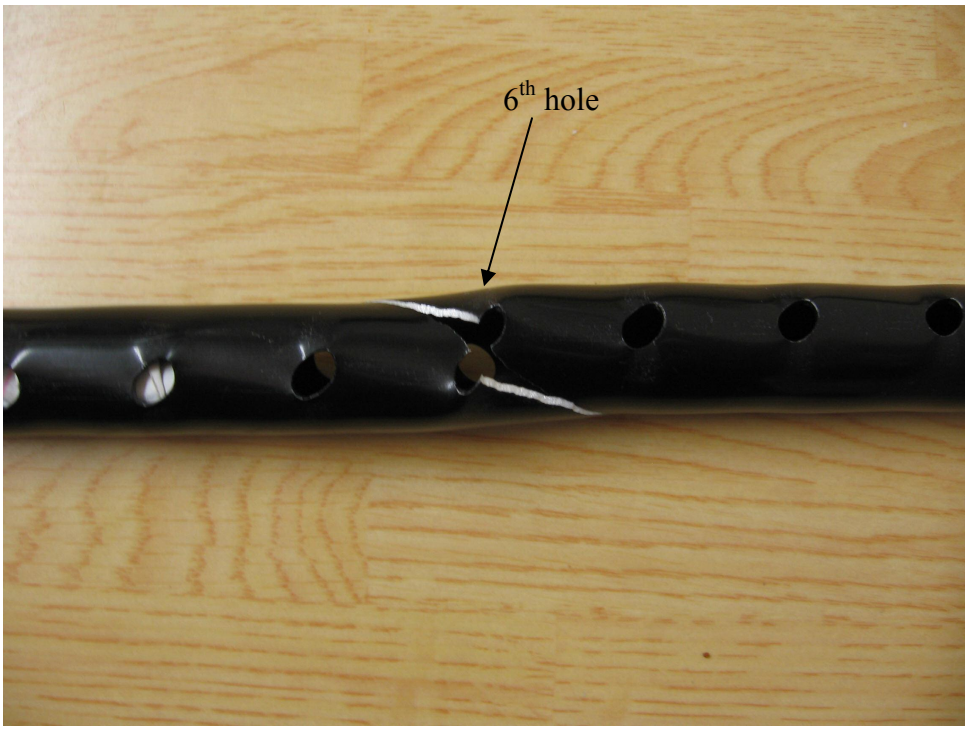

Figure 3.21: Fracture surface of test specimen 1 (Figure 3.18), fractured at 360 degrees/min.

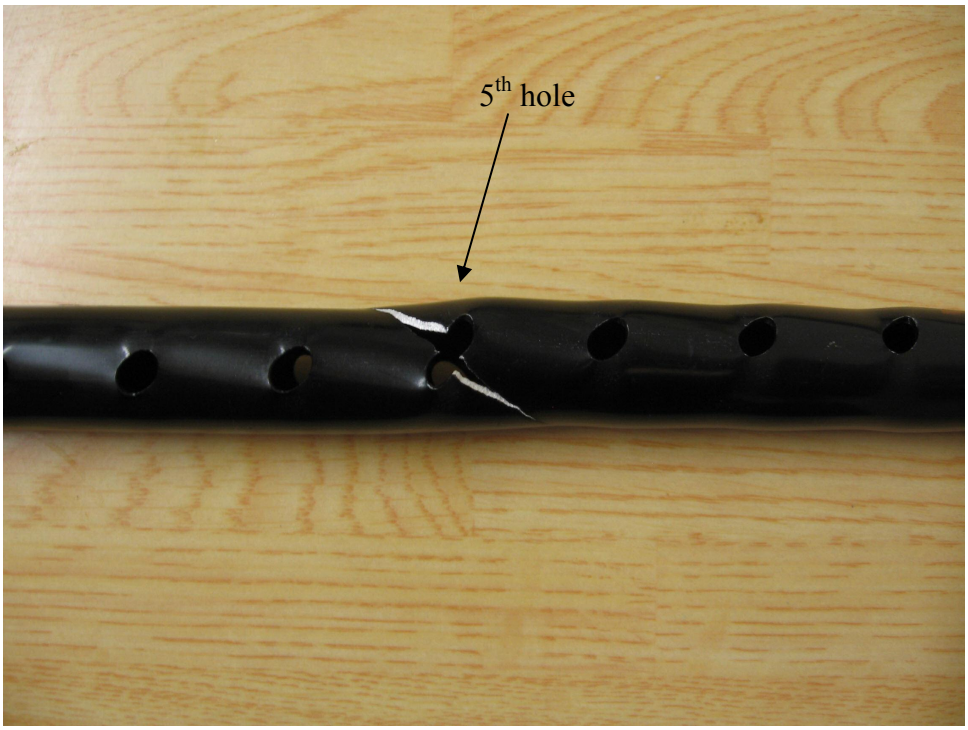

Figure 3.22: Fracture surface of test specimen 2 (Figure 3.19), fractured at 200 degrees/min.

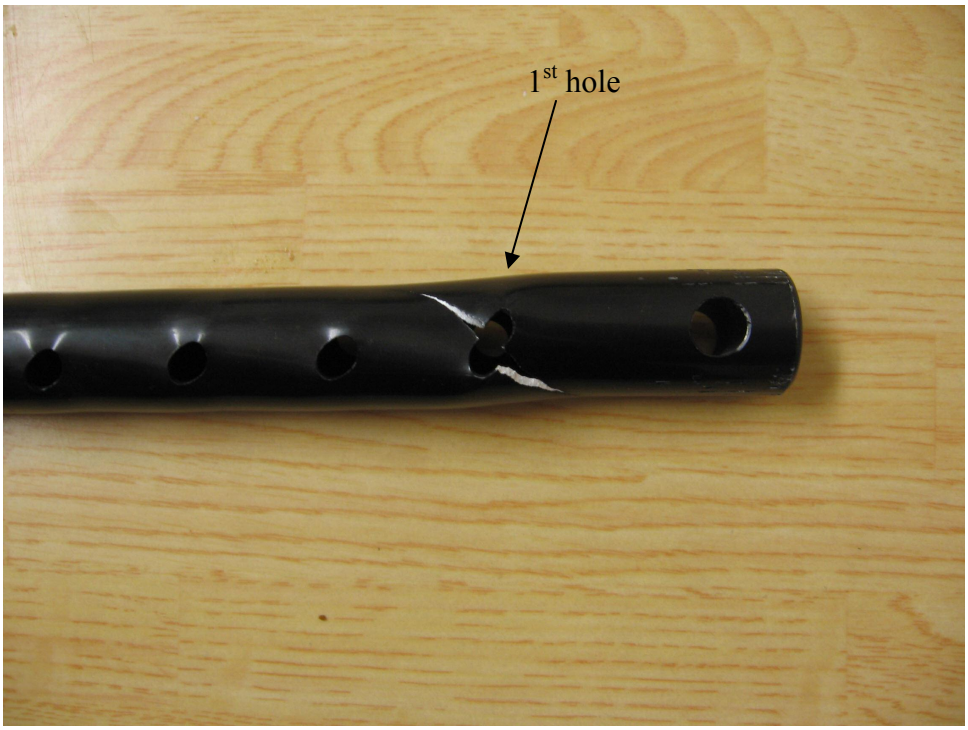

Figure 3.23: Fracture surface of test specimen 3 (Figure 3.20), fractured at 80 degrees/min.

3.5 FEM Analysis

Three loadings; axial, combined axial-bending and torsion of aluminum tubes with holes are examined using finite element method (FEM). The FEM is performed using Pro/Mechanica in conjunction with a vertical support tube modeled in Pro/Engineer Wildfire v1.0. FEM analysis is also used to explain the observed cracks in both the axial-bending tests and the torsion tests. The hypothesis is that the cracks start where the stresses are the highest. When the shoulder support of a conventional crutch is loaded by the user's weight, the support tubes are stressed axially. However, if the axillary support is cantilevered on the vertical supports then the same load will cause the vertical members to be in state of combined loading, compression and bending. The combined loading is larger than the pure compression. To see how much, the compressive stress is

first calculated for a pure axial load and then compared to a bending load. An aluminum tube without adjustment holes with outer diameter (OD) 0.875 inch and inner diameter (ID) 0.765 inch with a 100 lb compressive force has a stress of 706 psi given by

$$\sigma_y = \frac{F}{A}. \tag{3.1}$$

6063-T832 aluminum a suitable material for crutch tubes has a yield stress of 39,000 psi. An aluminum tube similar to one used in the Strutter with 12 adjustment holes has stresses that are much greater than the same aluminum tube without adjustment holes when loaded axially. FEM predicts that an aluminum tube with 12 adjustment holes loaded axially has a maximum Mises stress of 2,300 psi near the holes when a 100 lb compressive force is applied to the top surface and the bottom surface is fixed (Figure 3.24). The Mises stress is defined as,

$$2\sigma_M^2 = (\sigma_x - \sigma_y)^2 + (\sigma_x - \sigma_z)^2 + (\sigma_y - \sigma_z)^2 + 6(\tau_{xy}^2 + \tau_{xz}^2 + \tau_{yz}^2). \tag{3.2}$$

From eqn 3.2, when loaded with only an axial load, σ_x, the Mises stress is equal to the axial stress. Using the equation for the stress concentration factor (Haslach and Armstrong 2004)

$$K_\sigma = \frac{\sigma_{\max}}{\sigma_{ave}}, \tag{3.3}$$

with 706 psi from eqn 3.1 as the average stress and an FEM predicted maximum of 2,300 psi around the adjustment holes (Figure 3.24), the tube has a stress concentration factor of 3.3 at the height adjustment hole when loaded axially.

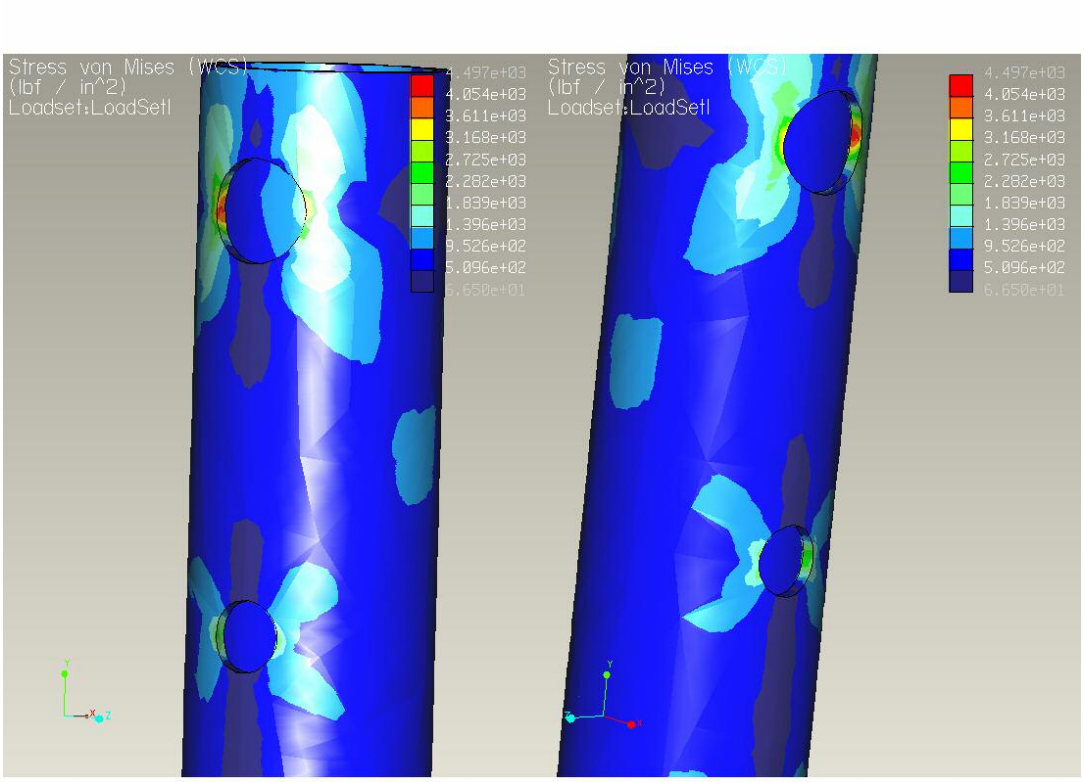

(a) (b)

Figure 3.24: Mini-Strutter vertical support tube with a 100lb load on the top surface shown from the font (a) and the back (b). The top hole is for a 3/8 inch aluminum rod that the shoulder support is cantilevered on.

When the shoulder support or handgrip of the Strutter is loaded in only the downward direction, the support tubes are stressed axially and in bending because the handgrip and axillary support is cantilevered. The stress equation for a tube with circular cross-section in combined bending and axial loading is given by

$$\sigma_y = \frac{F}{A} + \frac{My}{I}. \tag{3.4}$$

Assume $F = 100$ lb in Figure 3.25, the axial stress is 4,580 psi where $y = 3/16$ and the area moment of inertia, $I = 0.012$ in^4 (Figure 3.25). When the vertical support tube without holes is loaded axially and in bending, the stress is 6.5 times greater than when the vertical support tube is only loaded axially.

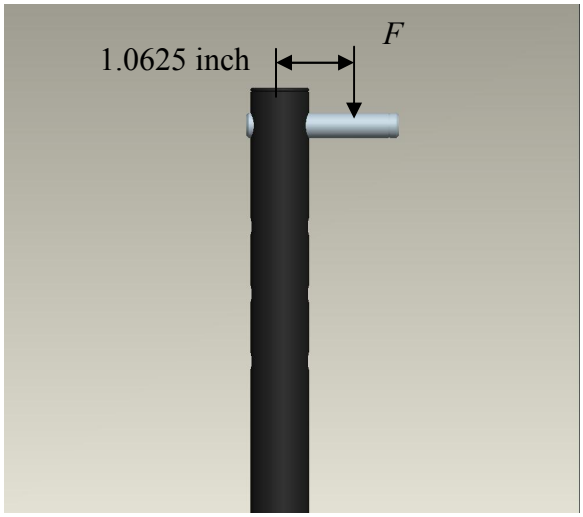

Figure 3.25: Diagram of the vertical support tube in combined axial and bending.

A vertical support tube with 12 adjustment holes, loaded axially and in bending, has a maximum Mises stress of 15,130 psi by FEM when $F = 100$ lb and the bottom surface is fixed (Figure 3.26). From eqn 3.2, the Mises stress is equal to the axial stress. Using 4,580 psi as the average stress and an FEM predicted maximum of 15,130 psi, the tube has an FEM predicted stress concentration factor of 3.3 at the height adjustment hole when loaded axially and in bending. The stress of a combined axial-bending load is 6.5 times larger than a pure axial load. The magnification factor around the holes in the aluminum tubes is 3.3 for both axial and axial-bending. Clearly eliminating the holes, the potential for combined loadings or both reduces the stress excursions experienced by the tubes which increases the useful lifetime of the tubes.

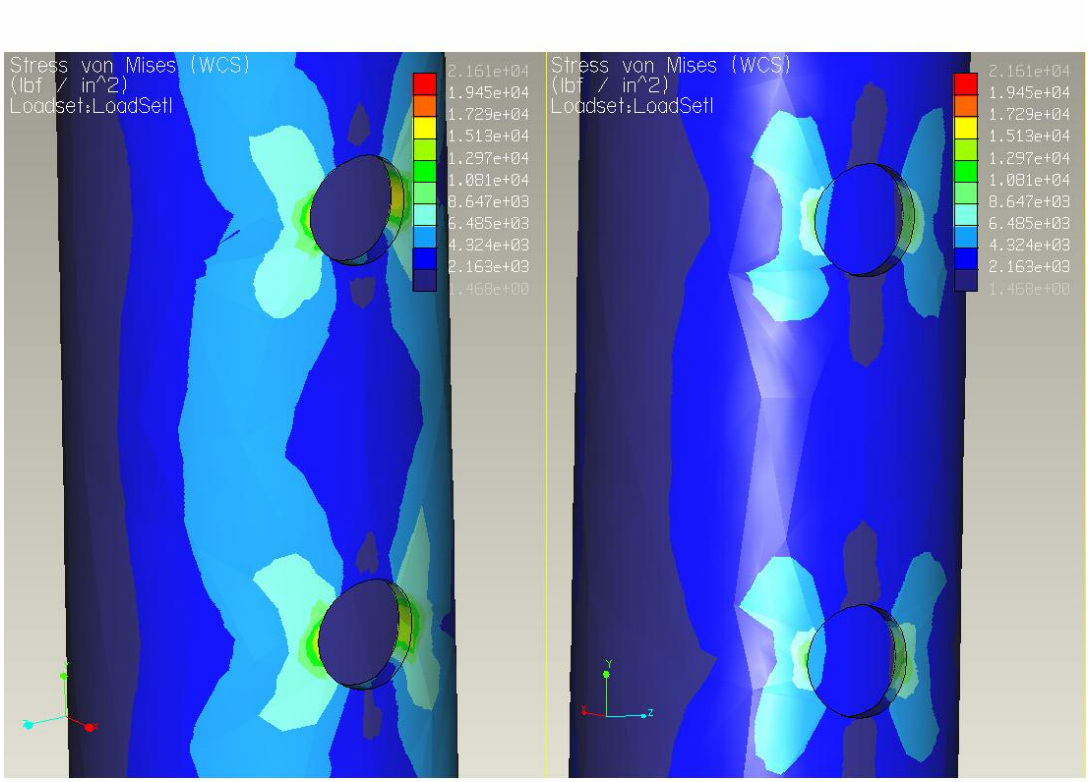

(a) (b)

Figure 3.26: Mini-Strutter vertical support tube with a 100lb moment on the top surface with a moment arm of 1.0625 inches shown from the front (a) and the back (b).

Loading the shoulder support or handgrip of the mini-Strutter in only the forward direction results in a torsion load. Assuming that 106.25 in-lb torque is exerted on the top of an aluminum tube without holes gives a stress of 1,945 psi with $c = 7/16$ in. and the polar area moment of inertia, $J = 0.0239$ in^4, using the stress equation for a member with a circular cross-section in torsion given by

$$\tau_{\max} = \frac{Tc}{J}. \tag{3.5}$$

The same aluminum tube with 12 adjustment holes, loaded in torsion, has a maximum Mises stress of 14,280 psi by FEM when a 106.26 in-lb torque is applied to the top of the tube and the bottom surface is fixed (Figure 3.24). Solving eqn 3.2 gives a

shear stress of 8,245 psi. The tube has a shear strength of 27,000 psi. Using 1,945 psi as the average stress and an FEM predicted shear stress of 8,245 psi around the adjustment holes, the tube has a stress concentration factor of 4.2 at the height adjustment hole when in torsion using eqn 3.3.

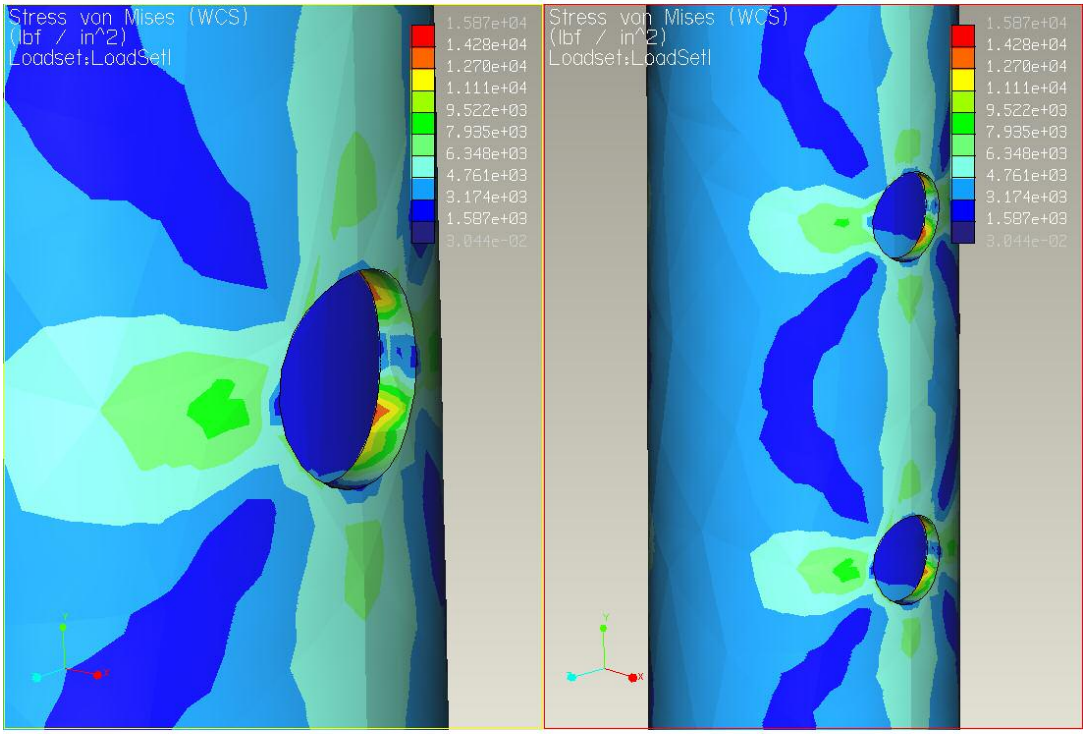

(a) (b)

Figure 3.27: Mini-Strutter vertical support tube with a 100lb torque on the surface of the top hole with a moment arm of 1.0625 inches shown from the front (a) and the back (b).

Figure 3.24 and Figure 3.26 show that the likely location for fracture of an aluminum tube with adjustment holes loaded axially or in bending is on the inner surface of the holes 90 degrees from the vertical where the highest normal stress is predicted. Figure 3.27 shows the likely location for fracture when loaded in torsion is on the inner surface of the holes 45 degrees from the vertical where the highest shear stress is predicted.

3.6 Discussion

Three combined loading (axial and bending) tests show that aluminum vertical support tubes with height adjustment holes support a maximum force of approximately 2,200 lbs before buckling. At fracture, cracks initiate around height adjustment holes at 90 degrees from the vertical axis of the tube. Cracks in the powder coating were observed. The cracks originate at the holes, 90 degrees from the vertical, which indicates higher stresses at the holes since the powder coating is not chipped in other places. FEM predicts the highest stresses for a tube with height adjustment holes at the holes, 90 degrees from the vertical under bending.

Three torsion tests show yielding occurs at approximately 400 in-lbs and fracture at approximately 600 in-lbs. At fracture, cracks initiate around the height adjustment holes in the tube 45 degrees from the vertical axis of the tube. There were no cracks in the powder coating observable under torsion. FEM predicts the highest stress at the holes at 45 degrees from the vertical axis of the tube under torsion.

If a user initiates cracks in the adjustment holes at some point during use, the stress required to increase the crack length may be less than the stress required to initiate a crack. If the cracks are 45 degrees from the vertical, a torque is responsible for the crack. If the cracks are 90 degrees from the vertical, a combined bending and axial load is responsible for the crack. A tube with a combined bending and axial load has stresses as much as 6.5 times as great as a tube with only an axial load if both tubes do not have height adjustment holes.

It is possible that a failure could occur from fatigue, FEM predicts stresses as high as 15,000 psi around the height adjustment holes for a static load of 100 lbs. An impulse

load could cause stresses up to three times as great in magnitude compared to static loads. The cantilevered shoulder support on the commercial mini-Strutter increases the likelihood of fatigue failure from combined loadings where stresses can be as high as 6.5 times greater than an axial load. The stresses in the vertical support tubes of the Strutter can be reduced by 6.5 times simply by putting the shoulder support and handgrip in the same plane as the vertical support tubes. Eliminating height adjustment holes and fitting each orthosis for the height of the user reduces the stress in the vertical support tubes by at least 3 times.

4 Behavior of a User Applied Force on the Axillary Support of the Strutter and Crutches

Bearing weight through the shoulder support of an axillary crutch is not recommended because such loadings may cause axillary nerve damage in the underarm. The manufacturer of the Strutter has made the axillary support different from a traditional crutch in an attempt to make it safe to load the axillary support with the user's weight. There are no guidelines for designing an axillary support that will not cause axillary nerve damage when supporting the user's weight. For the manufacturer to have succeeded, the Strutter should support the user's weight in a different manner than axillary crutches. In this study, the force and contact area between the axillary support and the underarm as well as the perceived comfort are measured in an effort to find a relationship between perceived comfort and loads in the normal direction at the axillary support/underarm interface.

4.1 Experimental Setup

The Fscan pressure sensor system (sensor #9811) by Tekscan, Inc, Boston MA is a thin compliant polyester sheet (Figure 4.1) with electrodes deposited in rows and columns in the middle of the sheet. There is resistive ink in between the rows and columns in the middle of the sensor. The pressure is correlated with changes in the resistance of the ink. The Fscan pressure sensor measures forces that are normal to the surface of the polyester sheet.

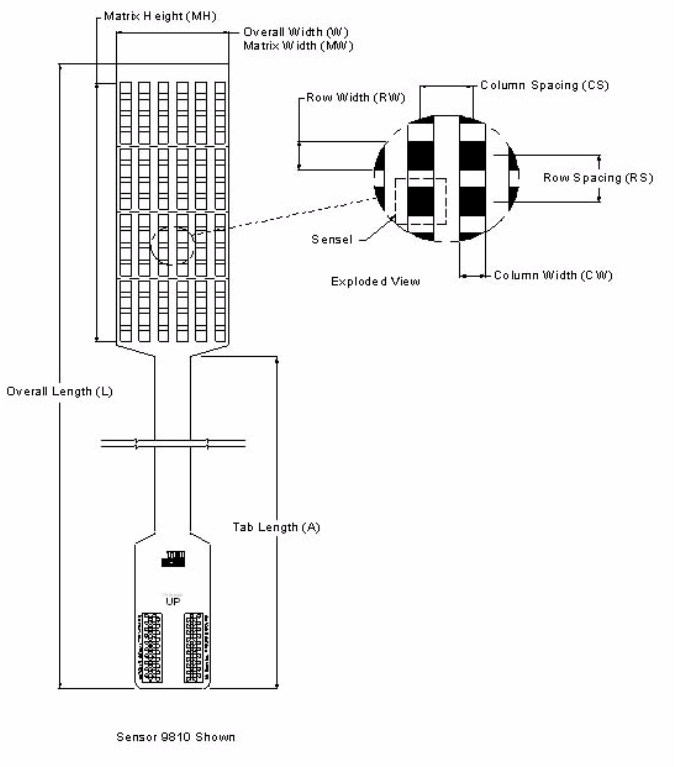

	General Dimensions			Sensing Region Dimensions								Summary	
	Overall	Overall	Tab	Matrix	Matrix								
Type	Length	Width	Length	Width	Height	Columns			Rows			No. of	Sensel
	L	*W*	*A*	*MW*	*MH*	*CW*	*CS*	*Qty.*	*RW*	*RS*	*Qty.*	Sensels	Density
US	(in)	(in)	(in)	(in)	(in)	(in)	(in)		(in)	(in)			(sensel per sq-in)
9811	24.5	3	15.5	3	8	0.25	0.50	6	0.31	0.5	16	96	4
Metric	(mm)	(mm)	(mm)	(mm)	(mm)	(mm)	(mm)		(mm)	(mm)			(sensel per sq-cm)
9811	622	76	394	76	203	6.35	12.7	6	7.87	12.7	16	96	0.62

Figure 4.1: Diagram of the Fscan pressure sensor and data sheet taken (tekscan.com, 2006).

A sensor is affixed to the axillary pad of an axillary crutch using double-sided tape (Figure 4.2). Notice that there are six columns of sensors. The two sensor columns in the middle are on top of the axillary support and the next two outermost sensor columns are in between the top and side. The next two outermost sensor columns are on the side of the axillary support.

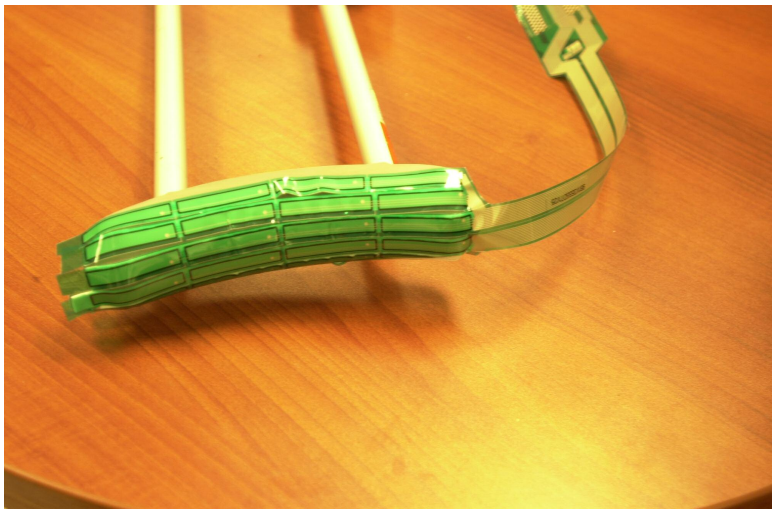

Figure 4.2: Axillary crutch pad with an Fscan pressure sensor taped to the cushion.

The intermediary between the sensor and the computer is called a handle (Figure 4.3). A cloth is wrapped around the vertical support of the crutch and the handle is connected to the cloth with Velcro.

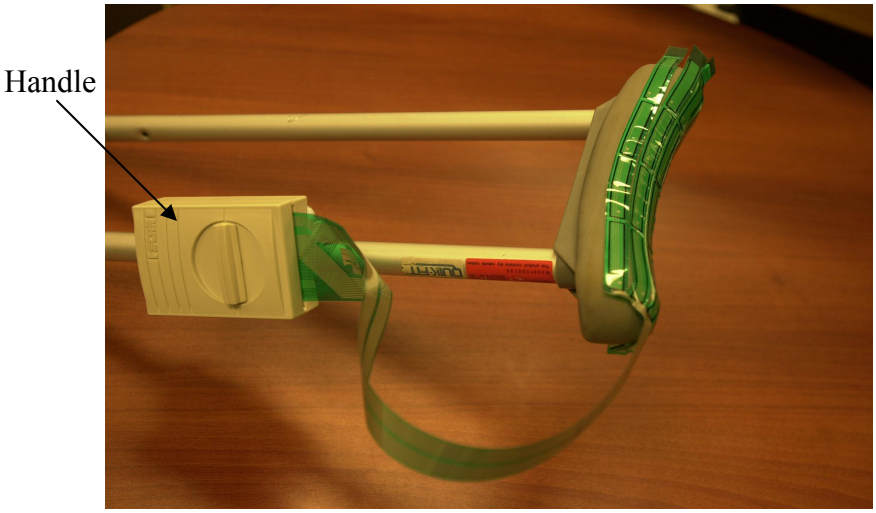

Figure 4.3: Axillary crutch with an Fscan sensor connected to the handle.

An Fscan sensor is affixed to the axillary pad on the Strutter (Figure 4.4). The axillary pad of the Strutter is made of polyethylene foam and rests on top of a rigid metal support. The axillary support has the middle two sensors on top and the outermost two

sensors on the side like the axillary crutch. The support and the pad are covered with a fabric cloth during use (Figure 4.4). Note that the sensor is wrinkled, this occurs during testing and the effect of which is discussed later. The pressure sensor is connected to a computer via a handle. The handle is secured to the vertical support member in a similar fashion as the axillary crutch using Velcro and a cloth wrap (Figure 4.5).

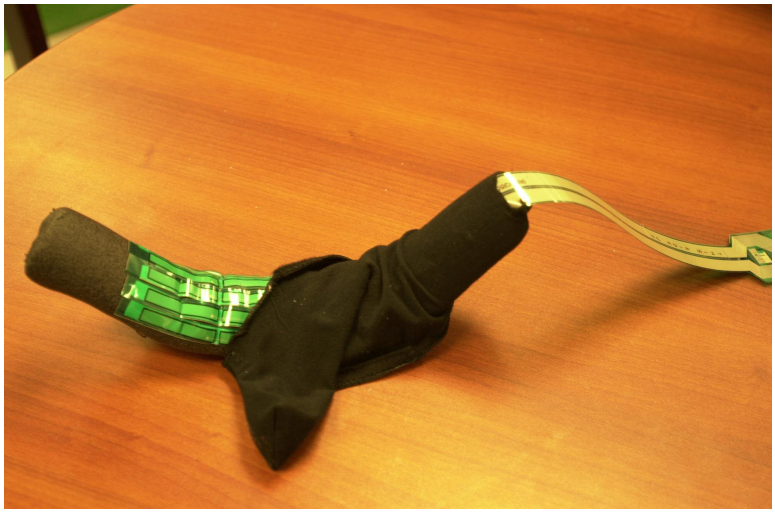

Figure 4.4: Strutter axillary support cushion with an Fscan pressure sensor attached.

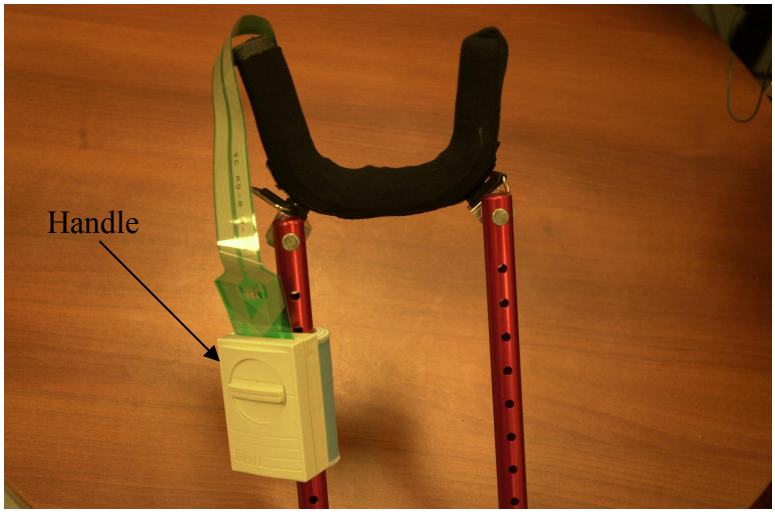

Figure 4.5: Strutter with the Fscan pressure sensor mounted.

The Fscan sensor measures pressure in the direction normal to the sensor only. Due to the shape of the axillary supports of the Strutter and axillary crutches, the normal force may not directly relate to weight bearing. The normal force is the socket pressure at the interface of the underarm and axillary support. To minimize the effect of twisting or snagging, the sensor is covered with a cotton fabric on the Strutter (by coincidence of design) and with subject's cotton t-shirts on axillary crutches (by coincidence of use). The low coefficient of friction between the sensor and cotton fabric helps reduce experimental error by reducing strain in the resistive ink in directions other than normal.

4.2 Experimental Procedure

Eight subjects between the ages of 21 and 25 were tested. The subjects were able-bodied college aged students with no history of shoulder trouble. The subject characteristics are shown in Table 4.1.

Subject	Sex	Age (yrs.)	Height (in.)	Weight (lbs.)	Handedness
1	M	25	70.5	165	R
2	M	22	71.25	161	R
3	M	25	72.25	196	R
4	M	21	67.25	188	R
5	F	22	64.75	132	R
6	F	21	64.5	142	R
7	F	24	65	121	R
8	F	22	67.5	202	R
Mean	-	22.75	67.5	163.38	-
Variance.	-	1.56	9.63	915.41	-

Table 4.1: Subject characteristics.

When using an orthosis with an axillary support, the user can support themselves through the handgrip and/or axillary support, which causes reaction forces at the hand and underarm. Some users may use the axillary support more than the handgrip. It is

already acceptable to do all the weight bearing through the hands as with axillary crutches and forearm crutches. The other cases of interest are a combination of hand and axillary support and axillary support.

The two strides considered in this experiment are 2-point swing-through gait using hand support and 2-point swing through without hand support. When subjects use a 2-point swing through without hand support, all of the forcing exerted on the othosis by the user goes through the axillary support. When using a 2-point swing through the underarm of the user can experience greater loads than in a 2-point swing through with hand support. In any 2-point swing through with hand support, the hands tend to support some of the weight of the body. The subjects perform one stride of each gait three times using each assistive device using a self-selected weight bearing and cadence. The subjects were NOT instructed to refrain from weight bearing through the axillary pad of either the Strutter or axillary crutches.

In a 2-point swing through with hand support, the subject advances both assistive devices to a comfortable distance in front of them, then supporting the weight of their body on the axillary support and handgrip of the device, the subject lifts both of their feet and swings them past the assistive devices (mid-stance). When the subject's feet come in contact with the ground, the subject comes to a complete stop and ceases weight bearing on the axillary support and handgrip. In a 2-point swing through without hand support the subject performs the stride as before except without supporting any weight on the handgrips.

A matched-pair test is used to analyze the data collected from the experiments with human subjects. A matched-pair test is a little different than a comparison of the means

between two populations. In a comparison of the means test, the mean of two populations is calculated

$$\mu_k = \frac{1}{n}\sum_{i=1}^{n} x_{ki} \quad k = 1,2 \tag{4.1}$$

where n is the size of the sample population, k is the sample population (control or experimental). The sample variance, s is calculated as follows,

$$s_k^2 = \frac{1}{n-1}\sum_{i=1}^{n}\left(x_{ki} - \mu_k\right)^2 \quad k = 1,2\,. \tag{4.2}$$

A possible null hypothesis is that the difference of the population means is equal to zero or that population means are the same,

$$H_0 : \mu_1 - \mu_2 = 0\,. \tag{4.3}$$

To test the null hypothesis, the student t test statistic is calculated,

$$t = \frac{\left(\mu_1 - \mu_2\right)}{\sqrt{s_1^2/n_1 + s_2^2/n_2}} \tag{4.4}$$

and the null hypothesis is rejected depending on the p-value. The p-value is the probability, assuming the null hypothesis to be true, that the test statistic has a value whose disagreement with the null hypothesis is as great as or greater than that actually observed (Navidid, 2006). If the p-value is smaller than a predetermined value, we reject the null hypothesis and if the p-value is larger, we fail to reject the null hypothesis. A good rule of thumb is to use a p-value of 0.05. Failing to reject the null hypothesis means that the null hypothesis is plausible.

In a matched-pairs experiment, the mean difference,

$$\overline{D} = \frac{1}{n}\sum_{i=1}^{n}\left(x_{1i} - x_{2i}\right), \tag{4.5}$$

is calculated by averaging the pair differences. The null hypothesis is that the mean difference is equal to zero,

$$H_0 : \overline{D} = 0 \tag{4.6}$$

is tested using the student *t* test statistic. The *t* test statistic is calculated with

$$t = \frac{\overline{D}}{s_D / \sqrt{n}} \tag{4.7}$$

where s_D is the sample standard deviation and n is the number of paired samples. Looking up the test statistic in statistical tables gives a corresponding p-value. The p-value measures the plausibility of H_0, the smaller the p-value, the stronger the evidence is against H_0. If the p-value is sufficiently small, it may be a good idea to abandon the assumption that H_0 is true and reject the null hypothesis. It can be shown by substituting eqn 4.1 into eqn 4.5 that the mean difference is equivalent to,

$$\overline{D} = \frac{1}{n}\sum_{i=1}^{n}\left(x_{1i} - x_{2i}\right) = \mu_1 - \mu_2 . \tag{4.8}$$

The sample standard deviation is

$$s_D^2 = \frac{1}{n-1}\sum_{i=1}^{n}\left(x_{1i} - x_{2i} - \overline{D}\right)^2 , \tag{4.9}$$

substituting eqn 4.2 into eqn 4.9 the sample standard deviation is found to be equivalent to,

$$s_D^2 = s_1^2 + s_2^2 . \tag{4.10}$$

where μ_1, μ_2, s_1 and s_2 are the control and experimental means and variances respectively.

In an ideal matched-pairs experiment identical twins are used. One twin is used in the control groups and one in the experimental group. This eliminates variation between groups due to physiological differences. Due to the rarity of identical twins, this is rarely utilized in practice. So often times subjects may receive both the control and experimental procedure or are paired using a predetermined method based on parameters such as age, physical fitness, height or any combination of factors if it is not possible for them to receive both treatments. In the matched-pair experiment conducted on the Strutter and axillary crutch, each subject acts as his or her own control and uses both the Strutter and axillary crutches. The order of assistive devices and order of gait patterns is chosen at random to reduce confounding and personal bias towards one orthosis.

4.3 Results

The Fscan sensor records the distributed load applied to the sensor by the underarm. Some common patterns observed during testing are discussed. The most commonly observed force distribution is a bean shape as in Figure 4.6 with areas of high force typically coinciding with the proximal anterior, proximal posterior and/or distal regions of the sensor. Users apply a force to the axillary support both on the top and on the sides. The force on top of the axillary support may directly represent the weight bearing of the user, but intuition suggests that the overall normal force on the axillary support is proportional to the perceived comfort.

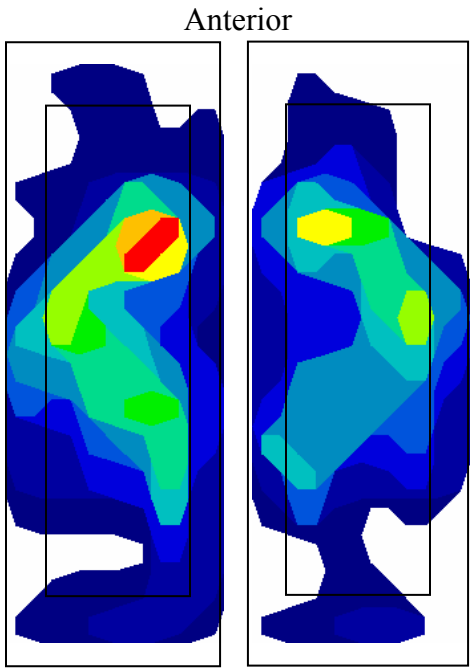

(a) (b)

Figure 4.6: Typical pressure distribution on the right (a) and left (b) axillary support. Areas of high pressure are in red and low pressure in blue. The top of the axillary support is boxed in.

Assume the axillary support is shaped like a rectangular prism and the user only forces the top of the support; the free body diagram of the cross-section of an axillary support from the side will look like the one in Figure 4.7.

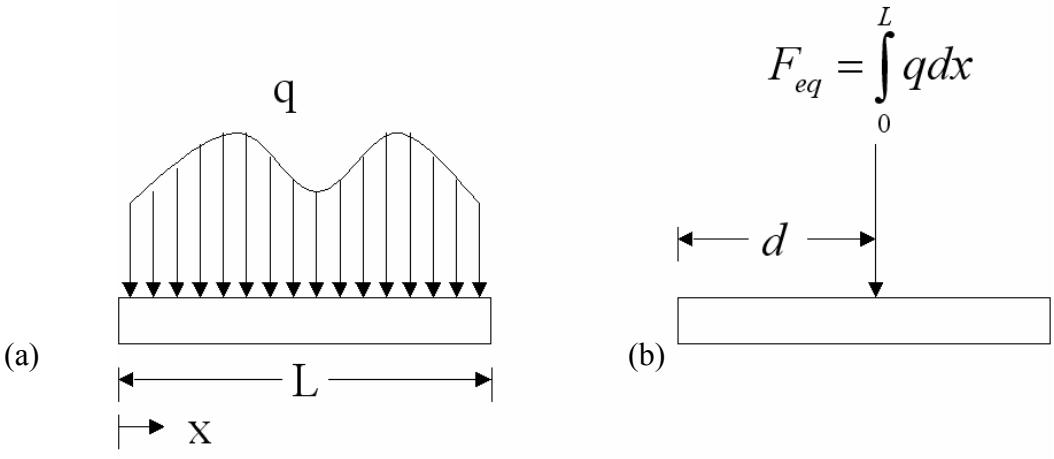

Figure 4.7: Free body diagram of a loaded axillary support shaped like a rectangular prism from the side (a) and the equivalent force and point of action at one instant (b).

Integrating the distributed load q over the length, L gives the equivalent force. The distance d from the edge, where the equivalent force acts is found using

$$d = \frac{\int_0^L qxdx}{\int_0^L qdx}. \tag{4.11}$$

The Fscan software finds the equivalent force and location where the equivalent force, F_{eq} acts (center of pressure) following a similar procedure except over a surface rather than a line. Figure 4.8 shows two commonly observed time histories of the equivalent total force exerted on an axillary support during one stride.

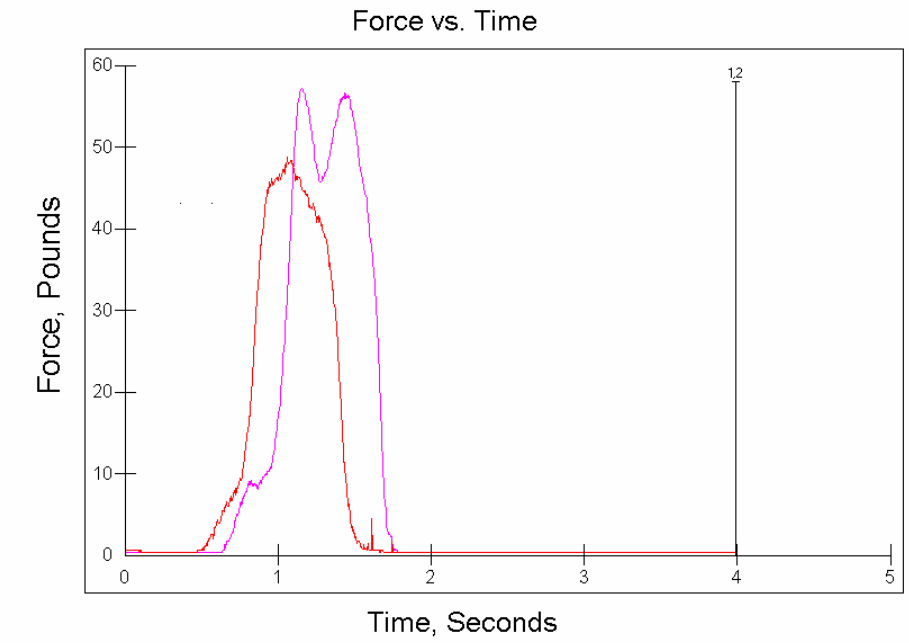

Figure 4.8: Typical time histories on the axillary support. Single peak in red and double peak in pink.

The time histories in Figure 4.8 are typical of 2-point gait with hand support and without hand support the only difference being the maximum force which is higher for 2-

point gait without hand support. Subjects begin with their legs and the orthosis in contact with the ground. The force on the axillary support starts at zero and increases until it reaches a maximum during mid-stance and then begins to decreases. Mid-stance is the period during a stride when the subject's legs are not in contact with the ground. Occasionally there is a maximum right before mid-stance and another maximum right after mid-stance. This may be caused by hesitation or a lack of fluidity in the motion or stride.

For both the Strutter and axillary crutches, the center of pressure follows the same general trend. The center of pressure starts in the middle of the sensor until mid-stance, after which the center of pressure heads toward the posterior. Axillary crutches are known to cause axillary nerve damage, and any characteristic pattern of axillary crutches could potentially indicate the reason damage occurs. Since the trajectory of the center of pressure is generally the same for the Strutter and axillary crutches, further testing could explore the effect of altering the path of the center of pressure so that the posterior muscles are not loaded, because such loadings may be a contributing factor in axillary nerve damage.

The findings of the UMD institutional review board approved pilot-study are now discussed. A copy of the institutional review board approval and informed consent papers are in the Appendix. First the left and right orthoses are compared to see if users prefer to load one orthosis instead of the other. Following this test each side of the Strutter and axillary crutches are compared, i.e. the left Strutter and the left axillary crutch. A two-tailed matched-pairs test compares the mean pair difference between the

left and right assistive ambulatory device (axillary crutches or the Strutter) while a subject uses a 2-point swing through with or without hand support.

The force exerted on each axillary support is divided by the subject's weight to obtain the body weight percent (BW%). In some cases, the BW% for the left or right orthosis may be greater than 50%. This is because some subjects sometimes prefer to support more of their weight on one orthosis, because they shift to one side or because they excessively squeeze the axillary support. The peak force, average force, peak contact area and average contact area are recorded during each stride. The peak force and peak contact area are the maximum equivalent force and maximum total contact area of one axillary support at one instant during a stride. The average force and average contact area are the average of the equivalent force and total contact area over the entire stride.

For subjects using an axillary crutch (Table 4.2) or using the Strutter (Table 4.3) while performing one stride with hand support, there is insufficient evidence to reject the null hypotheses that the peak force, average force, peak contact area and average contact area are the same for the left and right axillary support with the exception of the average contact area which, is the same for the left and right axillary crutch since the null hypothesis is rejected. The null hypothesis is rejected since the p-value is smaller than 0.05. However the null hypothesis that the average contact area is the same for the left and right crutch is not rejected, because the p-value is too close to 0.05.

In the case of axillary crutches without hand support (Table 4.4), there is insufficient evidence to reject the null hypotheses that the peak force, average force, peak contact area and average contact area are the same for the left and right axillary support. This

means it is plausible that the peak force, average force, peak contact area and average contact area between the left and right crutches are the same for axillary crutches.

Axillary 2-point							
		Min	Mean	Max	Var	Sample	P_value
Peak Force	Right	0.108	0.317	0.571	0.020	23	0.248
	Left	0.103	0.281	0.567	0.020	23	
Average Force	Right	0.030	0.170	0.330	0.010	23	0.113
	Left	0.039	0.130	0.367	0.010	23	
Peak Contact Area	Right	6.500	12.563	17.000	9.431	23	0.149
	Left	6.250	11.708	17.750	12.183	23	
Average Contact Area	Right	2.120	7.771	12.730	10.090	23	0.049
	Left	2.190	6.161	12.780	9.285	23	

Table 4.2: Matched-pair test of the peak force, average force, peak contact area and average contact area while using axillary crutches and performing one stride with hand support.

Strutter 2-point							
		Min	Mean	Max	Var	Sample	P_value
Peak Force	Right	0.043	0.175	0.491	0.015	23	0.473
	Left	0.033	0.166	0.410	0.013	23	
Average Force	Right	0.014	0.087	0.321	0.007	23	0.425
	Left	0.006	0.079	0.244	0.005	23	
Peak Contact Area	Right	3.000	8.946	19.000	17.397	23	0.244
	Left	1.750	8.348	17.000	18.845	23	
Average Contact Area	Right	1.020	4.694	14.420	13.338	23	0.248
	Left	0.370	4.233	11.590	11.495	23	

Table 4.3: Results of the matched-pair test of the peak force, average force, peak contact area and average contact area while using the Strutter and performing one stride with hand support.

Axillary 2-point with No Hands							
		Min	Mean	Max	Var	Sample	P_value
Peak Force	Right	0.371	0.441	0.595	0.003	23	0.239
	Left	0.365	0.459	0.568	0.003	23	
Average Force	Right	0.098	0.207	0.337	0.004	23	0.058
	Left	0.119	0.224	0.313	0.005	23	
Peak Contact Area	Right	10.750	14.348	18.000	5.283	23	0.284
	Left	11.250	14.641	17.750	5.181	23	
Average Contact Area	Right	4.860	9.101	13.680	5.413	23	0.108
	Left	6.470	9.492	13.420	5.478	23	

Table 4.4: Results of the matched-pair test of the peak force, average force, peak contact area and average contact area while using axillary crutches and performing one stride without hand support.

The null hypothesis that the average force, peak contact area and average contact area are the same for the left and right Strutter while performing one stride without hand support is rejected (Table 4.5). However there is insufficient evidence to reject the null hypothesis that the peak force between the left and right Strutter is the same. There is a general trend that the peak and average force is greater for the right orthosis, the dominant hand for the subjects. The difference is not statistically significant for this population size but may be statistically significant for larger population sizes.

Strutter 2-point with No Hands

		Min	Mean	Max	Var	Sample	P_value
Peak Force	Right	0.271	0.367	0.465	0.003	23	0.102
	Left	0.235	0.344	0.449	0.003	23	
Average Force	Right	0.082	0.182	0.259	0.003	23	0.005*
	Left	0.096	0.153	0.234	0.001	23	
Peak Contact Area	Right	10.000	15.760	19.250	7.557	23	<0.001*
	Left	9.750	14.406	17.500	6.684	23	
Average Contact Area	Right	4.480	9.257	13.200	7.020	23	<0.001*
	Left	4.480	7.981	11.380	5.460	23	

Table 4.5: Results of the matched-pair test of the peak force, average force, peak contact area and average contact area while using the Strutter and performing one stride without hand support. *Null hypothesis rejected.

The Strutter, in contrast to axillary crutches, is not rigid. It appears that when subjects use the Strutter without hand support the average force, peak contact area and average contact area is greater on the right side. This may be the result of subjects preferring to support weight on one side or from the tape holding the sensor to the axillary pad breaking loose during experiments. It was observed that the sensor slipped so far as to be folded over top of itself in some cases. The worst case observed had three sensels stacked on top of one another in corner of the Strutter's axillary pad (Figure 4.9).

Each sensel has an area of 0.25 $in.^2$, so three sensels overlapping each other will result in an error of 0.5$in.^2$. If all six columns of a sensor were to fold with three sensels in each column stacked on top of one another, the contact area reading will be 1.5 in. larger than it actually is. If this happens on both the front and back of the axillary support, the contact area would be 3 in. larger than it actually is. This may incorrectly show that users utilize a larger contact area with the Strutter than axillary crutches.

Figure 4.9: Location where the tape holding the sensor onto the axillary pad typically breaks free and folds.

A two-tailed matched-pair test with a significance level of 0.05 is used to compare the peak force, average force, peak contact area and average contact area of axillary crutches with the Strutter. The left axillary crutch is compared to the left Strutter and the right axillary crutch is compared to the right Strutter. The null hypothesis is that the mean pair difference is zero or that the population means are the same. For example one null hypothesis is that the mean pair difference of the peak force between axillary crutches and the Strutter on the right side of the user while performing one stride with hand support is zero.

The test shows that the subjects carried their weight differently on the right Strutter compared to the right axillary crutch (Table 4.6) and left Strutter compared to the left axillary crutch (Table 4.7) when using a 2-point gait with hand support. This is also true for the right (Table 4.8) and left (Table 4.9) devices while performing one stride without hand support. This means that it is plausible that the forces and contact area are different between axillary crutches and the Strutter for the left and right device except where noted as follows.

There is insufficient evidence to reject the null hypothesis that the matched-pair difference of the average contact area is the same for the right axillary crutch and the right Strutter while performing one stride without hand support (Table 4.8). Similarly there is insufficient evidence to reject the null hypothesis that the peak contact area is the same for the left axillary crutch and the left Strutter without hand support (Table 4.9). The failure to reject the null hypothesis that the peak contact area is the same for the left axillary crutch and the left Strutter without hand support may be caused by the sensor on the Strutter folding and giving a higher than true reading causing the mean difference to be indistinguishable from zero. The same may also be true for the failure to reject the null hypothesis that the right axillary and right Strutter average contact areas are the same without hand support as a result of the sensor folding.

Comparison of the Right Orthoses for a 2-point Gait							
		Min	Mean	Max	Var	Sample	P_value
Peak Force	Axillary	0.108	0.317	0.571	0.020	23	<0.001*
	Strutter	0.043	0.175	0.491	0.015	23	
Average Force	Axillary	0.030	0.170	0.330	0.010	23	<0.001*
	Strutter	0.014	0.087	0.321	0.007	23	
Peak Contact Area	Axillary	6.500	12.563	17.000	9.431	23	<0.001*
	Strutter	3.000	8.946	19.000	17.397	23	
Average Contact Area	Axillary	2.120	7.771	12.730	10.090	23	<0.001*
	Strutter	1.020	4.694	14.420	13.338	23	

Table 4.6: Matched-pair test of the peak force, average force, peak contact area and average contact area between axillary crutches and the Strutter on the user's right side while performing one stride with hand support. *Null hypothesis rejected

Comparison of the Left Orthoses for a 2-point Gait							
		Min	Mean	Max	Var	Sample	P_value
Peak Force	Axillary	0.103	0.281	0.567	0.020	23	<0.001*
	Strutter	0.033	0.166	0.410	0.013	23	
Average Force	Axillary	0.039	0.130	0.367	0.010	23	0.007*
	Strutter	0.006	0.079	0.244	0.005	23	
Peak Contact Area	Axillary	6.250	11.708	17.750	12.183	23	<0.001*
	Strutter	1.750	8.348	17.000	18.845	23	
Average Contact Area	Axillary	2.190	7.771	12.730	10.090	23	0.007*
	Strutter	0.370	4.233	11.590	11.495	23	

Table 4.7: Matched-pair test of the peak force, average force, peak contact area and average contact area between axillary crutches and the Strutter on the user's left side while performing one stride with hand support. *Null hypothesis rejected.

Comparison of the Right Orthoses for a 2-point Gait with No Hands							
		Min	Mean	Max	Var	Sample	P_value
Peak Force	Axillary	0.371	0.441	0.595	0.003	23	<0.001*
	Strutter	0.271	0.367	0.465	0.003	23	
Average Force	Axillary	0.098	0.207	0.337	0.004	23	0.012*
	Strutter	0.082	0.182	0.259	0.003	23	
Peak Contact Area	Axillary	10.750	14.348	18.000	5.283	23	<0.001*
	Strutter	10.000	15.760	19.250	7.557	23	
Average Contact Area	Axillary	4.860	9.101	13.680	5.413	23	0.764
	Strutter	4.480	9.257	13.200	7.020	23	

Table 4.8: Matched-pair test of the peak force, average force, peak contact area and average contact area between axillary crutches and the Strutter on the user's right side while performing one stride without hand support. *Null hypothesis is rejected

Comparison of the Left Orthoses for a 2-point Gait with No Hands							
		Min	Mean	Max	Var	Sample	P_value
Peak Force	Axillary	0.365	0.459	0.568	0.003	23	<0.001*
	Strutter	0.235	0.344	0.449	0.003	23	
Average Force	Axillary	0.119	0.224	0.313	0.005	23	<0.001*
	Strutter	0.096	0.153	0.234	0.001	23	
Peak Contact Area	Axillary	11.250	14.641	17.750	5.181	23	0.358
	Strutter	9.750	14.406	17.500	6.684	23	
Average Contact Area	Axillary	6.470	9.492	13.420	5.478	23	0.002*
	Strutter	4.480	7.981	11.380	5.460	23	

Table 4.9: Matched-pair test of the peak force, average force, peak contact area and average contact area between axillary crutches and the Strutter on the user's left side while performing one stride without hand support. *Null hypothesis is rejected.

4.4 Summary

There is a general trend that the subjects, all of whom were right handed, have higher forces and contact areas on the right orthosis, Strutter or axillary crutches. This is not statistically significant at the $p = 0.05$ level for this sample size. However, the difference may become statistically significant for larger subject populations. The results of the matched-pair test show that it is plausible that the peak force, average force, peak contact area and average contact area are the same between left and right axillary crutches. The same is true for the left and right Strutters when subjects perform one stride with hand support or without hand support. Except in the case of the average force, peak contact area and average contact area, which are different between the right and left orthosis when using the Strutter without hand support. Subjects likely prefer loading the right Strutter when using a gait without hand support.

The matched-pair test shows that it is plausible that the peak force, average force, peak contact area and average contact area are different for axillary crutches and for the Strutter with axillary crutches having larger forces and contact area than the Strutter. The previous statement has two exceptions, the case of the average contact area of the right

axillary crutch and right Strutter with hand support and the peak contact area for the left axillary crutch and left Strutter without hand support, where it is plausible that the means are the same.

4.5 Discussion

Nyland et al. (2002) says there is an available contact area of 96.8 cm^2 on the Strutter and 32.3 $in.^2$ on an axillary crutch and therefore the force/area should be lower and safer on the Strutter. Although the available contact area of the Strutter is far greater than an axillary crutch, on average, the peak contact area and average contact area utilized by users during one stride with hand support is smaller for Strutter users. There is a statistically significant difference in the peak force and average force attained between the Strutter and axillary crutch for gaits with and without hand support. There is a statistically significant difference in the peak contact area and average contact area between the Strutter and axillary crutches for a 2-point gait. Typically the subjects exhibit a lower peak and average BW% on the Strutter. On average, subjects utilize a greater contact area on both the left and right side when using axillary crutches.

The subjects were asked to fill out a questionnaire rating the perceived comfort of the Strutter and axillary crutches on a scale from one to ten. The Strutter is rated more comfortable than axillary crutches (Table 4.10), although not by much of a margin. Since the scale is perceived, there is no way to tell if a one-point increase in user perceived comfort means that the axillary support has crossed the threshold into the "safe axillary support" region.

Perceived Comfort and Stability	
Strutter Comfort	5.889
Axillary Crutch Comfort	4.667
Strutter Stability	6.333
Axillary Crutch Stability	6

Table 4.10: Average comfort and stability score of axillary crutches and the Strutter as perceived by study participants

The higher perceived comfort rating of the Strutter may have to do with lower normal forces or from lower contact area compared to axillary crutches. Intuitively it seems that an axillary support with lower normal forces should be more comfortable, however lower contact area being more comfortable is puzzling. The reason the Strutter is perceived as more comfortable compared to axillary crutches cannot be fully explained by just the normal forces and contact area. The increased comfort could potentially be caused by the axillary support and handgrip staying horizontal during a stride or from other factors. The force in the tangential direction at the axillary support may also be an important factor in perceived comfort but was not measured directly in this experiment. A dynamic model of the Strutter and axillary crutches will be presented next in an attempt to estimate the magnitude of forces accelerating the Strutter or axillary crutches during gait.

5 Dynamic Analysis of the Strutter and Axillary Crutches

Possible forces in the tangential direction for a 2-point gait with no hands are estimated to further investigate the relationship between the underarm/axillary support reactions and perceived comfort. The pin reactions for two loadings at the axillary support of the Strutter are used to calculate the time varying internal pin reactions for the orthosis during a stride.

5.1 Equation of Motion of the Strutter

The Strutter is essentially a modified four bar-linkage, Figure 5.1. The coupler link (axillary support) and the ground link (footpad) have the same length. The two follower links (vertical support members) have the same length but are much longer than the coupler links. The handgrip and the spring support act as two more coupler links. The axillary support, the handgrip and the spring support members are always horizontal during a stride. The Strutter differs from a four bar-linkage in that neither of the vertical support members acts as the crank link. The axillary support, handgrip and spring support members, which are traditionally coupler links, acts as the crank links, the links that accelerates the system.

The free-body diagram of the Strutter is shown in Figure 5.1. The range of motion of the Strutter is limited by its geometry with θ increasing counter clockwise from $-\pi/6$ to $\pi/6$ which corresponds to the user traveling to the left in Figure 5.1. Theta is the angle the vertical support member makes with respect to the y-axis. When the user travels to the left, the horizontal members translate. So a force tangential or normal to the handgrip

or axillary support will be in the *x* or *y* directions in the inertial frame in Figure 5.1 respectively.

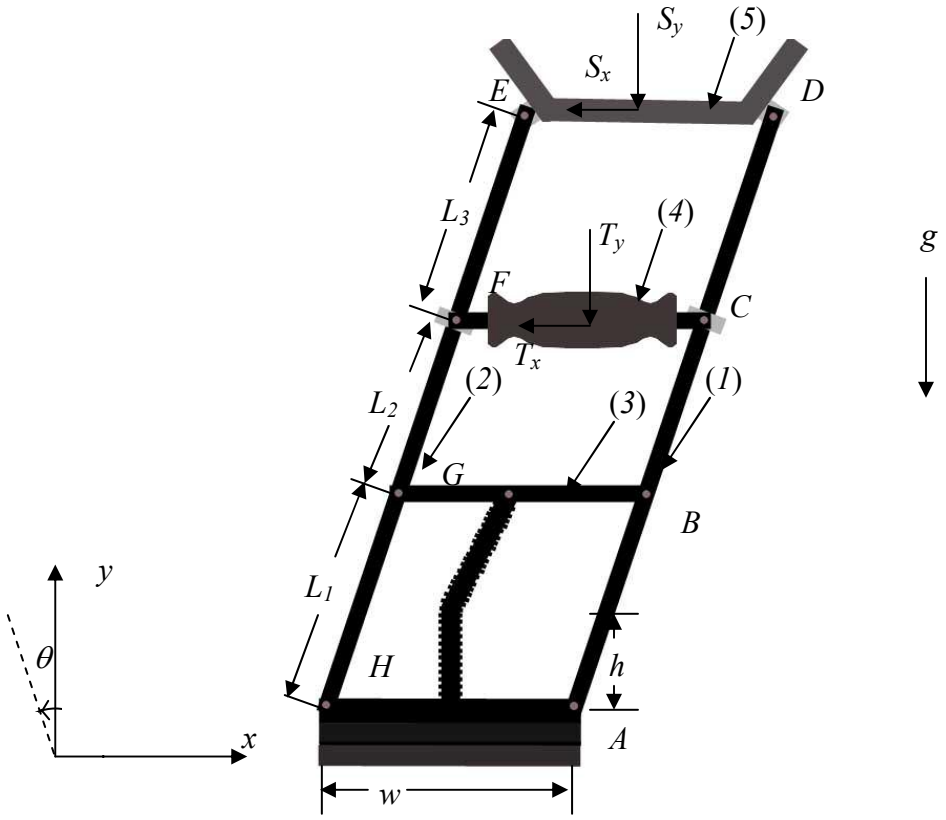

Figure 5.1: Free-body diagram of the Strutter

The subscripts of the external forces are the direction in which they act in the inertial frame and coincidently in the normal and tangential directions because the handgrip and shoulder support of the Strutter translates only. The external force on the axillary support consists of components in the *x*-direction (inertial frame), S_x and the *y*-direction (inertial frame), S_y. The external force on the handgrip consists of components T_x and T_y. The external forces are assumed to be acting on the centroid of the axillary support and handgrip. Let m_i be the mass of the i^{th} member and the members are assumed rigid.

Assume that the axillary support and handgrip are centered over the vertical supports, not cantilevered as they are in production.

Using Hamilton's principle, an equation for the angular acceleration, $\ddot{\theta}$, is found as a function of θ. Hamilton's principle says the integral of the sum of the variation of the kinetic energy and the virtual work, called the action, is equal to zero,

$$\int_{t_1}^{t_2} \left(\delta T + \delta W\right) dt = 0 \,. \tag{5.1}$$

The total kinetic energy of the Strutter is the sum of the kinetic energy of the individual vertical support members T_1, T_2, T_3, T_4 and T_5. The kinetic energies of the individual members are

$$T_1 = \frac{1}{2} I\dot{\theta}^2 = \frac{1}{6} m_1 \left(L_1 + L_2 + L_3\right)^2 \dot{\theta}^2 \,, \tag{5.2}$$

$$T_2 = \frac{1}{2} I\dot{\theta}^2 = \frac{1}{6} m_2 \left(L_1 + L_2 + L_3\right)^2 \dot{\theta}^2 \tag{5.3}$$

where L_1, L_2 and L_3 are shown on Figure 5.1. Members 3, 4 and 5 do not rotate but translate with velocity $r_i\dot{\theta}^2$, where r_1 is the distance from the footpad to the center of mass of spring support member (L_1), r_2 is the distance from the footpad to the handgrip ($L_1 + L_2$) and r_3 is the distance from the footpad to the shoulder support ($L_1 + L_2 + L_3$). The kinetic energies are

$$T_3 = \frac{1}{2} m_3 {L_1}^2 \dot{\theta}^2 \,, \tag{5.4}$$

$$T_4 = \frac{1}{2} m_4 \left(L_1 + L_2\right)^2 \dot{\theta}^2 \,, \tag{5.5}$$

and

$$T_5 = \frac{1}{2} m_5 \left(L_1 + L_2 + L_3\right)^2 \dot{\theta}^2, \tag{5.6}$$

where L_i are shown in Figure 5.1. The variation of the kinetic energy is equal to

$$\delta T = \frac{\partial T}{\partial \dot{\theta}} \delta \dot{\theta}, \tag{5.7}$$

Using integration by parts, the variation of the kinetic energy can be written,

$$\int \frac{\partial T}{\partial \dot{\theta}} \delta \dot{\theta} dt = \frac{\partial T}{\partial \theta} \delta \theta \Big|_{t_1}^{t_2} - \int_{t_1}^{t_2} \frac{d}{dt}\left(\frac{\partial T}{\partial \dot{\theta}}\right) \delta \theta = -\int_{t_1}^{t_2} \frac{d}{dt}\left(\frac{\partial T}{\partial \dot{\theta}}\right) \delta \theta . \tag{5.8}$$

The virtual rotations, $\delta\theta$ are arbitrary and chosen so that $\delta\theta = 0$ at t_1 and t_2.

The total variation of the kinetic energy is $\delta T = \delta T_1 + \delta T_2 + \delta T_3 + \delta T_4 + \delta T_5$ and the variations of kinetic energy of the individual members are by eqn 5.8,

$$\delta T_1 = \frac{1}{3} m_1 \left(L_1 + L_2 + L_3\right)^2 \dot{\theta} \delta \dot{\theta} = -\frac{1}{3} m_1 \left(L_1 + L_2 + L_3\right)^2 \ddot{\theta} \delta \theta, \tag{5.9}$$

$$\delta T_2 = \frac{1}{3} m_2 \left(L_1 + L_2 + L_3\right)^2 \dot{\theta} \delta \dot{\theta} = -\frac{1}{3} m_2 \left(L_1 + L_2 + L_3\right)^2 \ddot{\theta} \delta \theta, \tag{5.10}$$

$$\delta T_3 = m_3 {L_1}^2 \dot{\theta} \delta \dot{\theta} = -m_3 {L_1}^2 \ddot{\theta} \delta \theta, \tag{5.11}$$

$$\delta T_4 = m_4 \left(L_1 + L_2\right)^2 \dot{\theta} \delta \dot{\theta} = -m_4 \left(L_1 + L_2\right)^2 \ddot{\theta} \delta \theta, \tag{5.12}$$

and

$$\delta T_5 = m_5 \left(L_1 + L_2 + L_3\right)^2 \dot{\theta} \delta \dot{\theta} = -m_5 \left(L_1 + L_2 + L_3\right)^2 \ddot{\theta} \delta \theta . \tag{5.13}$$

It is convenient to separate the virtual work into two parts, the work done by conservative forces and the work done by non-conservative forces,

$$\delta W = \delta W_{nc} - \delta V \,. \tag{5.14}$$

Conservative forces depend on position alone or are constant, (Meirovich 2001). Assuming the external forces on the Strutter are non-conservative the total potential energy of the Strutter due to gravitational forces is the sum of the five members V_1, V_2, V_3, V_4, V_5 and the potential due to the spring, V_{spring} with $\theta = 0$ taken as the datum. The potential energies are,

$$V_1 = -\frac{1}{2} m_1 g\left(L_1 + L_2 + L_3\right)\left(1 - \cos\theta\right), \tag{5.15}$$

$$V_2 = -\frac{1}{2} m_2 g\left(L_1 + L_2 + L_3\right)\left(1 - \cos\theta\right), \tag{5.16}$$

$$V_3 = -m_3 g L_1\left(1 - \cos\theta\right), \tag{5.17}$$

$$V_4 = -m_4 g\left(L_1 + L_2\right)\left(1 - \cos\theta\right), \tag{5.18}$$

$$V_5 = -m_5 g\left(L_1 + L_2 + L_3\right)\left(1 - \cos\theta\right). \tag{5.19}$$

and the potential energy of the spring is given by

$$V_{spring} = \frac{1}{2} k \Delta x^2 \,. \tag{5.20}$$

The spring is stretched when the Strutter is rotated away from the vertical. The stretch of the spring Δx,

$$\Delta x = \sqrt{\left(L_1 \cos\theta - h\right)^2 + {L_1}^2 \sin^2\theta} - L_0 \,, \tag{5.21}$$

is equal to the difference of the stretched length of the spring and the un-stretched length of the spring, L_0 (Figure 5.2),

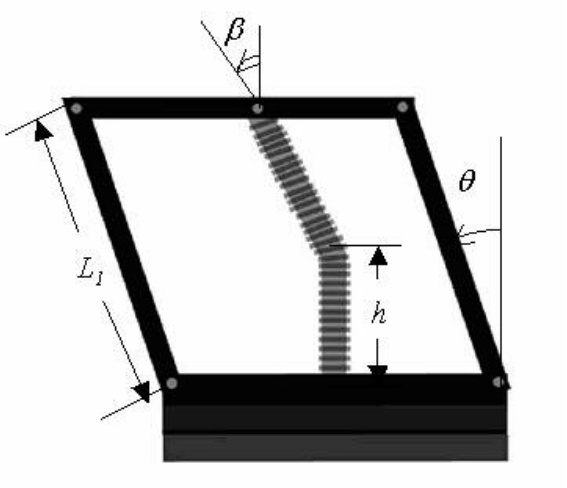

Figure 5.2: Geometry of the spring and spring support system.

Substituting eqn 5.21 into eqn 5.20 gives the potential energy of the spring,

$$V_{spring} = \frac{1}{2}k\left\{L_1^2 + h^2 + L_0^2 - 2L_1 h\cos\theta - 2L_0\sqrt{L_1^2 + h^2 - 2L_1 h\cos\theta}\right\}, \tag{5.22}$$

The variations of the potential energy for each member are

$$\delta V_1 = \frac{\partial V_1}{\partial\theta}\delta\theta = -\frac{1}{2}m_1 g\left(L_1 + L_2 + L_3\right)\sin\theta\delta\theta\,, \tag{5.23}$$

$$\delta V_2 = \frac{\partial V_2}{\partial\theta}\delta\theta = -\frac{1}{2}m_2 g\left(L_1 + L_2 + L_3\right)\sin\theta\delta\theta\,, \tag{5.24}$$

$$\delta V_3 = \frac{\partial V_3}{\partial\theta}\delta\theta = -m_3 g L_1\sin\theta\delta\theta\,, \tag{5.25}$$

$$\delta V_4 = \frac{\partial V_4}{\partial\theta}\delta\theta = -m_4 g\left(L_1 + L_2\right)\sin\theta\delta\theta\,, \tag{5.26}$$

$$\delta V_5 = \frac{\partial V_5}{\partial\theta}\delta\theta = -m_5 g\left(L_1 + L_2 + L_3\right)\sin\theta\delta\theta\,, \tag{5.27}$$

$$\delta V_{spring} = \frac{\partial V_{spring}}{\partial\theta}\delta\theta = khL_1\sin\theta\delta\theta - \frac{kL_0 L_1 h\sin\theta}{\sqrt{L_1^2 + h^2 - 2hL_1\cos\theta}}\delta\theta\,. \tag{5.28}$$

Summing eqn 5.23 through 5.28 gives the total variation of the kinetic energy. The work done by the external forces is,

$$\delta W_{nc} = \vec{T}\delta\vec{r}_4 + \vec{S}\delta\vec{r}_5, \tag{5.29}$$

where the position vector for member 4, is given by,

$$\vec{r}_4 = (L_1 + L_2)(-\sin\theta\,\vec{i} + \cos\theta\,\vec{j}), \tag{5.30}$$

and the variation of the position of member 4 is given by,

$$\delta\vec{r}_4 = \frac{\partial\vec{r}_4}{\partial\theta}\partial\theta = (L_1 + L_2)(-\cos\theta\,\vec{i} - \sin\theta\,\vec{j})\delta\theta. \tag{5.31}$$

The position vector for member 5 is given by,

$$\vec{r}_5 = \frac{\partial\vec{r}_5}{\partial\theta}\partial\theta = (L_1 + L_2 + L_3)(-\sin\theta\,\vec{i} + \cos\theta\,\vec{j}), \tag{5.32}$$

and the variation of the position of member 5 is,

$$\delta\vec{r}_5 = (L_1 + L_2 + L_3)(-\cos\theta\,\vec{i} - \sin\theta\,\vec{j})\delta\theta. \tag{5.33}$$

Substituting eqn 5.31 and eqn 5.33 into eqn 5.29 gives the variation of the non-conservative work,

$$\begin{aligned}\delta W_{nc} = {} & \{T_x(L_1 + L_2) + S_x(L_1 + L_2 + L_3)\}\cos\theta\delta\theta \\ & + \{T_y(L_1 + L_2) + S_y(L_1 + L_2 + L_3)\}\sin\theta\delta\theta\end{aligned} \tag{5.34}$$

Substituting the total variation of the kinetic energy, eqn 5.23 through eqn 5.28, the total variation of the potential energy, eqn 5.9 through eqn 5.13 and the work done by the external forces, substitute eqn 5.34 into eqn 5.1 using eqn 5.14 gives,

$$\int_{t_1}^{t_2}\Bigg[-\left\{\frac{1}{3}m_1(L_1+L_2+L_3)^2+\frac{1}{3}m_2(L_1+L_2+L_3)^2+m_3{L_1}^2+m_4(L_1+L_2)^2+m_5(L_1+L_2+L_3)^2\right\}\ddot{\theta}$$

$$+\left\{\frac{1}{2}m_1(L_1+L_2+L_3)+\frac{1}{2}m_2(L_1+L_2+L_3)+m_3L_1+m_4(L_1+L_2)+m_5(L_1+L_2+L_3)\right\}g\sin\theta$$

$$-hL_1\sin\theta+\frac{L_0L_1h\sin\theta}{\sqrt{L_1^2+h^2-2hL_1\cos\theta}}+\left\{T_x(L_1+L_2)+S_x(L_1+L_2+L_3)\right\}\cos\theta$$

$$+\left\{T_y(L_1+L_2)+S_y(L_1+L_2+L_3)\right\}\sin\theta\Bigg]\delta\theta\,dt=0\,. \qquad (5.35)$$

Equation 5.35 is true for any arbitrary variation of $\delta\theta$, so the coefficient of $\delta\theta$ must equal zero,

$$-\left\{\frac{1}{3}m_1(L_1+L_2+L_3)^2+\frac{1}{3}m_2(L_1+L_2+L_3)^2+m_3{L_1}^2+m_4(L_1+L_2)^2+m_5(L_1+L_2+L_3)^2\right\}\ddot{\theta}$$

$$+\left\{\frac{1}{2}m_1(L_1+L_2+L_3)+\frac{1}{2}m_2(L_1+L_2+L_3)+m_3L_1+m_4(L_1+L_2)+m_5(L_1+L_2+L_3)\right\}g\sin\theta$$

$$-hL_1\sin\theta+\frac{L_0L_1h\sin\theta}{\sqrt{L_1^2+h^2-2hL_1\cos\theta}}+\left\{T_x(L_1+L_2)+S_x(L_1+L_2+L_3)\right\}\cos\theta$$

$$+\left\{T_y(L_1+L_2)+S_y(L_1+L_2+L_3)\right\}\sin\theta=0\,. \qquad (5.36)$$

Solving eqn 5.36 for $\ddot{\theta}$,

$$\ddot{\theta}=\frac{\left\{\frac{1}{2}m_1(L_1+L_2+L_3)+\frac{1}{2}m_2(L_1+L_2+L_3)+m_3L_1+m_4(L_1+L_2)+m_5(L_1+L_2+L_3)\right\}g\sin\theta}{\frac{1}{3}m_1(L_1+L_2+L_3)^2+\frac{1}{3}m_2(L_1+L_2+L_3)^2+m_3{L_1}^2+m_4(L_1+L_2)^2+m_5(L_1+L_2+L_3)^2}$$

$$+\frac{-hL_1\sin\theta+\frac{L_0L_1h\sin\theta}{\sqrt{L_1^2+h^2-2hL_1\cos\theta}}+\left\{T_x(L_1+L_2)+S_x(L_1+L_2+L_3)\right\}\cos\theta+\left\{T_y(L_1+L_2)+S_y(L_1+L_2+L_3)\right\}\sin\theta}{\frac{1}{3}m_1(L_1+L_2+L_3)^2+\frac{1}{3}m_2(L_1+L_2+L_3)^2+m_3{L_1}^2+m_4(L_1+L_2)^2+m_5(L_1+L_2+L_3)^2}\,,$$

(5.37)

gives $\ddot{\theta}$ as a function of the external forces and θ. Re-writing eqn 5.37 as,

$$\ddot{\theta} = \frac{M_{grav} g \sin\theta - \psi + \xi_x + \xi_y}{M_{kinetic}}, \tag{5.38}$$

where the following relationships are used for notational convenience,

$$\xi_x = \left\{ T_x \left(L_1 + L_2 \right) + S_x \left(L_1 + L_2 + L_3 \right) \right\} \cos\theta, \tag{5.39}$$

$$\xi_y = \left\{ T_y \left(L_1 + L_2 \right) + S_y \left(L_1 + L_2 + L_3 \right) \right\} \sin\theta, \tag{5.40}$$

$$\psi = hL_1 \sin\theta - \frac{L_0 L_1 h \sin\theta}{\sqrt{L_1^2 + h^2 - 2hL_1 \cos\theta}}, \tag{5.41}$$

$$M_{grav} = \frac{1}{2} m_1 \left(L_1 + L_2 + L_3 \right) + \frac{1}{2} m_2 \left(L_1 + L_2 + L_3 \right) + m_3 L_1 + m_4 \left(L_1 + L_2 \right)$$

$$+ m_5 \left(L_1 + L_2 + L_3 \right), \tag{5.42}$$

and

$$M_{kinetic} = \frac{1}{3} m_1 \left(L_1 + L_2 + L_3 \right)^2 + \frac{1}{3} m_2 \left(L_1 + L_2 + L_3 \right)^2 + m_3 {L_1}^2 + m_4 \left(L_1 + L_2 \right)^2$$

$$+ m_5 \left(L_1 + L_2 + L_3 \right)^2. \tag{5.43}$$

Angular acceleration is defined as,

$$\ddot{\theta} = \frac{d\dot{\theta}}{dt} \tag{5.44}$$

where $\dot{\theta}$ is the angular velocity. The chain rule gives

$$\ddot{\theta} = \frac{d\dot{\theta}}{d\theta} \frac{d\theta}{dt} = \dot{\theta} \frac{d\dot{\theta}}{d\theta}. \tag{5.45}$$

Separating variables and integrating gives

$$\int_{\theta_0}^{\theta} \ddot{\theta}\, d\theta = \int_{\theta_0}^{\theta} \dot{\theta}\, d\dot{\theta}\,. \tag{5.46}$$

Using the fact that

$$\int \psi\, d\theta = V_{spring}\,, \tag{5.47}$$

and substituting eqn 5.38 into eqn 5.46 and integrating gives

$$\left.\frac{-M_{grav} g \cos\theta - V_{spring}}{M_{kinetic}}\right|_{\theta_0}^{\theta} + \int_{\theta_0}^{\theta}\left(\frac{\xi_x \cos\theta + \xi_y \sin\theta}{M_{kinetic}}\right) d\theta = \left.\frac{1}{2}\dot{\theta}^2\right|_{\theta_0}^{\theta}\,. \tag{5.48}$$

Equation 5.48 gives a means of computer $\omega(\theta)$. Using the definition

$$\dot{\theta} = \frac{d\theta}{dt}\,, \tag{5.49}$$

separating variables and integrating from θ_0 to θ gives the time, t, that it takes for the user to go through the angles θ_0 and θ,

$$t = \int_{\theta_0}^{\theta} \dot{\theta}^{-1} d\theta\,. \tag{5.50}$$

We have some idea of the normal forces present on the axillary support and the stride time. Using eqn 5.48 which is arrived at via eqn 5.38 and eqn 5.50, possible functions for the tangential force at the axillary support can be guessed for one stride. One stride is defined as moving from total weight support by the legs to total weight support by the orthoses at mid-stance and returning to total weight support by the legs.

5.2 *Equation of Motion of Axillary Crutches*

Following a similar approach as in section 5.1, the equation of motion of an axillary crutch is found. A simplified free body diagram of an axillary crutch where the external forces at the shoulder support in the tangential and normal direction S_t and S_n respectively and the external forces at the handgrip in the tangential and normal directions T_t and T_n respectively is shown in Figure 5.3.

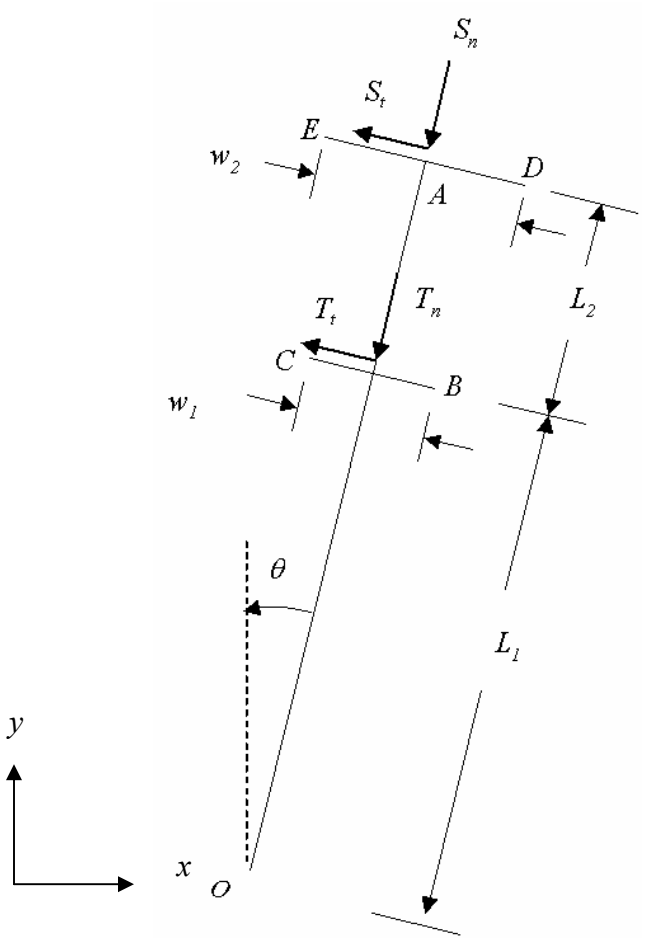

Figure 5.3: Free body diagram of an axillary crutch.

Using the parallel axis theorem the mass moment of inertia for the crutch is

$$I = (I_{OA})_O + (I_{BC})_O + (I_{CD})_O = \frac{1}{3} m_1 (L_1 + L_2)^2 + \frac{1}{12} m_2 {w_1}^2$$

$$+ m_2 L_1^{\,2} + \frac{1}{12} m_3 w_2^{\,2} + m_3 \left(L_1 + L_2\right)^2 \ . \tag{5.51}$$

The kinetic energy of the crutch is

$$T = \frac{1}{2} I \dot{\theta}^2 . \tag{5.52}$$

Using integration by parts as before, the variation of the kinetic energy is,

$$\delta T = I \dot{\theta} \delta \dot{\theta} = -I \ddot{\theta} \delta \theta . \tag{5.53}$$

Taking $\theta = 0$ as the datum, the total potential energy is

$$V = -\left[m_1 \left(\frac{L_1 + L_2}{2} \right) + m_2 L_1 + m_3 \left(L_1 + L_2\right) \right] g \left(1 - \cos\theta\right). \tag{5.54}$$

The variation of the potential energy is

$$\delta V = -\left[m_1 \left(\frac{L_1 + L_2}{2} \right) + m_2 L_1 + m_3 \left(L_1 + L_2\right) \right] g \sin\theta . \tag{5.55}$$

The work done by non-conservative forces is

$$\delta W_{nc} = \vec{T} \delta r_{BC} + \vec{S} \delta r_{DE} . \tag{5.56}$$

The position vector of member *BC* is

$$r_{BC} = L_1 \theta \vec{e}_t + L_1 \vec{e}_n , \tag{5.57}$$

and the variation of the position vector of the center of mass of member *BC* is

$$\delta r_{BC} = L_1 \delta\theta \vec{e}_t . \tag{5.58}$$

The position vector of the center of mass of member *DE* is,

$$r_{DE} = \left(L_1 + L_2\right) \theta \vec{e}_t + \left(L_1 + L_2\right) \vec{e}_n , \tag{5.59}$$

and the variation of the position vector of the center of mass of member *DE* is

$$\delta r_{DE} = (L_1 + L_2)\delta\theta\,\vec{e}_t\,. \tag{5.60}$$

Using Hamilton's principle, the action is given by

$$\int_{t_1}^{t_2}\left[-I\ddot{\theta} + \left\{m_1\left(\frac{L_1+L_2}{2}\right) + m_2L_1 + m_3(L_1+L_2)\right\}g\sin\theta + T_tL_1 + S_t(L_1+L_2)\right]\delta\theta\,dt = 0\,. \tag{5.61}$$

Hamilton's principle is valid for arbitrary $\delta\theta$, so the coefficient of $\delta\theta$ must equal zero. Rearranging eqn 5.61 and solving for $\ddot{\theta}$ gives,

$$\ddot{\theta} = \frac{g\sin\theta\left\{m_1\left(\frac{L_1+L_2}{2}\right) + m_2L_1 + m_3(L_1+L_2)\right\} + T_tL_1 + S_t(L_1+L_2)}{I}\,. \tag{5.62}$$

The angular velocity and corresponding stride time can be found using eqn 5.62 and eqn 5.46,

$$\left.\frac{-\left\{m_1\left(\frac{L_1+L_2}{2}\right) + m_2L_1 + m_3(L_1+L_2)\right\}g\cos\theta}{I}\right|_{\theta_0}^{\theta}$$

$$+\int_{\theta_0}^{\theta}\left(\frac{T_tL_1 + S_t(L_1+L_2)}{I}\right)d\theta = \frac{1}{2}\dot{\theta}^2\Big|_{\theta_0}^{\theta}\,. \tag{5.63}$$

The angular velocity, $\dot{\theta}$, (5.63) and angular acceleration, $\ddot{\theta}$, (5.62) of axillary crutches is dependent on the external forces in the tangential direction only where $\dot{\theta}$ and $\ddot{\theta}$ depend on the external forces on the axillary support in the tangential and normal directions for the Strutter.

5.3 Discussion

The experimental data obtained from the Fscan software (Chapter 4) and the dynamic analysis of axillary crutches and the Strutter provides a basis to estimate the forcing in the direction tangential to the axillary support. The force in the tangential direction must be estimated because a direct measurement of the force in the tangential direction by a strain gauge is impossible. A force in the tangential direction causes an axial strain and a force in the normal direction also causes an axial strain. The force in the normal direction causes a strain that is an order of magnitude larger than the tangential force making it impossible to measure the axial strain.

For the following examples, the Strutter is adjusted for an example user approximately 6 feet tall. The Strutter's spring is assumed linear with spring constant, $k = 100$ lbs/ft and the rest of the dimensions of the Strutter are in Table 5.1. The spring on the commercially available Strutter has changed a couple of times and is generally about 100 lbs/ft. See Figure 5.1 for the free body diagram of the Strutter.

Dimensions			
	Length (feet)		**Weight (lbs)**
L_1	1.25	m_1	0.786
L_2	3	m_2	0.786
L_3	1.5	m_3	0.0952
H	0.5	m_4	0.316
w	0.5	m_5	0.296
L_0	0.4375		

Table 5.1: Parameters of the commercially available Strutter.

Experimental data shows that normal force is 0 percent body weight (BW%) at the beginning of the stride. The force increases to a maximum around the middle of the duration of a user's stride, with approximately 50 BW% loaded on the shoulder support

when the handgrip is not used. Then the force falls off to 0 BW% at the end of the second double stance.

Without any knowledge of the relationship between θ and time, some assumptions must be made. Assume that the normal force and ω are even functions with initial and final angular velocities equal to zero, $\dot{\theta}_i = \dot{\theta}_f = 0$. Furthermore, assume that initial, θ_i and final angle, θ_f are equal and opposite, $\theta_i = -\theta_f$. In assuming ω is an even function, $\ddot{\theta}$ must be an odd function. For these assumptions it follows that

$$\int_{\theta_i}^{T/2} \dot{\theta}^{-1} d\theta = \int_{T/2}^{\theta_f} \dot{\theta}^{-1} d\theta \tag{5.64}$$

where $T = \theta_f - \theta_i$, which corresponds to the Strutter reaching the vertical, $\theta = 0$ at the middle of the duration of a stride. Assume a user weight of 200 lbs and the user utilizes the entire range of motion of the Strutter, $-\pi \leq \theta \leq \pi$. Assume S_y starts at 0 BW% at $\theta_i = -\pi/6$. Then S_y increases to a maximum of 100 BW% in the middle of the stride, $\theta = 0$ then S_y decreases to 0 BW% at $\theta_f = \pi/6$. Supporting 100 BW% is the worst case for a controlled stride and will unlikely be common in use, but should be expected to occur once if not several times during the lifetime of a Strutter. An equation of the force at the shoulder support that meets these conditions is given by

$$S_y = 200 \cos\left(\frac{\theta - \theta_i}{\theta_f - \theta_i} \right). \tag{5.65}$$

A graph of S_y as a function of θ is shown in Figure 5.4.

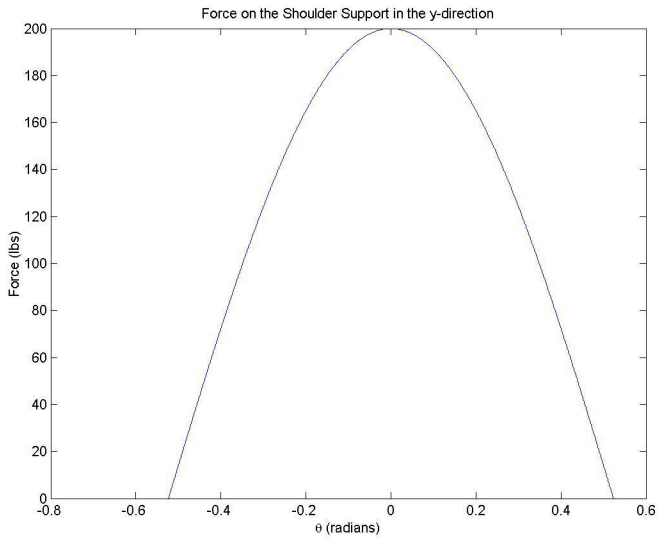

Figure 5.4: Assumed force in the *y*-direction at the shoulder support.

In a gait without hand support, there is no force at the handgrip the only unknown is S_x assuming S_y is known. Solving eqn 5.38 for $\ddot{\theta} = 0$ gives the force S_x required for static equilibrium at each θ,

$$S_x = \frac{-M_{grav} g \sin\theta + \psi - S_y (L_1 + L_2 + L_3)\sin\theta}{(L_1 + L_2 + L_3)\cos\theta}. \tag{5.66}$$

The term ψ is the function of θ given in eqn 5.41, and M_{grav} is a constant given by eqn 5.42. The force in the tangential direction on the shoulder support arises from the user applying a force to it. In order for the orthosis to move, there must be an initial angular acceleration produced by S_x. In this example there is no initial angular velocity, so S_x must initially be different from eqn 5.66. For the device to move forward, the user must initially apply a force greater than eqn 5.66. Adding an arbitrary function P to eqn 5.66 gives,

$$S_x = \frac{-M_{grav} g \sin\theta + \psi - S_y (L_1 + L_2 + L_3)\sin\theta}{(L_1 + L_2 + L_3)\cos\theta} + P. \tag{5.67}$$

Substituting eqn 5.67 into eqn 5.38 gives

$$\ddot{\theta} = \frac{P(L_1 + L_2 + L_3)\cos(\theta)}{M_{kinetic}} \quad . \tag{5.68}$$

It was stated earlier that the angular velocity, $\dot{\theta}$ should be an even function. Since the angular velocity, $\dot{\theta}$ is the time derivative of the angular acceleration, $\ddot{\theta}$, the angular acceleration needs to be an odd function if $\dot{\theta}$ is to be an even function. The function P needs to be odd so that $\ddot{\theta}$ is odd. Assume that in eqn 5.67, $P = W\sin(-\pi\theta/(\theta_f - \theta_i))$, where W is an arbitrary magnitude. For this choice of P, the graph of S_x versus θ is plotted with $W = 0$, $W = 1$ and $W = 2$ (Figure 5.5).

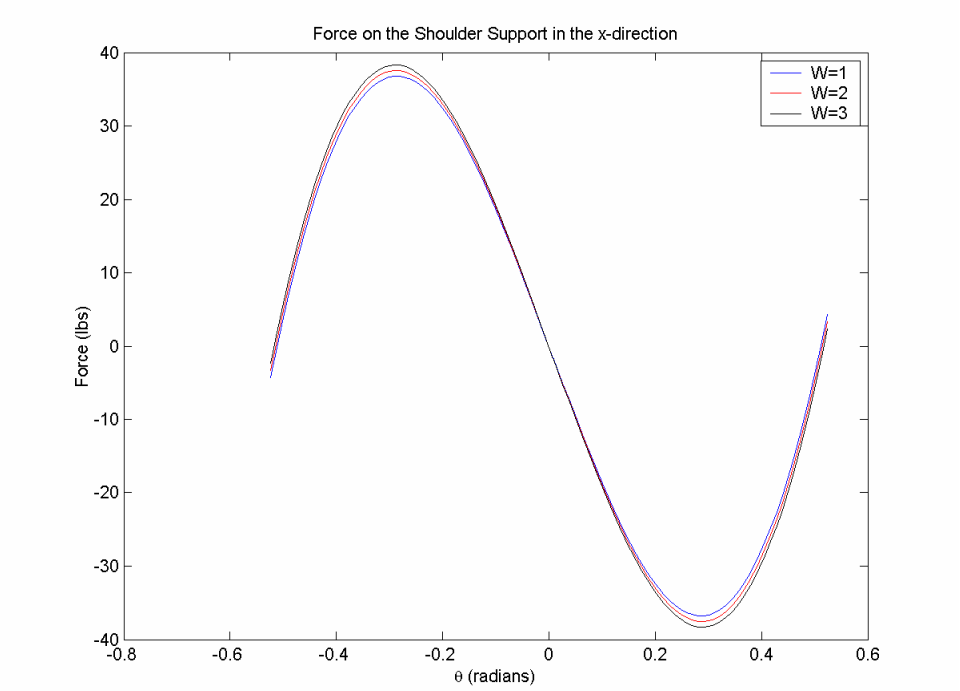

Figure 5.5: Plot of the assumed force in the x-direction at the shoulder support for $W = 0$, $W = 1$ and $W = 2$.

The angular velocity for $W = 1$, $W = 2$ and $W = 3$ are shown in Figure 5.6.

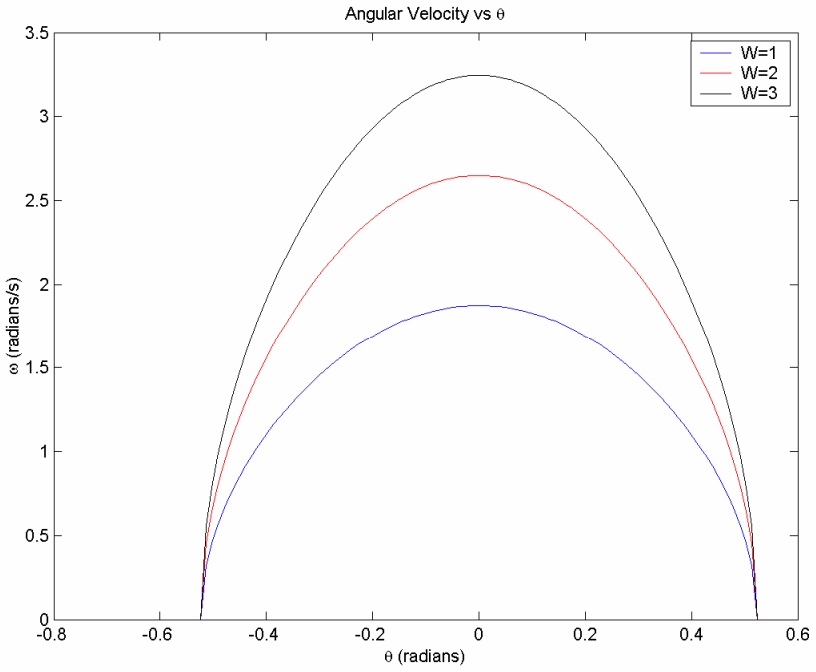

Figure 5.6: Angular velocity versus theta for $W = 1$, $W = 2$ and $W = 3$.

When $W = 1$, $W = 2$ and $W = 3$, stride times of 0.953 s, 0.674 s and 0.550 s are obtained respectively from eqn 5.50. A good value for W is 0.4, which gives a stride time of 1.5 s, which is a moderate cadence. Equation 5.67 with P~0.4sin(θ) gives one possible forcing on the shoulder support for a stride that starts and stops at rest. There are many possible functions, P, that are admissible and would satisfy the required conditions.

See Figure 5.3 for a free body diagram of an axillary crutch. Table 5.2 shows the parameters of the axillary crutch used in this example.

Dimensions			
	Length (feet)		**Weight (lbs)**
L_1	4.25	m_1	0.786
L_2	1.5	m_2	0.316
w_1=w_2	0.5	m_3	0.316

Table 5.2: Parameters of an axillary crutch.

Setting $\ddot{\theta} = 0$ gives the force, S_t, required for static equilibrium at each θ,

$$S_t = \frac{g \sin\theta \left\{ m_1 \left(\frac{L_1 + L_2}{2} \right) + m_2 L_1 + m_3 \left(L_1 + L_2 \right) \right\}}{\left(L_1 + L_2 \right)}. \tag{5.69}$$

Adding a arbitrary function $P = W\sin(-\pi\theta/(\theta_f - \theta_i))$ to eqn 5.69 gives,

$$S_t = \frac{g \sin\theta \left\{ m_1 \left(\frac{L_1 + L_2}{2} \right) + m_2 L_1 + m_3 \left(L_1 + L_2 \right) \right\}}{\left(L_1 + L_2 \right)} + W \sin\left(-\frac{\pi\theta}{\theta_f - \theta_i} \right). \tag{5.70}$$

Substituting eqn 5.70 into eqn 5.62 gives,

$$\ddot{\theta} = \frac{W}{I} \sin\left(-\frac{\pi\theta}{\theta_f - \theta_i} \right). \tag{5.71}$$

for values of W of 1, 2 and 3 the corresponding stride times are 0.78 s, 0.55 s and 0.45 s respectively. The corresponding tangential force at the axillary support and angular velocity, $\dot{\theta}$ are shown in Figure 5.7 and Figure 5.8. A good value for W is 0.25, which gives a stride time of 1.5 s.

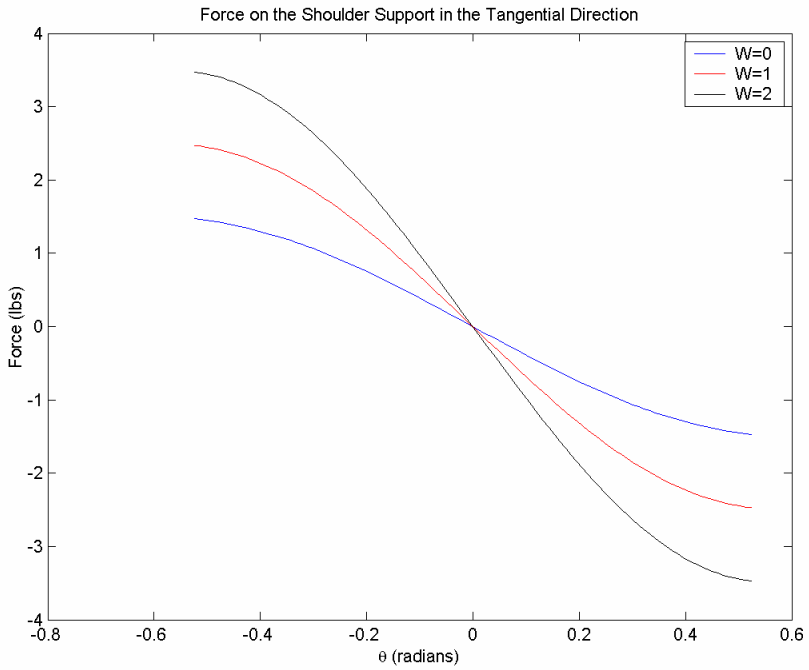

Figure 5.7: Plot of the assumed force in the tangential direction at the shoulder support of an axillary crutch for W values of 0, 1 and 2.

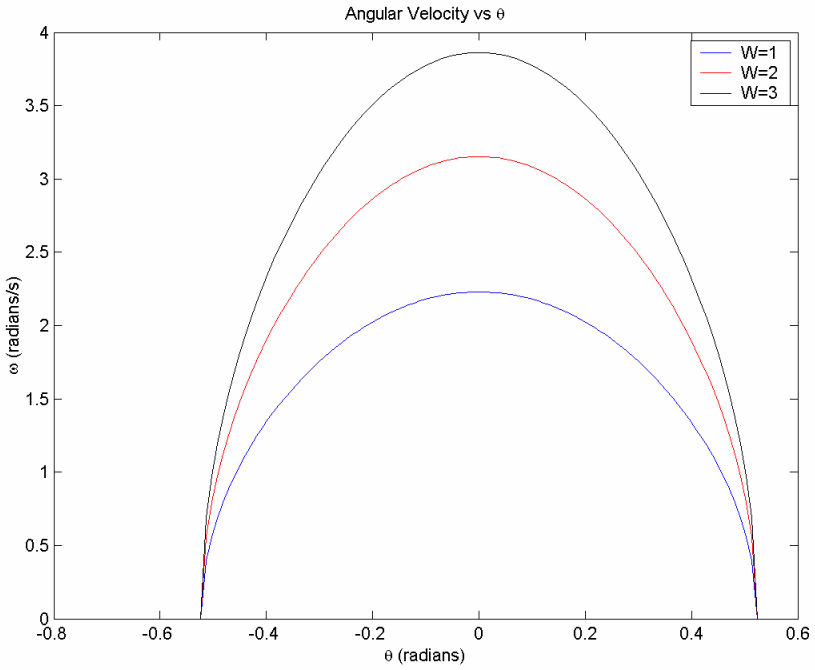

Figure 5.8: Angular velocity for an axillary crutch with W values 1, 2 and 3.

The stride time of the Strutter is dependent on the normal and tangential force on the axillary support whereas the stride time of axillary crutches depends only on the tangential force. Assume S_y on the Strutter is given by eqn 5.65 then for the Stutter to have a stride time of 1.5 s, S_x is given in Figure 5.9. The force, S_t for axillary crutches to have the same stride time is also plotted in Figure 5.9. The force in the tangential direction is clearly much larger for the Strutter.

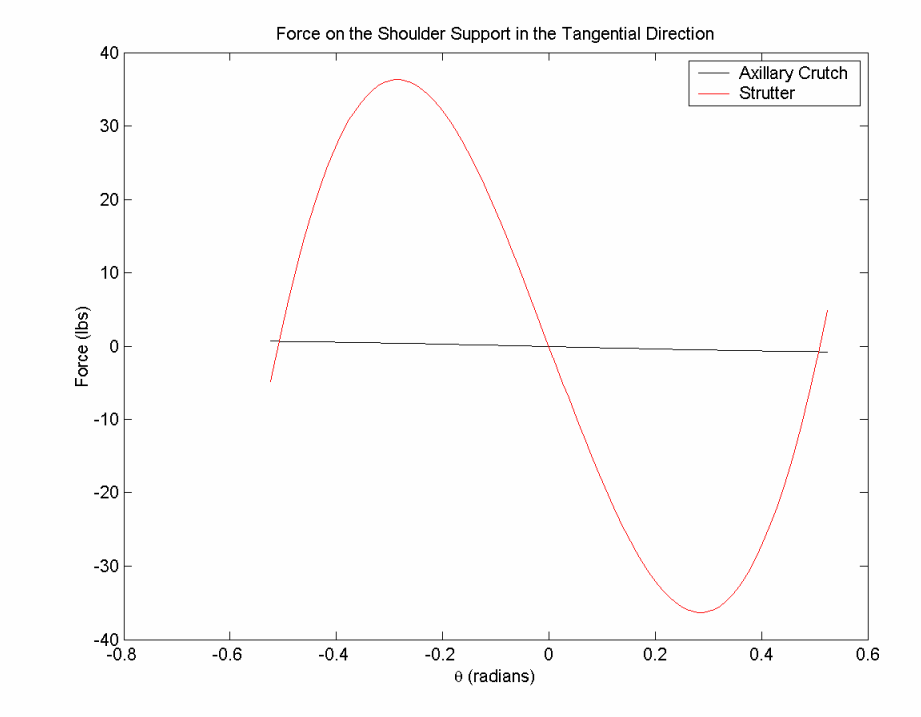

Figure 5.9: Comparison of the force in the tangential direction of the Strutter and axillary crutches. The tangential force gives a stride time of 1.5 s for the Strutter and 1.5 s for axillary crutches.

For the maximum force in the tangential direction to be approximately equal for the Strutter and axillary crutches with a stride time of 1.5 s, the force in the normal direction for the Strutter can be no greater than

$$S_y = 15\cos\left(\frac{\theta\pi}{\theta_f - \theta_i}\right). \tag{5.72}$$

However the angle, θ, where the maximum occurs is still not the same for axillary crutches and the Strutter. The maximum for axillary crutches occurs at the extremes of the range while the Strutter has maximums between the endpoints and the midpoint. If the spring constant is increased from 100 ft/lbs to 200 ft/lbs, then for the maximum force in the tangential direction to be approximately equal for the Strutter and axillary crutches, the force in the normal direction for the Strutter must be

$$S_y = 25\cos\left(\frac{\theta\pi}{\theta_f - \theta_i}\right). \tag{5.73}$$

Subjects applied normal forces to the axillary support as great as 50% of their body weight during experiments. The subjects had an average weight of 163.38. Anytime the subjects were supporting more than 9% (9% of 163.38 lbs is more than the maximum of eqn 5.72) of their body weight on the axillary support, the force in the tangential direction was greater than the maximum force necessary with axillary crutches for the same stride time.

5.4 Summary

The angular acceleration, angular velocity and the stride time for the Strutter are functions of the external forces and theta. The angular acceleration, angular velocity and stride time for axillary crutches are functions of the external forces in the tangential direction and theta. The force at the shoulder support in the tangential direction is greater for Strutter users versus axillary crutch users using a 2-point gait without hand support for the same stride time.

This model predicts a larger force required in the tangential direction for the Strutter compared to axillary crutches if the orthoses have the same stride time. The angle, θ

where the maximum tangential force occurs is different for the Strutter and axillary crutches, this may play a role in perceived comfort or the tangential force is not that important in terms of perceived comfort.

5.5 Dynamic Force Balance

Having estimated the external forces on the Strutter during a stride, the reactions at the pins can be found. The mini-Strutter and Strutter currently use the same size pins at the shoulder support, handgrip, spring support member and the footpad. Minor weight savings may be realized by optimizing pin size based on weight bearing expectations. The pins are assumed frictionless and the members are rigid. The free-body and kinetic diagrams for the vertical support member 1 are shown in Figure 5.10.

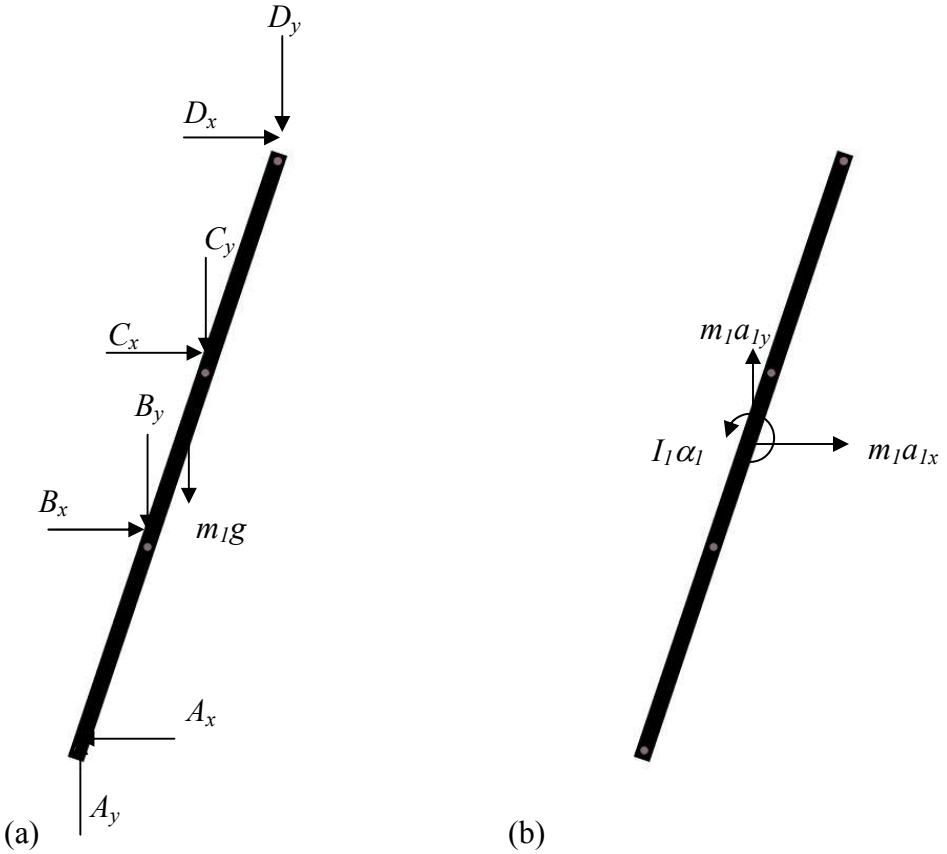

Figure 5.10: (a) Free-body diagram of member 1. (b) Kinetic diagram of member 1.

Summing the forces in the *x*-direction,

$$\sum F_x : m_1 a_{1x} = -A_x + B_x + C_x + D_x \,. \tag{5.74}$$

Summing the forces in the *y*-direction,

$$\sum F_y : m_1 a_{1y} = A_y - B_y - C_y - D_y - m_1 g \,. \tag{5.75}$$

Summing the moments about *A*,

$$\sum M_A : \frac{1}{3} m_1 (L_1 + L_2 + L_3)^2 \alpha_1 = -(B_x(L_1) + C_x(L_1 + L_2) + D_x(L_1 + L_2 + L_3))\cos\theta$$

$$+ (B_y(L_1) + C_y(L_1 + L_2) + D_y(L_1 + L_2 + L_3))\sin\theta + m_1 g \sin\theta\left(\frac{L_1 + L_2 + L_3}{2}\right), \tag{5.76}$$

where the acceleration of member 1 is given by

$$a_{1x} = \left(-\ddot{\theta}\cos\theta + \dot{\theta}^2 \sin\theta\right)\left(\frac{L_1 + L_2 + L_3}{2}\right) \tag{5.77}$$

and

$$a_{1y} = -\left(\ddot{\theta}\cos\theta + \dot{\theta}^2 \sin\theta\right)\left(\frac{L_1 + L_2 + L_3}{2}\right). \tag{5.78}$$

The force and acceleration diagrams for the other vertical support, member 2 are similar to those of member 1 since they both have the same motion, shown in Figure 5.11.

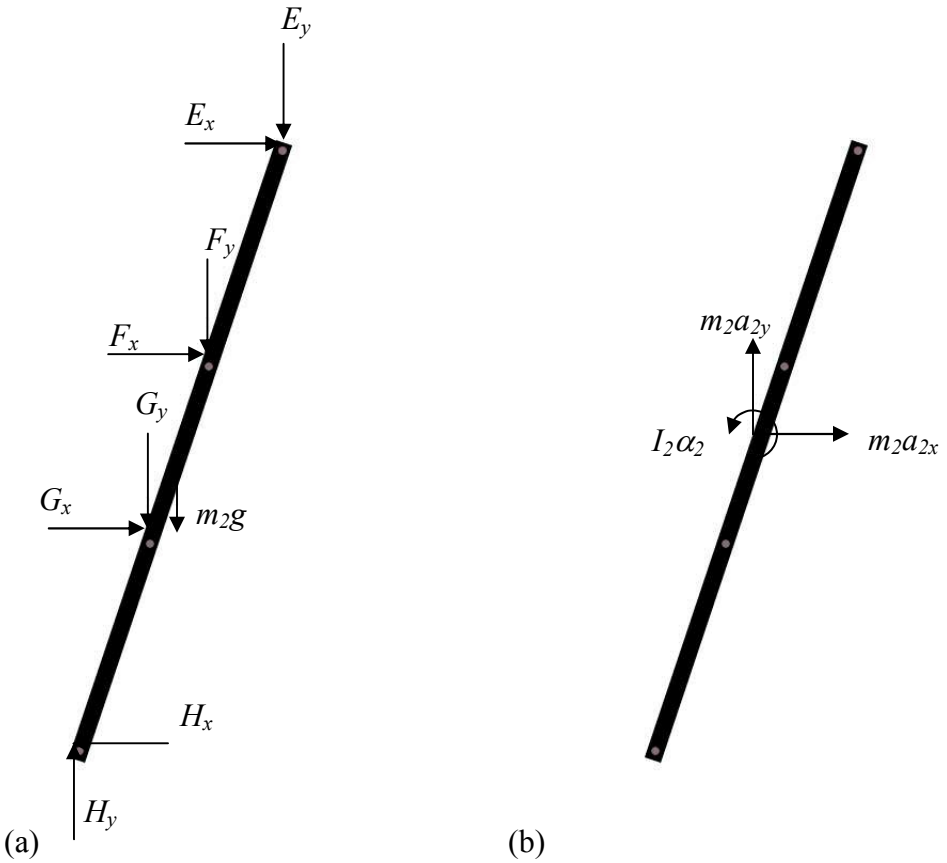

Figure 5.11: (a) Free-body diagram of member 2. (b) Kinetic diagram of member 2.

Summing the forces in the *x*-direction,

$$\sum F_x : m_1 a_{1x} = E_x + F_x + G_x - H_x \,. \tag{5.79}$$

Summing the forces in the *y*-direction,

$$\sum F_y : m_2 a_{2y} = -E_y - F_y - G_y + H_y - m_2 g \,. \tag{5.80}$$

Summing the moments about *H*,

$$\sum M_H : \frac{1}{3} m_2 \left(L_1 + L_2 + L_3\right)^2 \alpha_2 = -(G_x(L_1) + F_x(L_1 + L_2) + E_x(L_1 + L_2 + L_3))\cos\theta$$

$$+ (G_y(L_1) + F_y(L_1 + L_2) + E_y(L_1 + L_2 + L_3))\sin\theta + m_2 g \sin\theta\left(\frac{L_1 + L_2 + L_3}{2}\right), \tag{5.81}$$

where the acceleration of member 2 is given by

$$a_{2x} = \left(-\ddot{\theta}\cos\theta + \dot{\theta}^2 \sin\theta\right)\left(\frac{L_1 + L_2 + L_3}{2}\right) \tag{5.82}$$

and

$$a_{2y} = -\left(\ddot{\theta}\cos\theta + \dot{\theta}^2 \sin\theta\right)\left(\frac{L_1 + L_2 + L_3}{2}\right). \tag{5.83}$$

In addition to forcing from the pins there is a spring forcing the spring support, member 3. The free-body and kinetic diagrams for member 3 are shown in Figure 5.12.

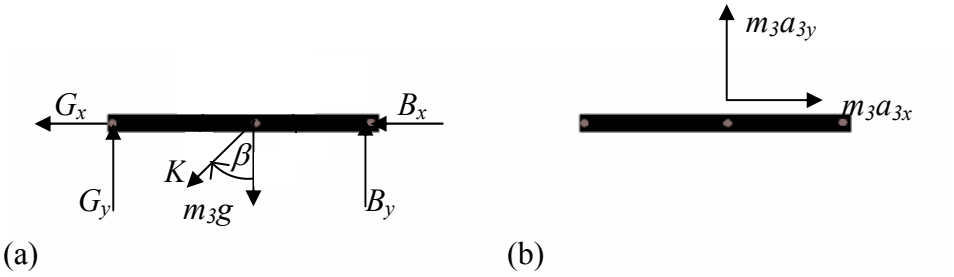

Figure 5.12: (a) Free-body diagram of member 3. (b) Kinetic diagram of member 3.

The force the spring in the Strutter exerts on member 3 when the Strutter rotates away from vertical is

$$\vec{\mathrm{K}} = -\mathrm{K}_x\,\vec{\mathrm{i}} - \mathrm{K}_y\,\vec{\mathrm{j}} \tag{5.84}$$

The angle at which the force of the spring $\vec{K}$ is exerted on member 3 is β in Figure 5.2 is

$$\beta = \tan^{-1}\frac{L_1 \sin\theta}{L_1 \cos\theta - h}. \tag{5.85}$$

The magnitude of the spring force is the spring constant, k times the stretch of the spring, Δx, substituting into eqn 5.84,

$$\vec{K} = k\Delta x \sin\beta\vec{i} - k\Delta x \cos\beta\vec{j} \,. \tag{5.86}$$

Summing the forces in the *x*-direction of Figure 5.12,

$$\sum F_x : m_3 a_{3x} = -B_x - G_x + K_x \,. \tag{5.87}$$

Summing the forces in the *y*-direction,

$$\sum F_y : m_3 a_{3y} = B_y + G_y - K_y - m_3 g \,. \tag{5.88}$$

Summing the moments about *B*,

$$\sum M_B : -m_3 a_{3y}\left(\frac{w}{2}\right) = -G_y(w) + m_3 g\left(\frac{w}{2}\right) + K_y\left(\frac{w}{2}\right), \tag{5.89}$$

where the acceleration of member 3 is given by

$$a_{3x} = \left(-\ddot{\theta}\cos\theta + \dot{\theta}^2 \sin\theta\right)(L_1) \tag{5.90}$$

and

$$a_{3y} = -\left(\ddot{\theta}\cos\theta + \dot{\theta}^2 \sin\theta\right)(L_1). \tag{5.91}$$

The force and acceleration diagrams for the handgrip, member 4 are shown in Figure 5.13

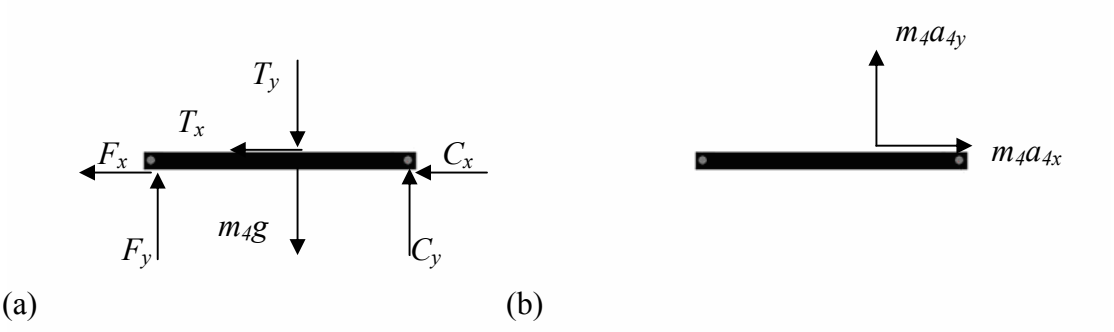

Figure 5.13: (a) Free-body diagram of member 4. (b) Kinetic diagram of member 4.

The external force acting on the centroid of the handgrip or member 4 is,

$$\vec{T} = -T_x \vec{i} - T_y \vec{j} \; . \tag{5.92}$$

Summing the forces in the *x*-direction,

$$\sum F_x : m_4 a_{4x} = -C_x - F_x - T_x \; . \tag{5.93}$$

Summing the forces in the *y*-direction,

$$\sum F_y : m_4 a_{4y} = C_y + F_y - T_y - m_4 g \; . \tag{5.94}$$

Summing the moments about C,

$$\sum M_C : -m_4 a_{4y} \left(\frac{w}{2} \right) = -F_y (w) + m_4 g \left(\frac{w}{2} \right) + T_y \left(\frac{w}{2} \right), \tag{5.95}$$

where the acceleration of member 4 is given by

$$a_{4x} = \left(-\ddot{\theta} \cos\theta + \dot{\theta}^2 \sin\theta \right) \left(L_1 + L_2 \right) \tag{5.96}$$

and

$$a_{4y} = -\left(\ddot{\theta} \cos\theta + \dot{\theta}^2 \sin\theta \right) \left(L_1 + L_2 \right). \tag{5.97}$$

The free-body diagram and kinetic diagram for member 5 are shown in Figure 5.14.

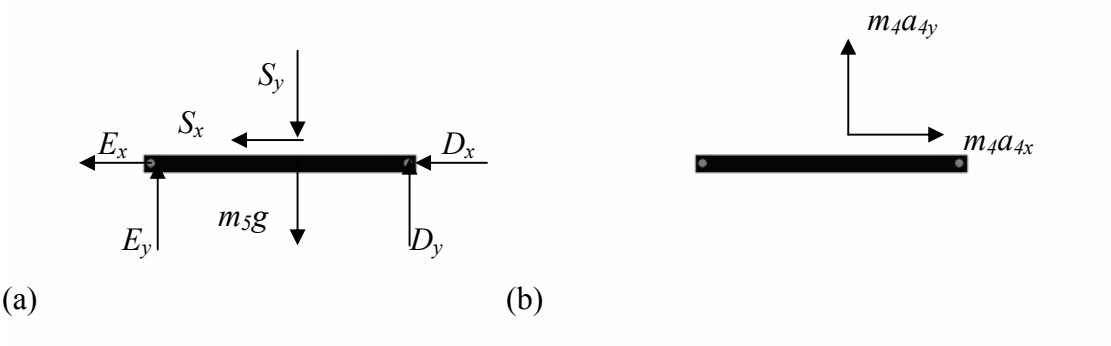

Figure 5.14: (a) Free-body diagram of member 5. (b) Kinetic diagram of member 5.

The external force acting at the centroid of the shoulder support, member 5 is,

$$\vec{S} = -S_x\vec{i} - S_y\vec{j}\,. \tag{5.98}$$

Summing the forces in the *x*-direction,

$$\sum F_x : m_5 a_{5x} = -D_x - E_x - S_x\,. \tag{5.99}$$

Summing the forces in the *y*-direction,

$$\sum F_y : m_5 a_{5y} = D_y + E_y - S_y - m_5 g\,. \tag{5.100}$$

Summing the forces about *D*,

$$\sum M_D : -m_5 a_{5y}\left(\frac{w}{2}\right) = -E_y(w) + m_5 g\left(\frac{w}{2}\right) + S_y\left(\frac{w}{2}\right), \tag{5.101}$$

where the acceleration of member 5 is

$$a_{5x} = \left(-\ddot{\theta}\cos\theta + \dot{\theta}^2\sin\theta\right)\left(L_1 + L_2 + L_3\right) \tag{5.102}$$

and

$$a_{5y} = -\left(\ddot{\theta}\cos\theta + \dot{\theta}^2\sin\theta\right)\left(L_1 + L_2 + L_3\right). \tag{5.103}$$

To solve for the pin reactions, eqn 5.89 is rearranged giving G_y,

$$G_y = \frac{1}{2}\left(m_3 a_{3y} + m_3 g + K_y\right). \tag{5.104}$$

Substituting eqn 5.104 into eqn 5.88 gives B_y,

$$B_y = \frac{1}{2}\left(m_3 a_{3y} + m_3 g + K_y\right), \tag{5.105}$$

therefore $B_y = G_y$. Rearranging eqn 5.95 gives F_y,

$$F_y = \frac{1}{2}\left(m_4 a_{4y} + m_4 g + T_y\right). \tag{5.106}$$

Substituting eqn 5.106 into eqn 5.94 gives C_y,

$$C_y = \frac{1}{2}\left(m_4 a_{4y} + m_4 g + T_y\right), \tag{5.107}$$

therefore $C_y = F_y$. Rearranging eqn 5.101 gives E_y,

$$E_y = \frac{1}{2}\left(m_5 a_{5y} + m_5 g + S_y\right). \tag{5.108}$$

Substituting eqn 5.108 into eqn 5.100 gives D_y,

$$D_y = \frac{1}{2}\left(m_5 a_{5y} + m_5 g + S_y\right), \tag{5.109}$$

therefore $D_y = E_y$. Substituting eqn 5.105, eqn 5.107 and eqn 5.107 into eqn 5.75 gives A_y,

$$A_y = \frac{1}{2}\left(m_3 a_{3y} + m_4 a_{4y} + m_5 a_{5y} + m_3 g + m_4 g + m_5 g + K_y + T_y + S_y\right)$$

$$+ m_1 g + m_1 a_{1y}\,. \tag{5.110}$$

Substituting eqn 5.104, eqn 5.106 and eqn 5.108 into eqn 5.80 eqn gives H_y,

$$H_y = \frac{1}{2}\left(m_3 a_{3y} + m_4 a_{4y} + m_5 a_{5y} + m_3 g + m_4 g + m_5 g + K_y + T_y + S_y\right) + m_2 a_{2y} + m_2 g \quad (5.111)$$

.

The pinned-pinned boundary conditions of the Strutter and prototype make the structure statically indeterminate because there are three equations of motion and four unknown reactions. Since ω is the same for members 1 and 2, the forces in the x-direction must be equivalent so assume that B_x equals G_x. Substituting this relationship into eqn 5.87,

$$B_x = G_x = \frac{1}{2}\left(-m_3 a_{3x} + K_x\right). \quad (5.112)$$

Also assume that C_x equals F_x. Solving eqn 5.93 gives,

$$C_x = F_x = \frac{1}{2}\left(-m_4 a_{4x} - T_x\right). \quad (5.113)$$

Setting D_x equal to E_x and substituting into eqn 5.99 gives,

$$D_x = E_x = \frac{1}{2}\left(-m_5 a_{5x} - S_x\right). \quad (5.114)$$

Substitute eqn 5.112, eqn 5.113, eqn 5.114 into eqn 5.74 gives A_x,

$$A_x = -m_1 a_{1x} + \frac{1}{2}\left(-m_3 a_{3x} + K_x - m_4 a_{4x} - T_x - m_5 a_{5x} - S_x\right) \quad (5.115)$$

Substitute eqn 5.112, eqn 5.113, eqn 5.114 into eqn 5.79 gives H_x,

$$H_x = -m_2 a_{2x} + \frac{1}{2}\left(-m_3 a_{3x} + K_x - m_4 a_{4x} + T_x - m_5 a_{5x} + S_x\right). \quad (5.116)$$

If the boundary conditions are relaxed to a pinned-rolling support, the forces in the *y*-direction are the same, however the reaction at the pinned support is then the sum of the reactions at A_x and H_x for the pinned-pinned boundary conditions. So it is possible for one of the pins to bear a force greater than that predicted here.

We are concerned with the worst case loading to consider the safety of the pins. Assume that a 200 lb user applies the same S_x given by eqn 5.67 with $W = 3$ and S_y given in eqn 5.65, the forces are repeated again here for convenience (Figure 5.15).

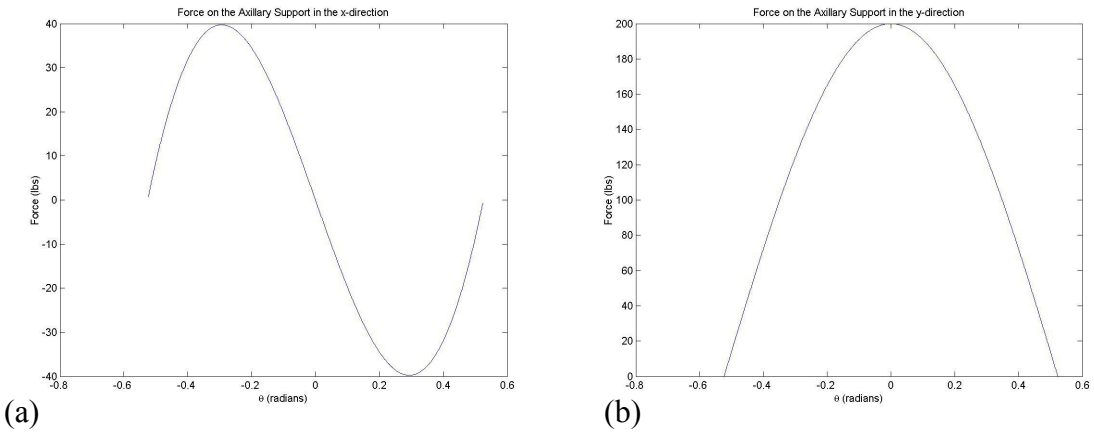

(a) (b)

Figure 5.15: External force at the shoulder support in the *x*-direction (a) and *y*-direction, (b).

Since the user initially supports a smaller amount of weight on the axillary support, the force in the *x*-direction required to begin motion is rather small. The force the user exerts on the axillary support in the *x*-direction can be from pushing on the ground with the feet during double support or from swinging the legs or torso during crutch stance. The external forces S_x and S_y cause $\dot{\theta}$ shown in Figure 5.6 for $W = 3$ and corresponding $\ddot{\theta}$ shown in Figure 5.16.

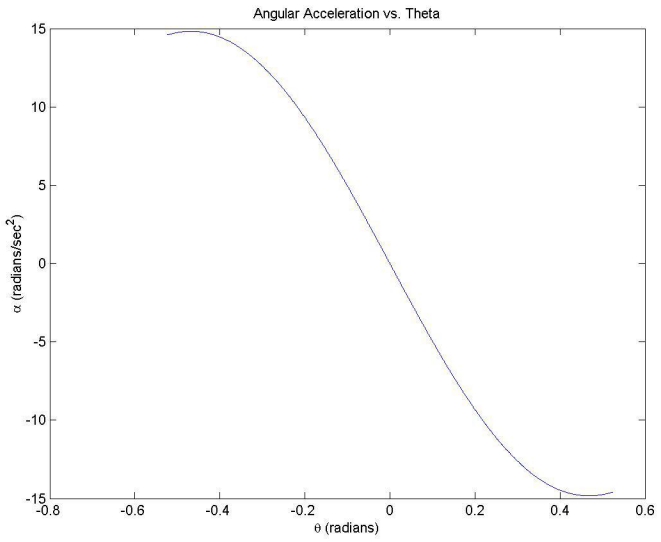

Figure 5.16: Angular acceleration of the Strutter for external forces shown in Figure 5.15.

The pin reactions are functions of the angular acceleration, $\dot{\theta}$ and the external forces. The pin reactions of the axillary support are at *D* and *E*. The pin reactions of *D* and *E* are assumed equal as in eqn 5.108, eqn 5.109 and eqn 5.114. The reaction in the *x*-direction and *y*-direction are shown in Figure 5.17. The reactions at the handgrip, pins *C* and *F* are also assumed equal as in equations eqn 5.106, eqn 5.107 and eqn 5.113. The pin reactions at the pin *C* or *F* are shown in Figure 5.18. Since it is assumed that there is no external forcing on the handgrip, the pin reactions are small. The spring support member (Figure 5.2) is forced by the spring, which is stretched when the Strutter is rotated from the vertical. The pin reactions for pins *B* or *G* are shown in Figure 5.19. The reactions at the footpad, pins *A* and *H* are also assumed equal as in equations eqn 5.110, eqn 5.115 and eqn 5.116. The reactions are shown in Figure 5.20.

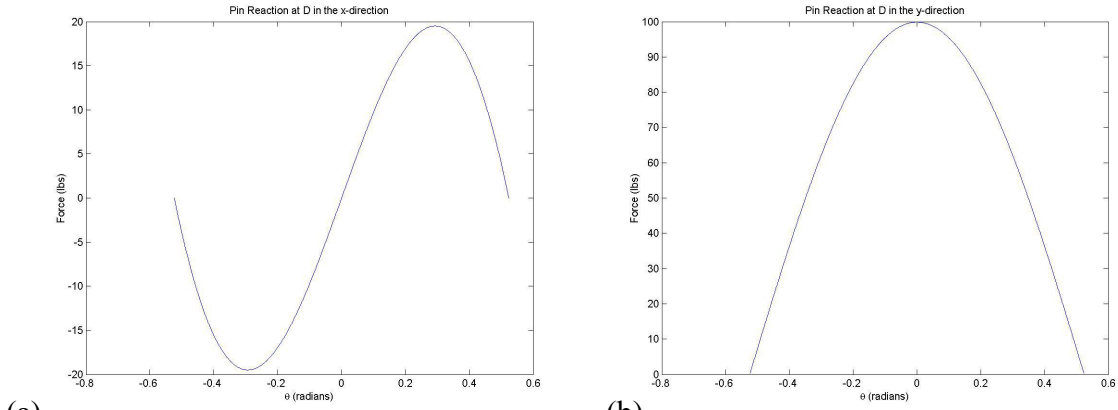

(a) (b)

Figure 5.17: Pin reactions at *D* in the *x*-direction (a) and the *y*-direction, (b).

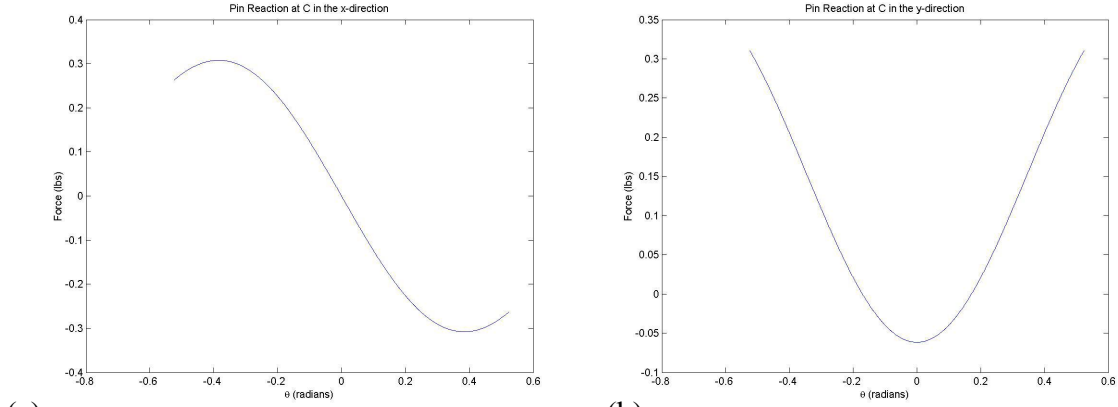

(a) (b)

Figure 5.18: Pin reactions at *C* in the *x*-direction (a) and the *y*-direction (b).

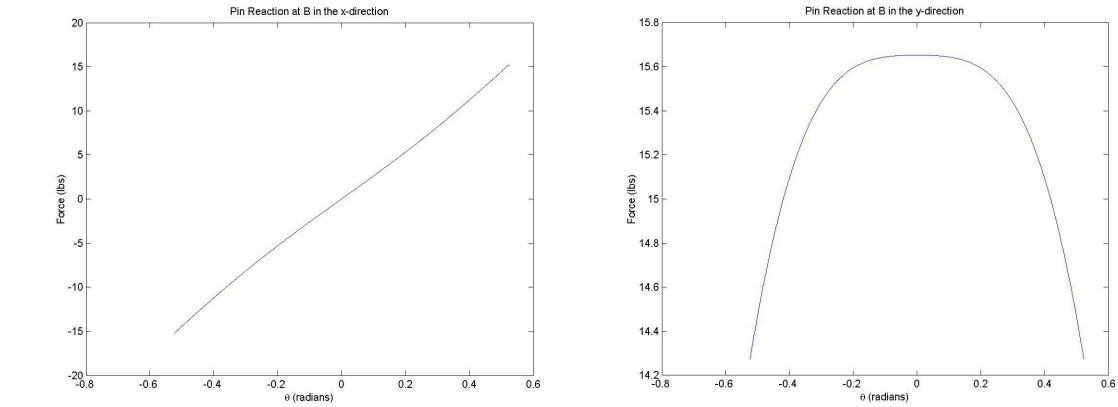

(a) (b)

Figure 5.19: Pin reactions at *B* in the *x*-direction (a) and the *y*-direction (b).

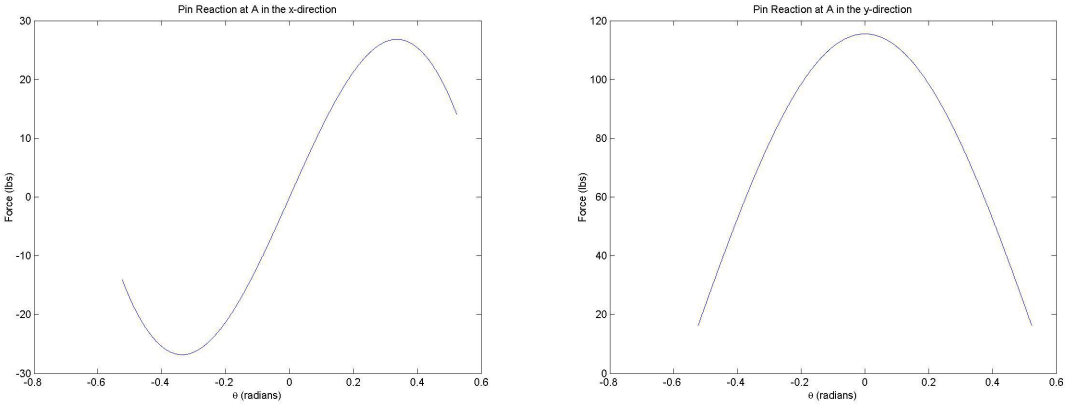

(a) (b)

Figure 5.20: Pin reactions at A in the x-direction (a) and the y-direction (b).

The previous example is of an optimized gait, where the user does not bear the entire body weight on the axillary support for the entire range of motion of the Strutter. Now S_y is considered a constant 200 lbs. This represents the device holding a user's entire body weight through the entire stride. Using eqn 5.67 with $W = 3$ again, gives a stride time of 0.55 s.

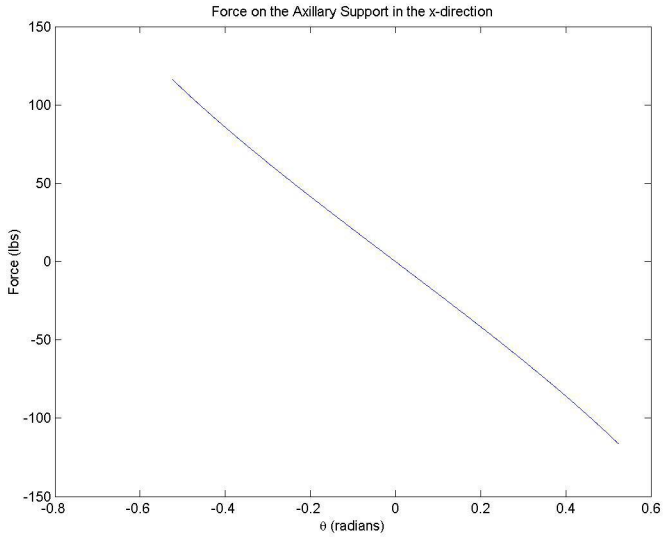

Figure 5.21: Force in the x-direction at the axillary support.

This forcing configuration gives $\ddot{\theta}$ and $\dot{\theta}$ equal to that found previously, $\ddot{\theta}$ and ω are shown again for convenience (Figure 5.22).

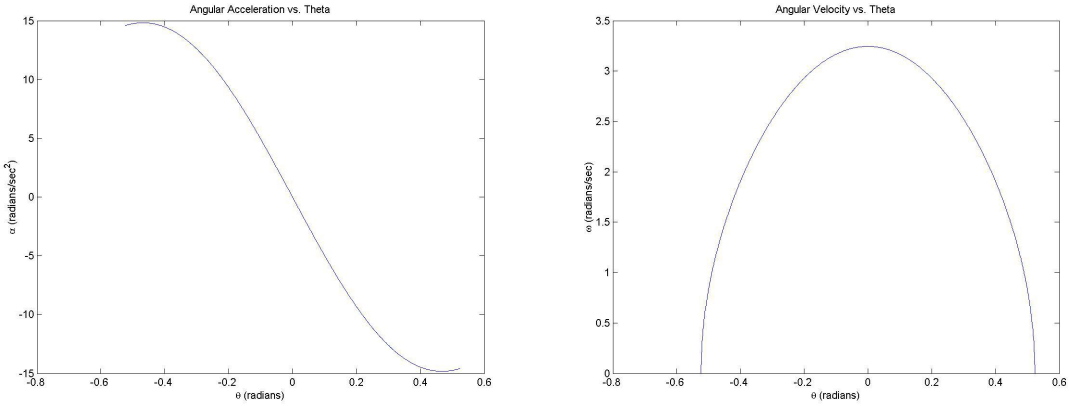

(a) (b)

Figure 5.22: Angular acceleration (a) and $\dot{\theta}$ resulting from the forcing of Figure 5.21.

The pin reactions at *D* are shown in Figure 5.23. The maximum reaction in the *x*-direction is 3 times greater than the reaction at *D* for the previous loading shown in Figure 5.17 and the reaction in the *y*-direction is about the same. The maximum occurs at $\theta = \pm\pi/6$ because the inertial force is highest at that point in the *y*-direction. The reactions at the pins *C* or *F* are the same as in Figure 5.18. The reactions at the pins *B* or *G* are the same as in Figure 5.19. The reactions at pins *A* or *H* are shown in Figure 5.24.

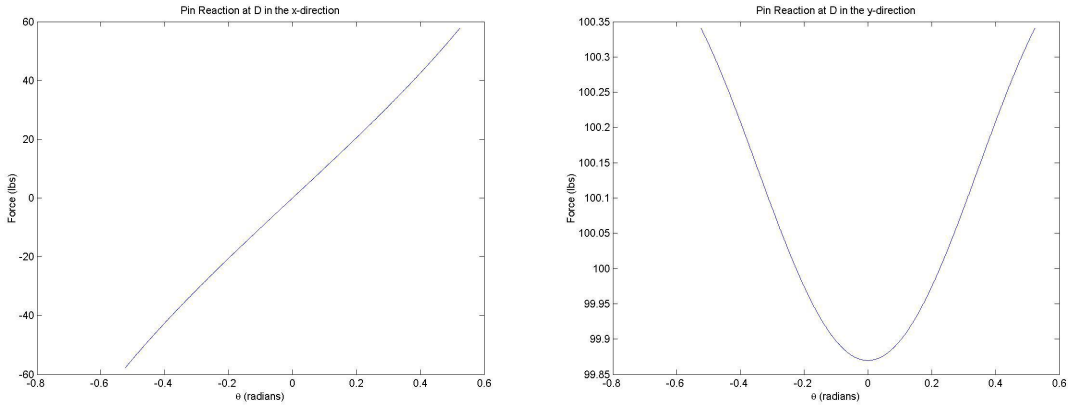

Figure 5.23: Pin reactions at *D* in the *x*-direction (a) and in the *y*-direction (b) for the forcing of Figure 5.21.

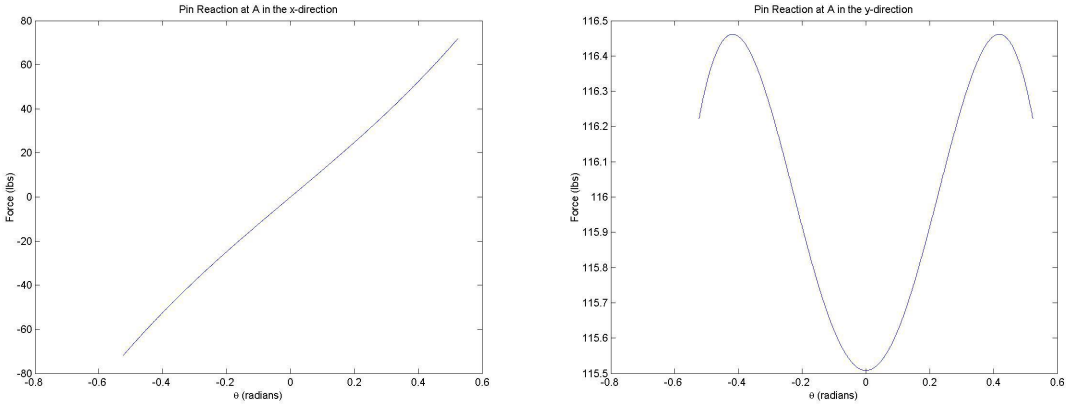

Figure 5.24: Pin reaction at *A* in the *x*-direction (a) and in the *y*-direction (b) for the forcing of Figure 5.21.

The pin reactions at *A* are 2.5 times as great as the reactions at *A* in the *x*-direction for the previous loading and approximately the same in the *y*-direction.

By the superposition principle the minimum pin diameter to prevent yielding can be calculated by assuming a force of 200 lbs. (sum of the reactions in the *x* and *y* directions at *A* or *H*). The minimum pin diameter can be calculated by assuming the pin is a pinned-roller connection as in Figure 5.25.

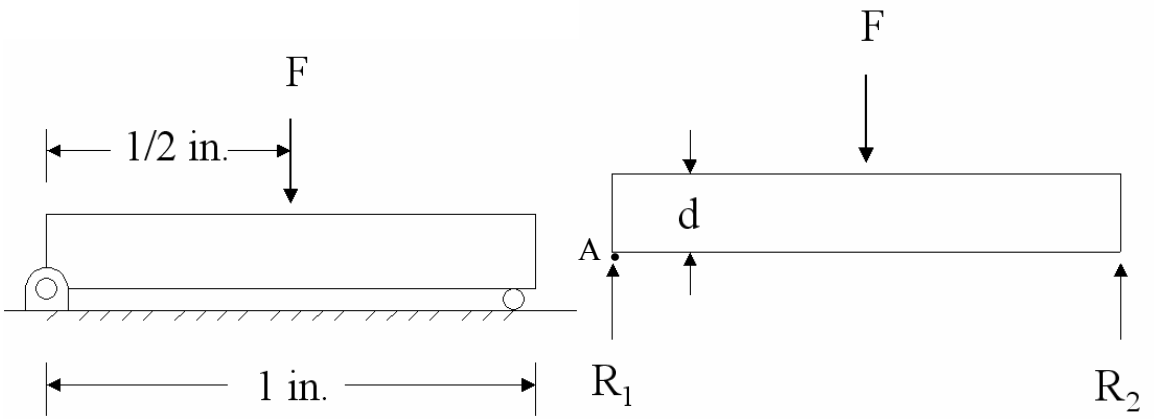

Figure 5.25: Free body diagram of the pin at *A* and *H* in the Strutter.

To solve for the pin reactions where $F = 200$ lbs the moments are summed at point A,

$$\sum M_A = 0 : R_2 L - \frac{1}{2} FL = 0 , \tag{5.117}$$

which gives $R_2 = 100$ lbs Summing the forces in the y-direction,

$$\sum F_y = 0 : R_1 + R_2 - F = 0 , \tag{5.118}$$

gives $R_1 = 100$ lbs Cutting the beam (Figure 5.26),

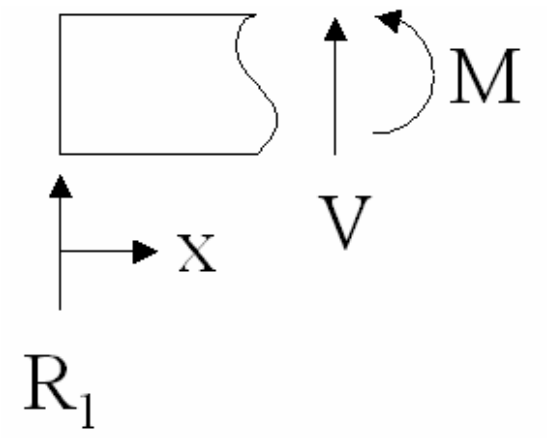

Figure 5.26: Cut section of the beam from Figure 5.25.

and solving for the maximum moment about the point of the cut,

$$\sum M = 0 : M(x) + R_1 x . \tag{5.119}$$

So the maximum moment $M = -R_1 x$ occurs at $x = L/2$. The maximum moment is equal to 50 in-lbs when $R_1 = 100$ lbs The axial stress for a member in bending is

$$\sigma = \frac{My}{I} . \tag{5.120}$$

Solving for the diameter of a member with a circular cross section,

$$d^3 = \frac{16M}{\pi\sigma} , \tag{5.121}$$

where $I = \pi d^4/32$. For a 200 lb user to have a safety factor of 2, $M = 100$ in-lbs. using 6063-T832 aluminum which has a yield strength of 39,000 psi the minimum pin diameter is 0.245 in.

When the user applies their full body weight on the shoulder support of one Strutter, the pin reaction in *y*-direction at the footpad can be as large as 1.15 times the body weight and the pin reaction in the *x*-direction can be as large as 0.60 times the body weight if the user has a stride time of 0.55 s. Loadings where the full weight bearing is not present for all θ but increases to full weight bearing around $\theta = 0$ reduces the reaction in the *x*-direction but the reaction in the *y*-direction is the same. Also more rapid accelerations of the Strutter increases the pin reactions and put higher stress on the members i.e. accelerations reached during a fall or loss of control.

5.6 Discussion

The pin reactions for the Strutter are found as a function of θ, $\dot{\theta}$, $\ddot{\theta}$ and the external forces. The angular acceleration and angular velocity are found as a function of θ and the external forces. The stride time is found as a function of the external forces. The stride time of the Strutter is dependent on the forces in the normal and tangential direction, whereas axillary crutches are dependent on the forces in the tangential direction. The maximum force in the tangential direction is larger for the Strutter than axillary crutches when they have the same stride time except when the Strutter is used for minimal weight bearing. This is because the Strutter is not rigid and the larger the weight bearing on the axillary support, the larger the tangential force must be for the Strutter to have the same stride time as axillary crutches. It appears that perceived comfort is not a function of tangential forces or total force but rather a function of the normal force on the axillary

support since the users rated the Strutter more comfortable than axillary crutches (chapter 4).

6 Force Impulse Transmission to the Underarm

During initial contact of the footpad of an orthosis with the ground the orthosis transmits a force to the user's underarm and/or hands. This force should be minimized through design of the device to prevent injury to the user's axillary region. In order to do so, the acceleration ratio of the orthosis must be modeled mathematically. The acceleration ratio is used to find the force transmitted to the underarm of a user. In this chapter the feasibility of modeling the acceleration ratio of the mini-Strutter and the prototype as a single degree of freedom (SDOF) system is explored.

6.1 Experimental Frequency Response Function

To find the acceleration ratio, the orthoses are subjected a harmonic excitation of the base using a shaker table. The shaker table is controlled by the Hewlett Packard (HP) Dynamic Signal Analyzer 35665A (Figure 6.1). The dynamic analyzer sends a signal to an amplifier, which excites the shaker at a random frequency. The acceleration at the base (excitation) and the shoulder support (response) are captured with accelerometers that are secured using reusable adhesive wax. The acceleration ratio is the ratio of the magnitude of the response over the magnitude of the excitation.

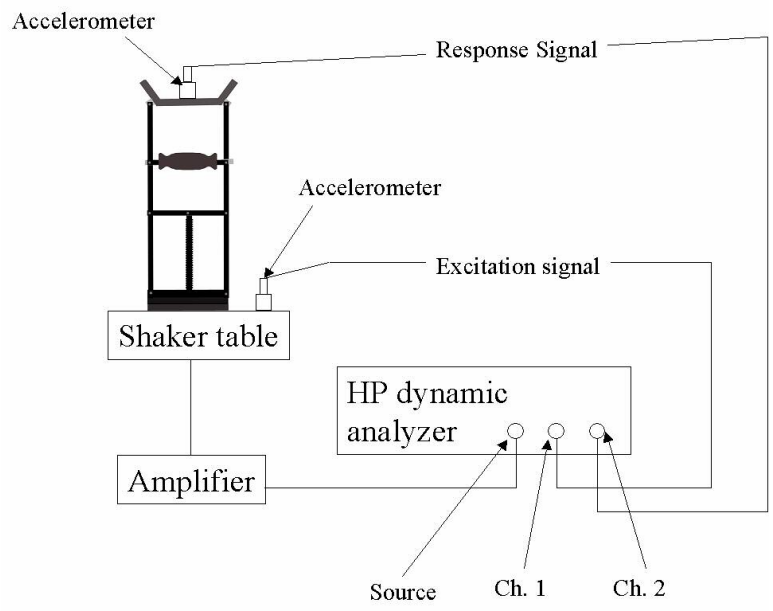

Figure 6.1: Experimental setup.

A fixture is used to connect the orthoses to the shaker table. The orthoses are secured to the fixture by passing two (2) screws through the lower u-channel. The orthoses can be secured to the fixture with the shock absorbing pad and footpad or without the shock absorbing pad and footpad. A close up of the Strutter secured to the fixture with and without the shock absorber or footpad is shown in Figure 6.2. When the orthoses are mounted without the shock absorber or footpad, aluminum spacers are used, as shown.

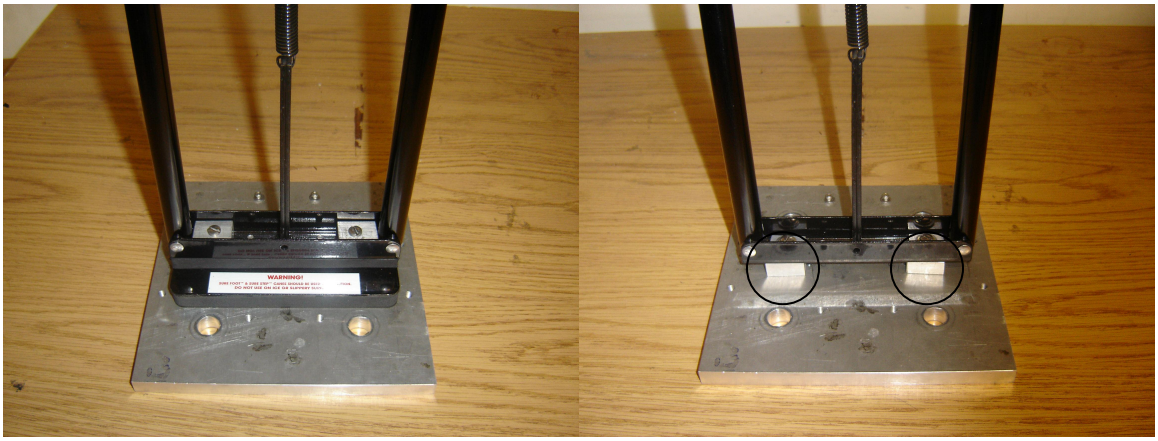

(a) (b)

Figure 6.2: Side view of the mini-Strutter secured to the fixture with the footpad and shock absorber (a) and with aluminum spacers (circled) used in place of the footpad and shock absorber (b).

The prototype and the mini-Strutter have shock absorbing materials below both of the respective axillary supports. The damping material of the mini-Strutter sits between the axillary support and the cantilevered support. The cantilevered axillary support of the mini-Strutter positions the axillary support outside of the plane of the parallelogram whereas the prototype's axillary support lies in the plane. The mini-Strutter has rubber gaskets, and the prototype has a shock absorbing pad (Figure 6.3) as well as dampers inside of the aluminum boxes on top of the damper.

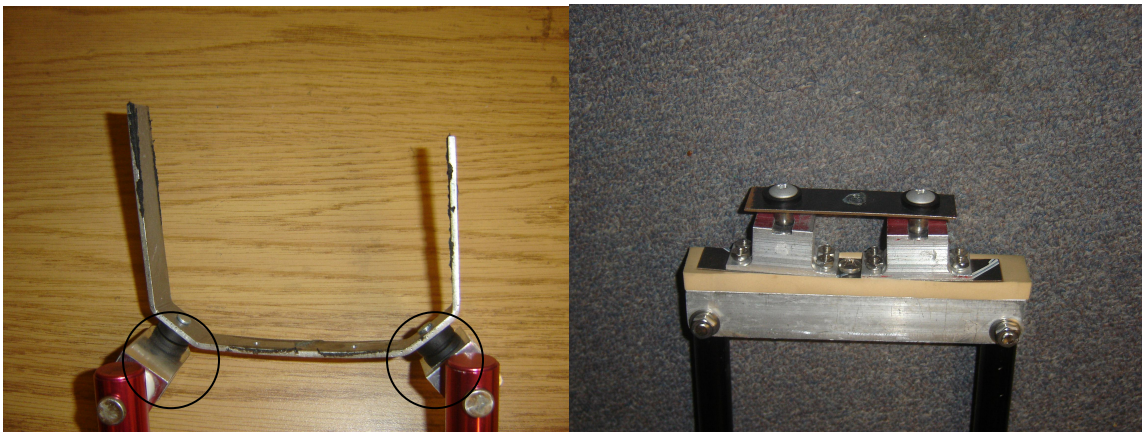

(a) (b)

Figure 6.3: Shock absorbing gasket circled on the mini-Strutter (a) and prototype with shock absorbing axillary support (shock absorber is yellow and there are also dampers in the two boxes) (b).

The vertical support member of the mini-Strutter has one tube inside of the other. The outer tube has 12 holes evenly spaced, 1 inch apart. To adjust the height of the device, the outer tube slides up and down the inner tube until a pin fits into the desired hole. People can use the mini-Strutter with underarm heights ranging from 2 feet to 3 feet from the ground. When the mini-Strutter is adjusted to the tallest height, the outer tube is completely above the inner tube. The mini-Strutter's acceleration ratio is measured with the orthosis setup in the shortest configuration, 2 feet and the tallest, 3 feet. The prototype is 3 feet and 7.5 inches tall and the height is not adjustable.

The assistive devices are tested without the shock absorber and footpad and with the shock absorber and footpad (Figure 6.2). Gillespie and Dickey (2003) claim that the frequency content of the initial ground reaction force when the heel of a subject walking barefooted strikes a force plate extends up to 400 Hz. Therefore, the orthoses are tested between the frequencies 0 and 400 Hz. The measured magnitude of the acceleration ratio and phase of the mini-Strutter at the shortest and tallest height and the Prototype are shown in Figure 6.4, Figure 6.5 and Figure 6.6 respectively. The phase angle is the

distance on the x-axis that the response leads the excitation. If the base of the orthosis is excited with a displacement of $y(t) = A\sin(\omega t)$, then the response will be of the form $x(t) = A\sin(\omega t + \phi)$, where ϕ is the phase angle.

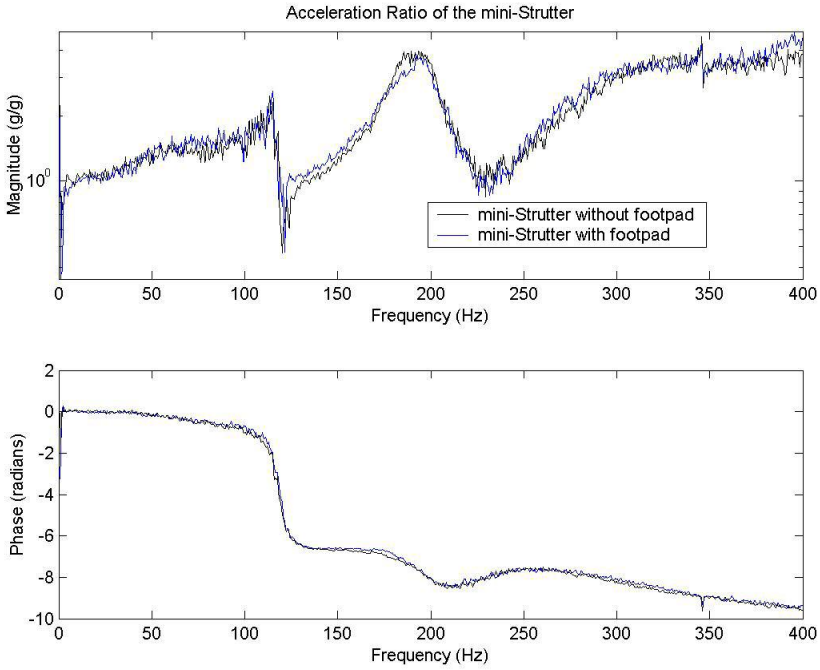

Figure 6.4: Magnitude and phase of the acceleration ratio of the mini-Strutter with a height of 24 inches in the range of 0-400 Hz.

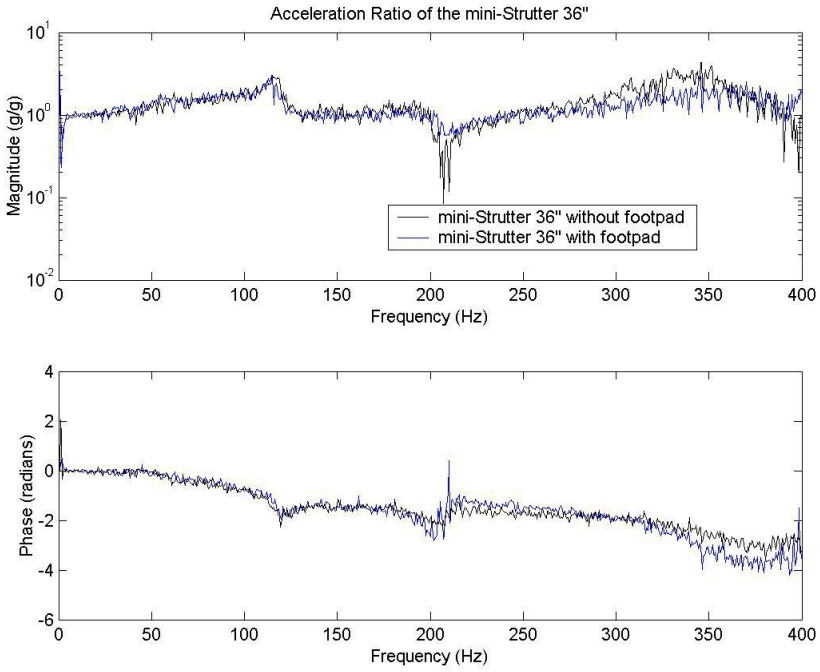

Figure 6.5: Magnitude and phase of the acceleration ratio of the mini-Strutter with a height of 36 inches in the range of 0-400 Hz.

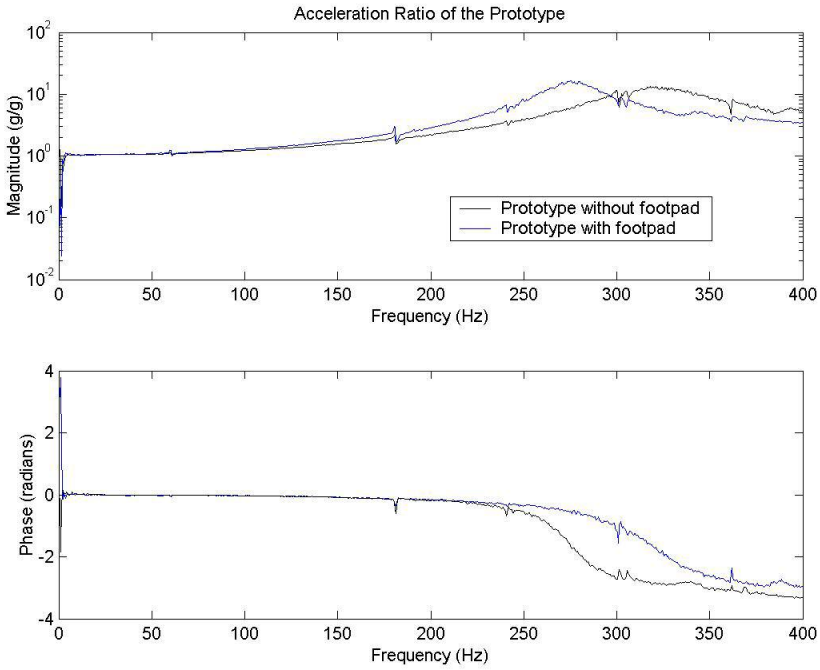

Figure 6.6: Magnitude and phase of the acceleration ratio of the Prototype in the range of 0-400 Hz.

Examining the response of the orthoses, we can tell if the data will lend itself to being modeled as a SDOF system. The details of a SDOF system will be elaborated further in the next section. For now it is enough to know the characteristic features include a sharp increase in the magnitude of the acceleration. The frequency where the magnitude has a sharp increase is called resonance. Before resonance, the response is in phase with the excitation. At resonance, the response is 90 degrees out of phase with the excitation and then for higher frequencies, the response is 180 degrees out of phase with the excitation.

The mini-Strutter at 24 inches (Figure 6.4) reaches response maximums at 113 Hz and at approximately 200 Hz. The response changes phase 180 degrees near 113 Hz but only 98 degrees around 200 Hz. The mini-Strutter at 36 inches does not appear to have a sufficient change in phase to demark a resonant frequency in the range of 0 to 400 Hz, although it is probable that the system has resonant frequencies near that of the mini-Strutter at 24 inches since the mini-Strutter at 36 inches has a smaller phase change at approximately the same frequency as the mini-Strutter at 24 inches, a phase change of 82 degrees around 116 Hertz and a phase change of 64 degrees around 210 Hertz.

As can be seen in Figure 6.4 and Figure 6.5, the shock absorber and footpad appear to have little effect on the response of the mini-Strutter compared to the prototype. The prototype exhibits behavior similar to that of a SDOF system, it has a sharp increase in magnitude and the phase changes 180 degrees around the increase. Also the additional shock absorber on the Prototype has the effect of decreasing the resonant frequency and increasing the response at resonance (Figure 6.6). This is consistent with decreasing the damping factor on a SDOF system. So it appears that it may be possible to model the

prototype as a SDOF system. The results are summarized in Table 6.1. The response of the prototype is much larger than the mini-Strutter at either height, possibly because the prototype is more rigid than the mini-Strutter from the lack of height adjustment holes and the upper and lower u-channels. A u-channel is used to mount the axillary support on top and the footpad on the bottom of the Strutter. Both the mini-Strutter and prototype use this method, however the u-channel on the prototype is twice as thick as the one on the mini-Strutter. The response of the mini-Strutter is not restricted to the direction of the excitation.

Magnitude and Frequency at Resonance

Device	Footpad	Height (in.)	Magnitude (g/g)	Frequency (Hz)
Mini Strutter	No	24	2.4605	113.5
	Yes	24	2.5875	115
Mini Strutter	No	36	4.3364	345.5*
	Yes	36	3.0125	114.5*
Prototype	No	43.5	13.3145	321
	Yes	43.5	16.469	275.5

Table 6.1: Magnitude and resonant frequency of the acceleration ratio of the assistive devices in the range of 0-400 Hz. *These are maximum values; these may/may not be a resonant frequency.

For a SDOF system, the frequency where a maximum or resonance occurs is inversely proportional to the mass. If the effect of a user increasing weight bearing on the axillary support of an orthoses can be modeled as an increasing inertial mass, then the effect is to lower the frequency where resonance occurs. So resonant frequencies that occur just above the range of interest could enter the range of interest for larger weight bearing requirements. In order to adequately characterize the systems, resonant frequencies above 400 Hz need to be considered. The response of the orthoses without the shock absorber and footpad are examined between the frequencies 0 and 1600 Hz. The magnitude and phase of the acceleration ratio for the mini-Strutter at a height of 24

inches and 36 inches and the prototype are shown in Figure 6.7, Figure 6.8 and Figure 6.9 respectively.

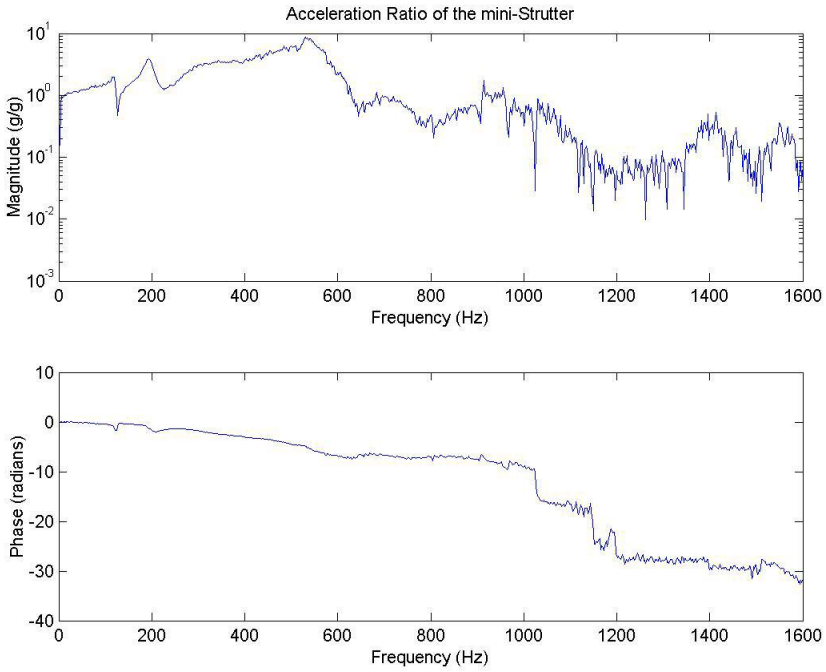

Figure 6.7: Magnitude and phase of the acceleration ratio of the mini-Strutter with a height of 24 inches in the range of 0-1600 Hz.

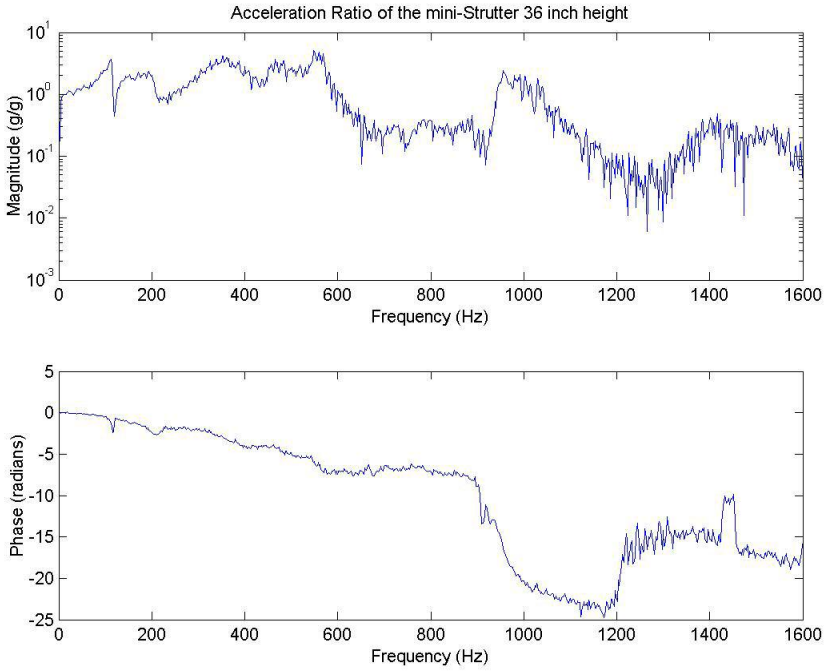

Figure 6.8: Magnitude and phase of the acceleration ratio of the mini-Strutter with a height of 36 inches in the range of 0-1600 Hz.

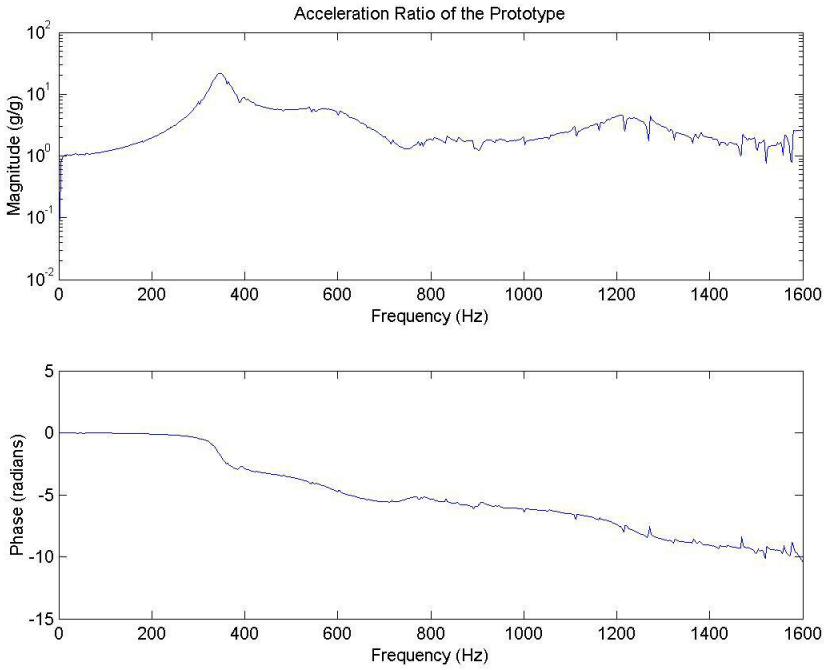

Figure 6.9: Magnitude and phase of the acceleration ratio of the prototype in the range of 0-1600 Hz.

The prototype has no resonant frequencies above the one at about 350 Hz. The mini-Strutter at 24 and 36 inches both appear to potentially have resonant frequencies around 100 Hz, 200 Hz, 350 Hz, 550 Hz and 1000 Hz. The response characteristics of the mini-Strutter at the 24 and 36 inch heights make it nearly impossible to model the systems as a SDOF system. In addition, the application of a greater load to the axillary support can potentially decrease the frequency where resonance occurs. So the mini-Strutter could potentially have multiple resonant frequencies in the range of interest. Multiple resonant frequencies will likely decrease user comfort. The response characteristics of the prototype make it an excellent candidate for modeling as a SDOF system as will be shown in the subsequent section.

6.2 Model for the force transmitted to the underarm for a SDOF system

To estimate the parameters of the orthosis, a theoretic acceleration ratio is curve fit to the experimental data. The simplest model is a SDOF system as shown in Figure 6.10. Adjusting the spring constant, k, the damping, c and mass, m, will cause the device to transmit varying amounts of the force to the user's underarm.

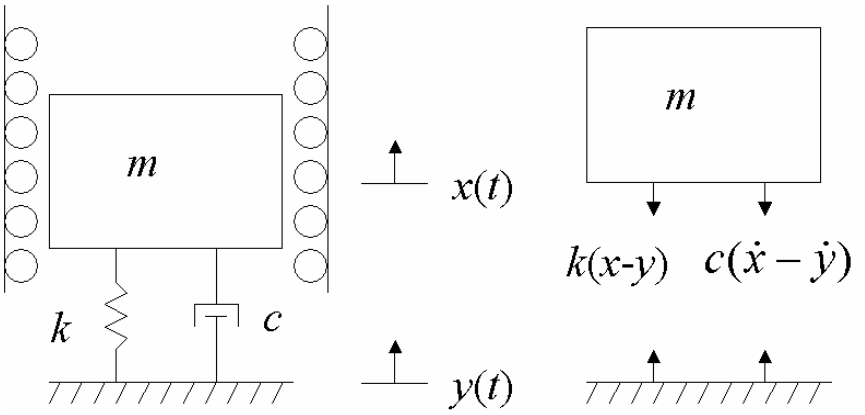

Figure 6.10: SDOF system subject to base excitation.

The equation of motion of a SDOF system mass, spring and damper system is

$$m\frac{d^2x}{dt^2} + c\frac{dx}{dt} + kx = c\frac{dy}{dt} + ky\,, \tag{6.1}$$

where m is the mass, c the coefficient of viscous damping, k the spring constant, $x(t)$ the displacement of the mass and $y(t)$ the displacement of the base. Assuming harmonic excitation of the base of the form

$$y(t) = Y\sin(\omega t), \tag{6.2}$$

and substituting the excitation into the equation of motion (6.1) gives

$$m\frac{d^2x}{dt^2} + c\frac{dx}{dt} + kx = c\omega Y\cos(\omega t) + kY\sin(\omega t). \tag{6.3}$$

Using trigonometric identities, the right hand side of eqn 6.3 can be re-written as

$$Y\sqrt{k^2 + (c\omega)^2}\,\sin(\omega t - \phi), \tag{6.4}$$

where

$$\phi = \tan^{-1}\left(-\frac{c\omega}{k}\right). \tag{6.5}$$

The response is assumed to be of the form

$$x(t) = C_1\sin(\omega t - \phi) + C_2\cos(\omega t - \phi). \tag{6.6}$$

Substituting the assumed response (6.6) and excitation (6.4) into the equation of motion (6.1), gives

$$\left[\left(k-m\omega^2\right)C_1-c\omega C_2\right]\sin(\omega t-\phi)+\left[\left(k-m\omega^2\right)C_2+c\omega C_1\right]\cos(\omega t-\phi)$$

$$=Y\sqrt{k^2+(c\omega)^2}\,\sin(\omega t-\phi). \tag{6.7}$$

Equating the coefficients of $\sin(\omega t - \phi)$ and $\cos(\omega t - \phi)$ and writing the equations in matrix form as

$$\begin{bmatrix}\left(k-m\omega^2\right) & -c\omega \\ c\omega & \left(k-m\omega^2\right)\end{bmatrix}\begin{bmatrix}C_1\\C_2\end{bmatrix}=\begin{bmatrix}Y\sqrt{k^2+(c\omega)^2}\\0\end{bmatrix}. \tag{6.8}$$

The solution of eqn 6.8 gives the coefficients C_1 and C_2,

$$C_1=\frac{\left(k-m\omega^2\right)Y\sqrt{k+(c\omega)^2}}{\left(k-m\omega^2\right)^2+(c\omega)^2}, \tag{6.9}$$

and

$$C_2=\frac{c\omega Y\sqrt{k+(c\omega)^2}}{\left(k-m\omega^2\right)^2+(c\omega)^2}. \tag{6.10}$$

Substituting eqn 6.9 and eqn 6.10 in to the assumed solution for $x(t)$, eqn 6.6 gives

$$x(t)=\frac{Y\sqrt{k+(c\omega)^2}}{\left(k-m\omega^2\right)^2+(c\omega)^2}\left[\left(k-m\omega^2\right)\sin(\omega t-\phi)+c\omega\cos(\omega t-\phi)\right]. \tag{6.11}$$

Using trigonometric identities eqn 6.11 can be rewritten as

$$x(t)=\frac{Y\sqrt{k+(c\omega)^2}}{\sqrt{\left(k-m\omega^2\right)^2+(c\omega)^2}}\sin(\omega t-\phi-\alpha), \tag{6.12}$$

where

$$\alpha=\tan^{-1}\left(\frac{c\omega}{k-m\omega^2}\right). \tag{6.13}$$

The phase angles ϕ and α are combined into one term

$$\psi = \phi - \alpha = \tan^{-1}\left(\frac{mc\omega^3}{k\left(k - m\omega^2\right) + \left(c\omega\right)^2}\right). \tag{6.14}$$

using the relation,

$$\tan^{-1} x \pm \tan^{-1} y = \tan^{-1} \frac{x \pm y}{1 \mp xy}. \tag{6.15}$$

Equation 6.12 can now be rewritten as

$$x(t) = \frac{Y\sqrt{k + \left(c\omega\right)^2}}{\sqrt{\left(k - m\omega^2\right)^2 + \left(c\omega\right)^2}} \sin\left(\omega t - \psi\right). \tag{6.16}$$

The magnitude of the displacement ratio is defined as the magnitude of eqn 6.16 divided by the magnitude of the excitation,

$$\frac{|x(t)|}{Y} = \frac{\sqrt{k + \left(c\omega\right)^2}}{\sqrt{\left(k - m\omega^2\right)^2 + \left(c\omega\right)^2}}. \tag{6.17}$$

Equation 6.17 is fit to experimental data in the next section to find the system parameters, the mass, *m* the spring constant, *k* and the damping, *c*.

6.3 System Design

The system parameters of the prototype are estimated using the least squares method. The Matlab program lsqnonlin is used with the experimental data shown in Figure 6.6 and the theoretical acceleration ratio magnitude (6.17). The estimates of system parameters for the prototype are shown in Table 6.2.

Prototype Parameters		
	w/o footpad	**w/ footpad**
k (lb/ft)	599940	599916
c (lb-s/ft)	20.171	19.429
m (lb-s^2/ft)	0.144	0.197
ζ (dimensionless)	0.034	0.028

Table 6.2: Estimate of the prototype's parameters.

In Table 6.2 all of the system parameters are affected by adding the footpad and damper, however the damping factor decreases. When adding dampers in series, the second damper must be much larger than the first damper to increase the equivalent damping of the system,

$$c_{eq} = \left(\frac{1}{c_1} + \frac{1}{c_2} \right)^{-1} = \frac{c_1 c_2}{c_1 + c_2}. \tag{6.18}$$

It will be shown in this section that the force transmitted is a function of the damping factor,

$$\zeta = \frac{c}{2\sqrt{km}}. \tag{6.19}$$

A study of different shock absorbers and footpads could be used to create a "toolbox" of footpad/damper combinations that can be fit for different weight bearing requirements. The experimental acceleration ratio of the prototype with and without the footpad is shown in Figure 6.11, with the curve fit.

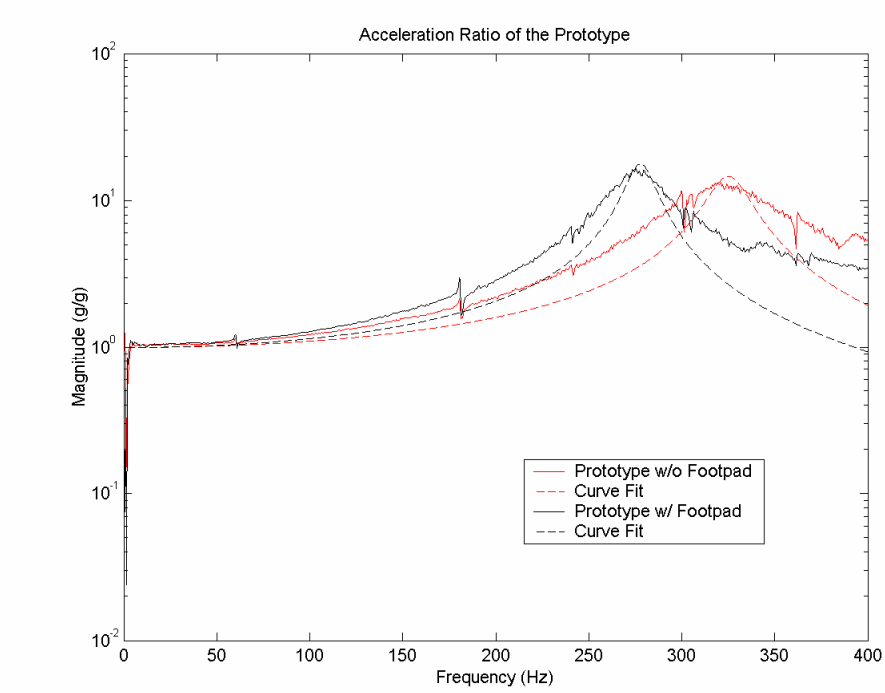

Figure 6.11: Experimental magnitude and phase of the acceleration ratio for the prototype with and without the shock absorber and footpad. Equation 9.17 is fit to the data in Table 6.2.

To find the transmissibility, assume that initial contact of the footpad with the ground occurs while $\theta = 0$ (Figure 5.1) and that the orthosis drops a distance h, at which time the stiffness, k and damping element, c contact the ground. Let x denote the displacement of the mass, m after contact with the ground. The vertical acceleration, a of the orthosis before initial contact is user controlled and is not the acceleration of the mass after contact (Figure 6.12).

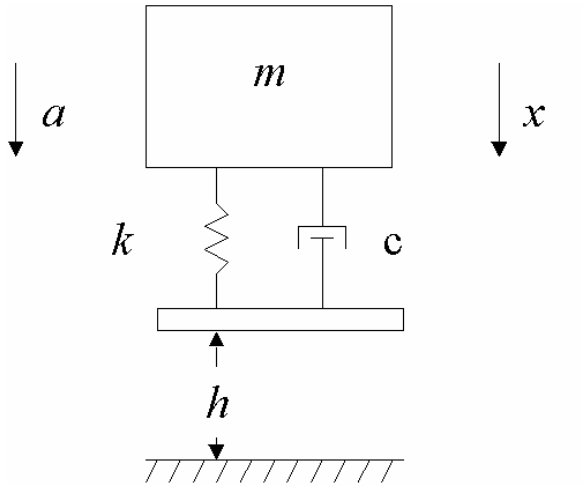

Figure 6.12: Model of orthosis initial contact with the ground.

The velocity of the inertial mass at the time of contact can be determined from conservation of energy,

$$mah = \frac{1}{2}mv^2 . \tag{6.20}$$

The free body diagram of the system after contact with the ground is shown in Figure 6.13.

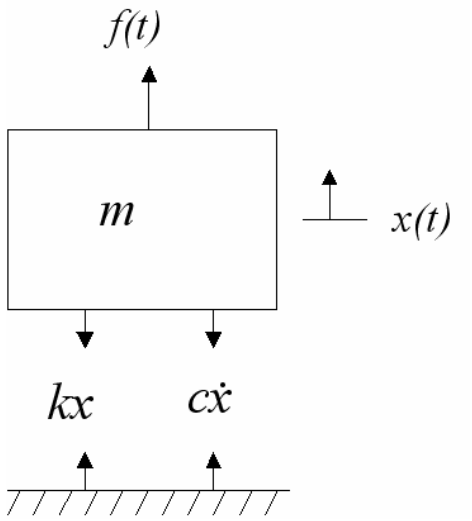

Figure 6.13: Free body diagram of a SDOF system subject to harmonic forcing.

The equation of motion for the system is given by,

$$m\ddot{x} + c\dot{x} + kx = f(t), \tag{6.21}$$

assuming that the footpad remains in contact with the ground after the initial contact. Equation 6.21 is solved using Laplace transforms. The Laplace transform of a time dependent function $z(t)$ is defined as

$$Z(s) = \int_0^\infty z(t)e^{-st}dt, \tag{6.22}$$

where s is in general a complex variable and has the form $s = x + iy$. This is the one-sided transform, which assumes that $z(t)$ is zero for $t<0$. The integral in eqn 6.22 is a transformation from the time domain to the s domain. The integral is a one-to-one transformation, there is no function $g(t)$ different from $z(t)$ that has $Z(s)$ as its Laplace transform. Tables of Laplace transforms are readily available. A convenient feature of the Laplace transform is that if the variable $s = i\omega$, the transformation is from the time domain to the frequency domain.

Applying the Laplace transform to eqn 6.21 and assuming that $f(t) = 0$ gives,

$$m\int_0^\infty \ddot{x}e^{-st}dt + c\int_0^\infty \dot{x}e^{-st}dt + c\int_0^\infty xe^{-st}dt = 0. \tag{6.23}$$

Performing the integration gives,

$$m\left[s^2X(s) - sx(0) - \dot{x}(0)\right] + c\left[sX(s) - x(0)\right] + kX(s) = 0. \tag{6.24}$$

Rearranging eqn 6.24,

$$ms^2X(s) + csX(s) + kX(s) = x(0)\left[ms + c\right] + m\dot{x}(0). \tag{6.25}$$

Assume *x(0) = 0* and $\dot{x}(0) = 1/m$ (for convenience) then eqn 6.25 is equal to,

$$ms^2X(s) + csX(s) + kX(s) = 1. \tag{6.26}$$

If we assume that the initial conditions are zero and *f(t)* is the unit impulse then the Laplace transform of eqn 6.21 is,

$$ms^2X(s) + csX(s) + kX(s) = 1. \tag{6.27}$$

Equation 6.26 and 6.27 say that an unforced system with an initial velocity of

$$\dot{x}(0) = \frac{1}{m} \tag{6.28}$$

is equivalent to a system with zero initial conditions subjected to a unit impulse. Rearranging eqn 6.27 gives

$$X(s) = \frac{1}{ms^2 + cs + k}. \tag{6.29}$$

Taking the inverse Laplace transform of eqn 6.29, which is defined as

$$f(t) = \frac{1}{2\pi i}\int_{x-i\infty}^{x+i\infty} F(s)e^{st}ds, \tag{6.30}$$

gives the response of the mass in the time domain,

$$x(t) = \frac{1}{m\omega_d}e^{-\zeta\omega_n t}\sin(\omega_d t). \tag{6.31}$$

It can be seen from Figure 6.13 that the force transmitted to the base is equal to the force transmitted to the mass through the spring and damper, which is,

$$F_{tr} = c\dot{x} + kx. \tag{6.32}$$

Substituting eqn 6.31 into eqn 6.32 gives,

$$F_{tr} = k\left[\frac{2\zeta\sqrt{1-\zeta^2}}{m\omega_d}\cos(\omega_d t) - \frac{2\zeta^2}{m\omega_d}\sin(\omega_d t) + \frac{1}{m\omega_d}\sin(\omega_d t)\right]e^{-\zeta\omega_n t}, \tag{6.33}$$

where the damping factor, the natural frequency and the damped natural frequency are given by,

$$\zeta = \frac{c}{2\sqrt{km}}, \tag{6.34}$$

$$\omega_n = \sqrt{\frac{k}{m}}, \tag{6.35}$$

and

$$\omega_d = \omega_n\sqrt{1-\zeta^2}, \tag{6.36}$$

respectively. Using trigonometric relationships, eqn 6.33 is equal to

$$F_{tr} = \frac{\omega_n}{\sqrt{1-\zeta^2}}e^{-\zeta\omega_n t}\sin(\omega_d t + \phi), \tag{6.37}$$

where

$$\phi = \tan^{-1}\left(\frac{2\zeta\sqrt{1-\zeta^2}}{1-2\zeta^2}\right). \tag{6.38}$$

Dividing both sides of eqn 6.37 by ω_n gives the normalized force transmitted to the mass. The maximum force transmitted occurs when the time derivative of eqn 6.37 is equal to zero. The derivative of eqn 6.37 with respect to time is

$$\frac{dF_{tr}}{dt} = \frac{\omega_n}{\sqrt{1-\zeta^2}}e^{-\zeta\omega_n t}\left(\omega_d\cos(\omega_d t + \phi) - \zeta\omega_n\sin(\omega_d t + \phi)\right). \tag{6.39}$$

Using trigonometric relationships gives

$$\frac{dF_{tr}}{dt} = \frac{\omega_n^2}{\sqrt{1-\zeta^2}} e^{-\zeta\omega_n t} \sin\left(\omega_d t + \phi - \psi\right), \tag{6.40}$$

where

$$\psi = \tan^{-1} \frac{\sqrt{1-\zeta^2}}{\zeta}. \tag{6.41}$$

Equation 6.41 is equal to zero when

$$\omega_d t = \psi - \phi. \tag{6.42}$$

Substituting eqn 6.42 into eqn 6.37 gives

$$F_{tr} = \frac{\omega_n}{\sqrt{1-\zeta^2}} e^{\frac{-\zeta(\psi-\phi)}{\sqrt{1-\zeta^2}}}. \tag{6.43}$$

Dividing both sides of eqn 6.43 by ω_n and plotting as a function of ζ is shown in Figure 6.14. Figure 6.14 is a plot of the normalized force transmitted to the base as a function of one variable, the damping factor, ζ.

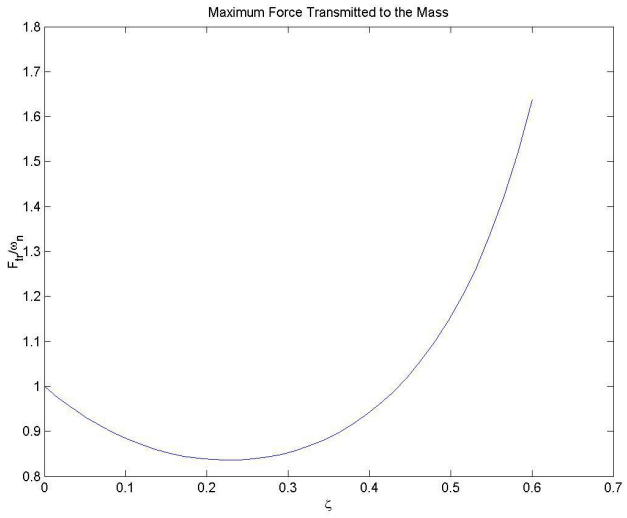

Figure 6.14: Maximum magnitude of an impulsive force transmitted to the mass.

As can be seen from eqn 6.37, the force transmitted is a function of the damping factor, ζ and the natural frequency of the system, ω_n. To reduce the force transmitted to

the mass, or the user's underarm, the natural frequency of the system should be minimized and ζ should be approximately 0.25 according to Figure 6.14. The maximum normalized transmissibility for the prototype is 0.951 without the footpad and 0.959 with the footpad. The maximum normal force at the axillary support is likely to coincide with maximum weight bearing. If the prototype acts like a SDOF system and can be modeled by an increasing mass as the user increases their weight bearing, then we would like ζ to be approximately 0.25 at maximum weight bearing

It is unlikely that the mini-Strutter can be fully represented by a SDOF system over the range of frequencies 0 to 400 Hz. It is possible that asymmetry and/or inadequate constraining during the experiment prevent the mini-Strutter from responding as a SDOF system. If the mini-Strutter spring length does not remain constant, the orthosis will oscillate in directions other than the excitation. Sufficient constraints are required to restrict motion to only the *z*-direction. If not, part of the excitation can cause oscillation/s in the *x* and/or *y* direction/s, as labeled in Figure 6.15.

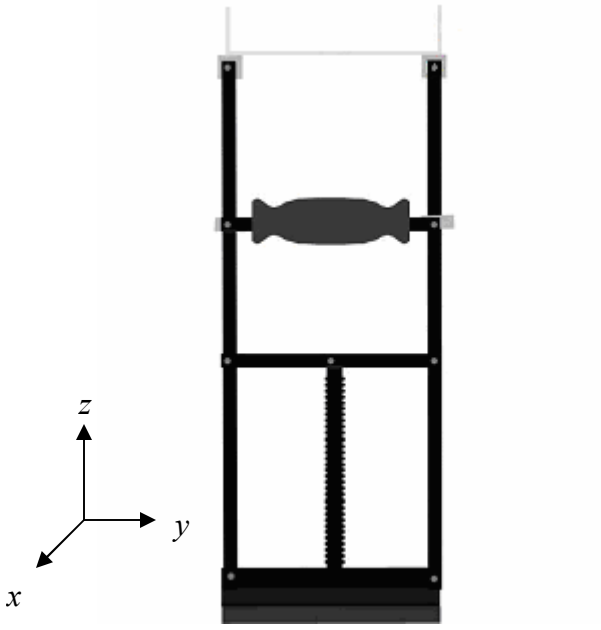

Figure 6.15: Coordinate system used for the 3-D acceleration ratio.

Accelerometers mounted in the three Cartesian directions are used to measure the oscillation in the *x*, *y* and *z* directions. The acceleration ratios of the mini-Strutter at 24 inches, 36 inches and the prototype are shown in Figure 6.16, Figure 6.17 and Figure 6.18.

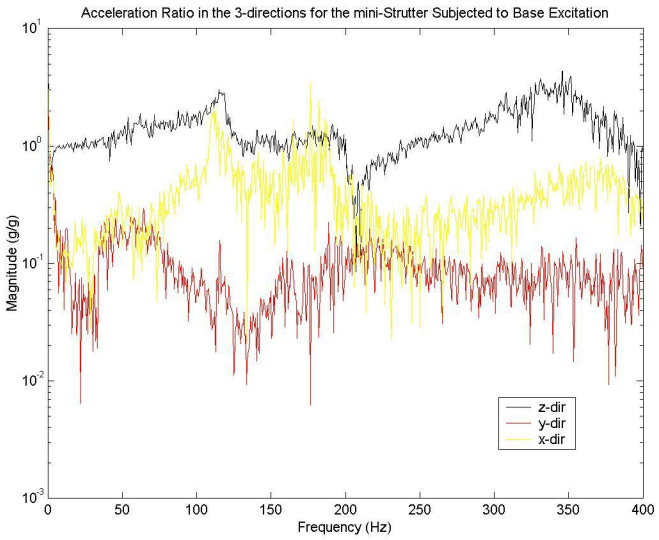

Figure 6.16: Magnitude of the displacement ratio of the mini-Strutter with a height of 24 inches subject to base excitation in the 3-directions between the frequencies 0 and 400 Hz.

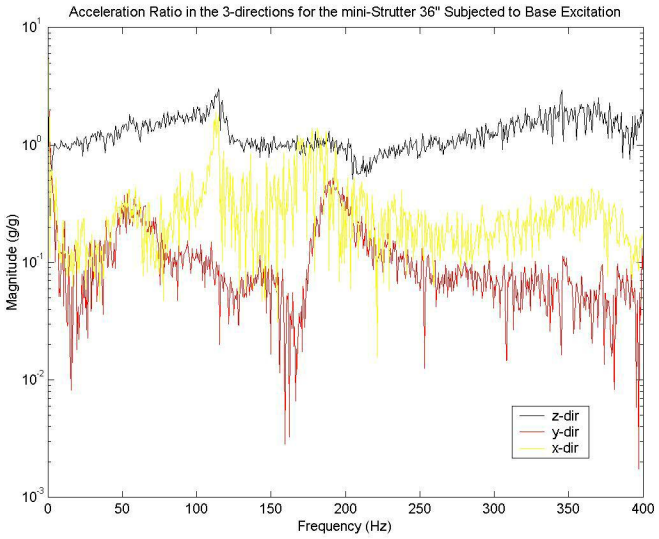

Figure 6.17: Magnitude of the displacement ratio of the mini-Strutter with a height of 36 inches subject to base excitation in the 3 directions between the frequencies 0 and 400 Hz.

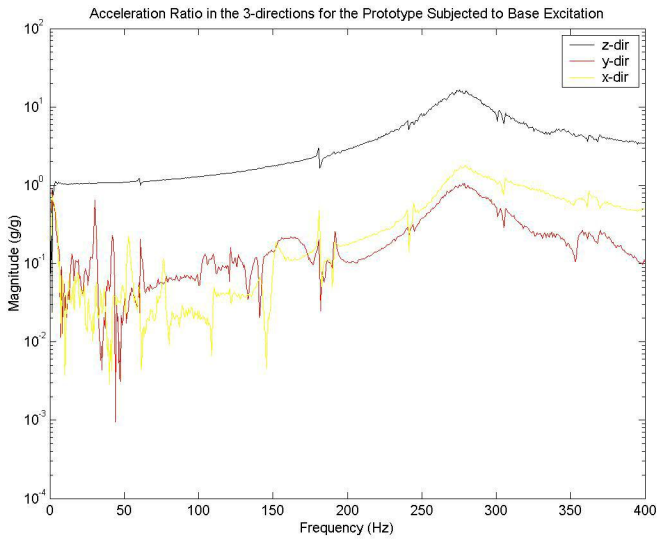

Figure 6.18: Magnitude of the displacement ratio of the prototype subject to base excitation in the 3 directions between the frequencies 0 and 400 Hz.

The mini-Strutter at the 24 and 36 inches height exhibits a greater acceleration ratio in the *x* and *y* direction for frequencies below 200 Hz when subjected to base excitation. The acceleration ratio of the prototype has a relatively smooth curve between 200 and 400 Hz. The smaller out of plane oscillations of the prototype can probably be explained by its lack of a cantilevered shoulder support and/or height adjustment tube.

6.4 Discussion

The responses of the mini-Strutter and the Prototype are found and a theoretic model of the response of the Prototype is determined. A SDOF system model cannot fully represent the behavior of the mini-Strutter because it does not have the characteristic features between the frequencies of interest. More sophisticated modeling techniques may be capable of modeling the behavior of the mini-Strutter between the frequencies of interest.

By eliminating the height adjustment tube and cantilevered shoulder support on the mini-Strutter as in the prototype, the response behaves more like a SDOF system and reduces low frequency (0-200 Hz) out of plane oscillations. Out of plane oscillations cause the user to apply a reaction force to counter-act the oscillations if they want to stay in the same position. With further testing of damping materials, a technique for picking a damping material depending on the weight bearing requirements of a user can be developed. Fitting a damper/footpad based on weight bearing requirements reduces the maximum normal force transmitted to the underarm of the user. Normal forces at the underarm/axillary support interface appear to be related to perceived comfort so reducing the normal forces as a result of initial contact of the footpad with the ground should also increase the user perceived comfort.

7 Conclusions and Recommendations

7.1 Conclusions

This thesis develops a comprehensive method by which assistive ambulatory devices with axillary supports are compared. The comparison accounts for forces during a stride and from impacts of the footpad with the ground at the beginning of a stride as well as measures the mechanical integrity of a device. The force transmitted to the underarm from the contact of the assistive ambulatory device's footpad with the ground should be minimized because in crutch walking there are bound to be multiple impacts with the ground throughout a day. These ground impacts cause normal impulses on the underarm that may cause damage to the axillary nerve. Since the normal force on the underarm during a stride appears related to perceived comfort, it is natural to assume that the impulse transmission is related to perceived comfort. However, the perceived comfort was measured for a gait with the footpad initially in contact with the ground, i.e. there was no initial contact of the footpad with the ground so that this cannot be validated. To minimize the force transmitted, the damping ratio of a device should be fit to a user's weight bearing requirements so that when they use the device for maximum weight bearing the force transmission is minimized. Also the impulse transmissibility of axillary crutches was not found so it cannot be said whether the Strutter or axillary crutches has a smaller transmissibility ratio.

Eliminating the cantilevered axillary support and height adjustment holes in the Strutter as in the prototype, reduces the stress in the vertical support tubes and allows the orthosis to be modeled as a single degree of freedom system so impacts with the ground

can be minimized. In use, for able-bodied users during a stride, the peak and average force normal to the axillary pad is higher for axillary crutches than the Strutter. The force in the tangential direction is higher than the Strutter compared to axillary crutches for the same stride time. Subjects rate the Strutter more comfortable than axillary crutches after participation in the experiment. It appears that the comfort of subjects is most heavily dependent on the normal force because the Strutter has lower forces in the normal direction.

The criteria for a good assistive mobility device with axillary support should be one that minimizes the reactions between the axillary support and the user's underarm during a stride and when the footpad initially makes contact with the ground. Axillary crutches and the Strutter have relatively poor user perceived comfort. Axillary crutches were rated a 4.7 while the Strutter was rated a 5.9 on a scale of 1 to 10 with a score of 10 being most comfortable. Clearly there is room for improvement. The axillary support needs to distribute the weight of the user in a way differently than the Strutter or axillary crutches do to further increase user perceived comfort.

7.2 Recommendations

The forces in the tangential direction on the axillary support of the Strutter +and axillary crutches had to be estimated but accelerometry could be used to determine the angular acceleration as a function of time, $\ddot{\theta}(t)$. Using a motion capture system, the angular velocity can be found as a function of the angle the device makes with the vertical, $\ddot{\theta}(\theta)$. Knowing $\ddot{\theta}(t)$ or $\ddot{\theta}(\theta)$ allows direct computation of the tangential force which can verify whether the estimated force is reasonable.

When users of the Strutter or axillary crutches make initial contact with the ground, the orthosis is rarely in the vertical position. Measuring the acceleration ratio for axillary crutches as well as for cases when the orthosis is in a position other than vertical makes a more realistic model of initial contact since users seldom if ever hold their orthosis in the vertical position during initial contact.

The handgrip and axillary support of the Strutter are always horizontal during a stride. The handgrip and axillary support of axillary crutches rotate through a stride. Despite this difference, the path that the center of pressure follows during a stride is the similar for both the Strutter and axillary crutches. The center of pressure begins in the middle of the axillary support then moves toward the posterior. This means the middle and anterior regions of the underarm are loaded during a stride. Whether or not loading the middle or anterior regions of the underarm affects perceived comfort remains to be determined. Most importantly a more concrete relationship between perceived comfort and safety must be established.

7.3 Contributions

This thesis develops a means of analyzing assistive devices with axillary supports to lay the foundation for the design of safe axillary supports specifically for individuals with low-level spinal cord injuries. In particular two assistive mobility devices with axillary supports are compared, axillary crutches and the Strutter. A correlation between the force normal to the axillary support applied by the underarm and user perceived comfort was found using the Fscan pressure sensor. A dynamic model for the Strutter and axillary crutches was developed. The model can be used to predict external forces that are not easily measured using a conventional strain gauge. A technique to minimize the

force transmitted to the underarm due to contact of the orthoses footpad with the ground was developed. Finally the fracture morphology of aluminum tubes with holes for height adjustment was found so that when confronted with a failure, investigators can deduce the cause of a failure.

8 Appendix

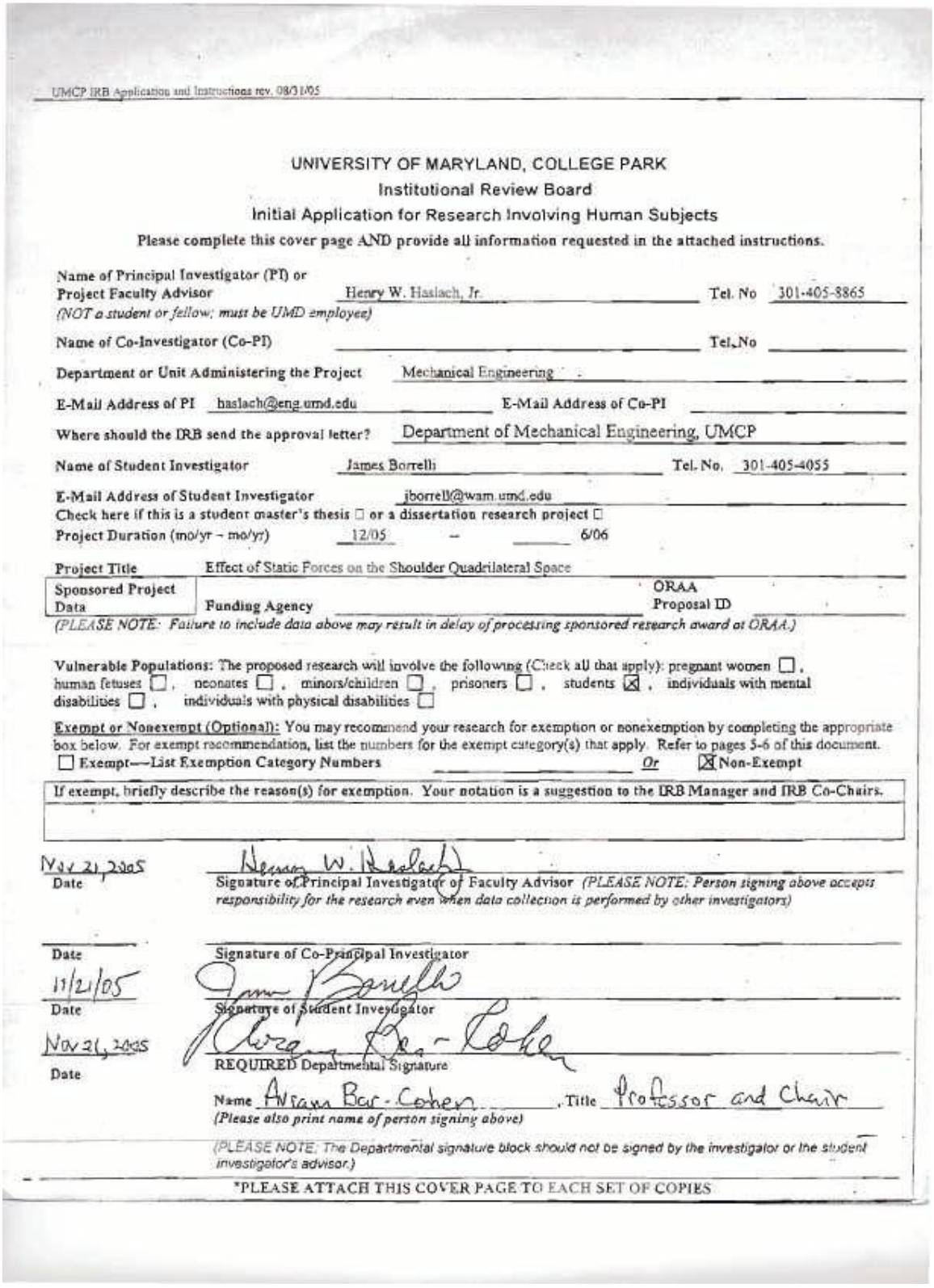

UMCP IRB Application and Instructions rev. 08/31/05

UNIVERSITY OF MARYLAND, COLLEGE PARK
Institutional Review Board
Initial Application for Research Involving Human Subjects

Please complete this cover page AND provide all information requested in the attached instructions.

Name of Principal Investigator (PI) or Project Faculty Advisor: Henry W. Haslach, Jr. Tel. No: 301-405-8865
(NOT a student or fellow; must be UMD employee)

Name of Co-Investigator (Co-PI): _____ Tel. No: _____

Department or Unit Administering the Project: Mechanical Engineering

E-Mail Address of PI: haslach@eng.umd.edu E-Mail Address of Co-PI: _____

Where should the IRB send the approval letter? Department of Mechanical Engineering, UMCP

Name of Student Investigator: James Borrelli Tel. No: 301-405-4055

E-Mail Address of Student Investigator: jborrell@wam.umd.edu

Check here if this is a student master's thesis ☐ or a dissertation research project ☐

Project Duration (mo/yr – mo/yr): 12/05 – 6/06

Project Title: Effect of Static Forces on the Shoulder Quadrilateral Space

Sponsored Project Data — Funding Agency: _____ ORAA Proposal ID: _____
(PLEASE NOTE: Failure to include data above may result in delay of processing sponsored research award at ORAA.)

Vulnerable Populations: The proposed research will involve the following (Check all that apply): pregnant women ☐, human fetuses ☐, neonates ☐, minors/children ☐, prisoners ☐, students ☒, individuals with mental disabilities ☐, individuals with physical disabilities ☐

Exempt or Nonexempt (Optional): You may recommend your research for exemption or nonexemption by completing the appropriate box below. For exempt recommendation, list the numbers for the exempt category(s) that apply. Refer to pages 5-6 of this document.
☐ Exempt—List Exemption Category Numbers _____ *Or* ☒ Non-Exempt

If exempt, briefly describe the reason(s) for exemption. Your notation is a suggestion to the IRB Manager and IRB Co-Chairs.

Nov 21, 2005 — Date
Henry W. Haslach — Signature of Principal Investigator or Faculty Advisor *(PLEASE NOTE: Person signing above accepts responsibility for the research even when data collection is performed by other investigators)*

Date — Signature of Co-Principal Investigator

11/21/05 — Date
James Borrelli — Signature of Student Investigator

Nov 21, 2005 — Date
Avram Bar-Cohen — REQUIRED Departmental Signature

Name Avram Bar-Cohen, Title Professor and Chair
(Please also print name of person signing above)

(PLEASE NOTE: The Departmental signature block should not be signed by the investigator or the student investigator's advisor.)

*PLEASE ATTACH THIS COVER PAGE TO EACH SET OF COPIES

CONSENT FORM

Initials _____ Date _____

Project Title	*Effect of Static Forces on the Shoulder Quadrilateral Space*
Why is this research being done?	*This is a research project being conducted by Henry Haslach at the University of Maryland, College Park. We are inviting you to participate in this research because you are at least 18 years of age and you are not currently experiencing any shoulder problems. The purpose of this research is to measure the effects of static forces on the integrity of the shoulder quadrilateral space as part of a study to prevent crutch palsy.*
What will I be asked to do?	*The procedures involve one session during which you will be asked to rest your weight on several types of crutch underarm supports while measurements are taken both as you stand stationary and as you take one stride. The total time for your participation will be 1 to 2 hours. The research will take place in the Department of Mechanical Engineering at the University of Maryland, College Park.*
What about confidentiality?	*We will do our best to keep your personal information confidential. To help protect your confidentiality: (1) your name will not be included on the surveys or other collected data; (2) a code will be placed on the survey and other collected data; (3) through the use of an identification key, the researcher will be able to link your survey to your identity; and (4) only the researcher will have access to the identification key. If we write a report or article about this research project, your identity will be protected to the maximum extent possible.* *Your information may be shared with representatives of the University of Maryland, College Park or governmental authorities if you or someone else is in danger or if we are required to do so by law.*
What are the risks of this research?	*There are some risks from participating in this research study. Putting your full weight on the underarm may cause discomfort. Normally, there are no long-term effects associated with placing your full weight on an underarm support for the period of time involved in this experiment.*
What are the benefits of this research?	*This research is not designed to help you personally, but the results may help the investigator learn more about how weight is bourn on an underarm support. We hope that, in the future, other people might benefit from this study through improved understanding of how to prevent excessive forces on the underarm and therefore reduce the risk of crutch palsy.*
Do I have to be in this research? **Can I stop participating at any time?**	*Your participation in this research is completely voluntary. You may choose not to take part at all. If you decide to participate in this research, you may stop participating at any time. If you decide not to participate in this study or if you stop participating at any time, you will not be penalized or lose any benefits to which you otherwise qualify.*

Initials _____ Date _____

Project Title	*Effect of Static Forces on the Shoulder Quadrilateral Space*	
Is any medical treatment available if I am injured?	*The University of Maryland does not provide any medical, hospitalization or other insurance for participants in this research study, nor will the University of Maryland provide any medical treatment or compensation for any injury sustained as a result of participation in this research study, except as required by law.*	
What if I have questions?	*This research is being conducted by Henry Haslach at the University of Maryland, College Park. If you have any questions about the research study itself, please contact Henry Haslach at: Department of Mechanical Engineering, University of Maryland, 2149 Glenn L. Martin Hall, 301-405-8865 or haslach@eng.umd.edu* *If you have questions about your rights as a research subject or wish to report a research-related injury, please contact:* **Institutional Review Board Office, University of Maryland, College Park, Maryland, 20742; (e-mail) irb@deans.umd.edu; (telephone) 301-405-0678** *This research has been reviewed according to the University of Maryland, College Park IRB procedures for research involving human subjects.*	
Statement of Age of Subject and Consent	*Your signature indicates that:* *you are at least 18 years of age;,* *the research has been explained to you;* *your questions have been answered; and* *you freely and voluntarily choose to participate in this research project.*	
Signature and Date	**NAME OF SUBJECT**	
	SIGNATURE OF SUBJECT	
	DATE	

******Please note: When consent form requires more than one page, please include a space for the subject to initial and date at the top right-hand corner of each page. The corner should appear as: Initials_____ Date_____ Also, each page must display a page range such as: Page 1 of 2, then Page 2 of 2. This step would confirm that the subject agreed to the entire contents of the consent form. ******

9 Bibliography

A. M. R. Agur, A. F. Dalley II, *Grant's Atlas of Anatomy*, Philadelphia: Lippincott, Williams & Wilkins, 2005.

F. C. Anderson, M. G. Pandy, "A Dynamic Optimization Solution for Vertical Jumping in Three Dimensions," *Computer Methods in Biomechanics and Biomedical Engineering*, vol. 2, pp. 201-231, 1999.

F. C. Anderson, M. G. Pandy, "Dynamic Optimization of Human Walking," *Journal of Biomechanical Engineering,* vol. 123 (5), pp. 381-390, Oct. 2001.

B. Balachandran, E. B. Magrab, *Vibration,* United Kingdom: Thomson-Engineering, 2003.

R. Bogey, "Individual Knee Muscle Force and Power in Normal Adult Walking," *American Journal of Physical Medicine and Rehabilitation,* vol. 82 (3), pp. 243, March 2003.

R. P. Brown, *Physical Testing of Rubber*, London: Chapman and Hall, 1996.

T. K. Cobb, K. An, W. P. Cooney, "Externally Applied Forces to the Palm Increase Carpal Tunnel Pressure," *The Journal of Hand Surgery,* vol. 20A (2), pp. 181-185, March 1995.

M. Comin, R. P. Puente, J. M. B. Lois, C. R. Ruiz, J. L. Peris, J. Sanchez-Lacuesta, C. S. Gracia, "Biomechanical Evaluation of Handgrips for the Design of Elbow Crutches," *Technology and Disability,* vol. 10 (2), pp. 115-121, 1999.

N. Doriot, L. Cheze, "A Three-Dimensional Kinematic and Dynamic Study of the Lower Limb During the Stance Phase of Gait Using an Homogeneous Matrix Approach," *IEEE Transactions on Biomedical Engineering,* vol. 51 (1), pp. 21-27, Jan. 2004.

A. J. Dalton, "Prospective Clinical Evaluation Comparing Standard Axillary Crutches with the Hands Free Crutch," *Physiotherapy Canada,* vol. 54 (2), pp. 110-115, 2002.

A. B. Deathe, "Canes, Crutches, Walkers and Wheelchairs; A Review of Metabolic Energy Expenditure," *Canadian Journal of Rehabilitation,* (4), pp. 217-230, 1992.

G. N. Duda, E. Schneider, E. Y. S. Chao, "Internal Forces and Moments in the Femur During Walking," *Journal of Biomechanics*, vol. 30 (9), pp. 933-941, Sept. 1997.

C. M. Duffy, A. E. Hill, A. P Cosgrove, I. S. Corry, R. A. B. Mollan, H. K. Graham, "Three-Dimensional Gait Analysis in Spina Bifida," *Journal of Pediatric Orthopaedics*, vol. 16 (6), pp. 786-791, 1996.

D. R. Feldman, I. Vujic, D. McKay, F. Callcott, R. Uflacker, "Crutch-Induced Axillary Injury," *Cardiovascular and Interventional Radiology,* vol. 18 (5), pp. 296-299, 1995.

S. A. Gard, D. S. Childress, "What Determines the Vertical Displacement of the Body During Normal Walking?" *Journal of Prosthetics and Orthotics*, vol. 13 (3), pp. 64-69, 2001.

K. A. Gillespie, J. P. Dickey, "Determination of the Effectiveness of Materials in Attenuating High Frequency Shock During Gait Using Filterbank Analysis," *Clinical Biomechanics*, vol. 18 (1), pp.50-59, 2003.

J. S. Gottschall, R. Kram, "Energy Cost and Muscular Activity Required for propulsion During Walking," *Journal of Applied Physiology,* vol. 94 (5), pp. 1776-1772, May 2003.

J. Hall, A. K. Clarke, "An Evaluation of Crutches," *Physiotherapy,* vol. 77 (3), pp. 156-160, 1991.

C. Fransson-Hall, A. Kilborn, "Sensitivity of the Hand to Surface Pressure," *Applied Ergonomics,* vol. 24 (3), pp. 181-189, 1993.

H. W. Haslach, R. W. Armstrong, *Deformable Bodies and Their Material Behavior*, Danvers, MA: John Wiley and Sons Inc, 2003.

http://www.spinal-research.org/display_section.asp?section=cord_injury, accessed June 2006.

http://www.tekscan.com/medical/catalog/9811.html, access July 2006.

H. L. P. Hurkmans, J. B. J. Bussman, E. Benda, J. A. N. Verhaar, H. J. Stam, "Techniques for measuring weight bearing during standing and walking," *Clinical Biomechanics*, vol. 18 (7), pp. 576-589, August 2003.

K. F. Janz, R. Smita, H. J. Baumann, "Measuring Children's Vertical Ground Reaction Forces with Accelerometry During Walking, Running, and Jumping: The Iowa Bone Development Study," *Pediatric Exercise Sceince,* vol. 15 (1), pp. 34-43, Feb. 2003.

B. Kingston, *Understanding Muscles A Practical Guide to Muscle Function*, New York: Chapman & Hall Medical, 1996.

Y. Laufer, "The Effect of Walking Aids on Balance and Weight-Bearing Patterns of Patients with Hemiparesis in Various Stance Positions," *Physical Therapy*, vol. 83 (2), pp.112-122, Feb. 2003.

M. A. Le Blanc, L. E. Carlson, T. Nauenberg, "A Quantitative Comparison of Four Experimental Axillary Crutches," *Journal of Prosthetics and Orthotics*, vol. 5 (1), pp. 20-28, 1993.

R. Y. W. Lee, "Energy Expenditure of Three-Point Non-Weight Bearing Walking with Axillary Crutches and Elbow Crutches," *The Journal of the Hong Kong Physiotherapy Association,* vol. 9, pp. 29-37, 1987.

B. McFall, N. Arya, C. Soong, B. Lee, R. Hannon, "Crutch Induced Axillary Artery Injury," *The Ulster Medical Journal,* vol. 73 (1), pp. 50-52, 2004.

L. Meirovitch, *Fundamentals of Vibrations,* Boston: McGraw Hill, 2001.

W. Navidi, *Statistics for Engineers and Scientists,* Boston: McGraw Hill, 2006.

M. Nordin, V. H. Frankel, D. Leger, K. Forssen, A. Lis, *Basic Biomechanics of the Musculoskeletal System*, Philadelphia, PA: Lippincott Williams &Wilkins, 2001.

M. J. O'Malley, "Normalization of Temporal-Distance Parameters in Pediatric Gait," *Journal of Biomechanics,* vol. 29 (5), pp. 619-625, May 1996.

M. J. O'Malley, D. L. M. de Paor, "Kinematic Analysis of Human Walking Gait Using Digital Image Processing," *Medical and Biological Engineering and Computing,* vol. 31 (4), pp. 392-298, 1993.

D. A. Neumann , *Kinesiology of the Musculoskeletal System Foundations for Physical Rehabilitation*, St. Louis, MO: Mosby Inc, 2002.

L. Noreau, L. Richards, F. Comeau, D. Tardif, "Biomechanical Analysis of Swing-Through Gait in Paraplegic and Non-Disabled Individuals," *Journal of Biomechanics,* vol. 28 (6), pp. 689-700, 1995.

J. Nyland, T. Bernasek, B. Markee, C. Dundore, "Comparison of the Easy Strutter Functional Orthosis Sysyem™ and axillary crutches during modified 3-point gait," *Journal of Rehabilitation Research & DevelopmentI*, vol. 41 (2), pp. 195-205, March/April 2004.

M. G. Pandy, N. Berme, "Quantitative Assessment of Gait Determinants During Single Stance Via a Three-Dimensional Model-Part 1. Normal Gait," *Journal of Biomechanics,* vol. 22 (6/7), pp. 717-724, June/July 1989.

M. G. Pandy, N. Berme, "Quantitative Assessment of Gait Determinants During Single Stance Via a Three-Dimensional Model-Part 2. Pathological Gait," *Journal of Biomechanics,* vol. 22 (6/7), pp. 725-733, June/July 1989.

G. S. Perlmutter, "Axillary Nerve Injury," *Clinical Orthopaedics and Related Research,* vol. 386, pp. 28-36, Nov. 1999.

T. M. Quinn, P. Dierickx, A. J. Grodzinsky, "Glycosaminoglycan Network Geometry May Contribute to Anisotropic Hydraulic Permeability in Cartilage Under Comppression," *Journal of Biomechanics,* vol. 34 (11), pp. 1483-1490, Nov. 2001.

P. J. Rasch, *Kinesiology and Applied Anatomy*, Philadelphia, PA: Lea & Febiger, 1989.

L. N. Rudin, L. Levine, "Bilateral Compression of the Radial Nerve," *Physical Therapy Review,* vol. 31 (6), pp. 229-231, 1951.

D. A. Sala, L. M. Leva, F. J. Kummer, A. D. Grant, "Crutch Handle Design: Effect on Palmar Loads During Ambulation," *Archives of Physical Medicine and Rehabilitation,* vol. 79 (11), pp. 1473-1476, Nov. 1998.

J. Stallard, "A Comparison of Axillary, Elbow and Canadian Crutches," *Rheumatology and Rehabilitation,* vol. 17 (4), pp. 237-239, 1978.

C. L. Vaughan, "Theories of Bipedal Walking: An Odyssey," *Journal of Biomechanics,* vol. 36 (4), pp. 513-523, April 2003.

E. N. Williams, N. S. Broughton, M. B. Menelaus, "Age-Related Walking in Children with Spina Bifida," *Developmental Medicine and Child Neurology*, vol. 41 (7), pp 446-449, 1999.